ΠΑΝΕΠΙΣΤΗΜΙΟ ΘΕΣΣΑΛΙΑΣ
ΣΧΟΛΗ ΕΠΙΣΤΗΜΩΝ ΥΓΕΙΑΣ
ΤΜΗΜΑ ΙΑΤΡΙΚΗΣ

Τομέας Βασικών και Εφαρμοσμένων Βιοϊατρικών Επιστημών

Εργαστήριο Φυσιολογίας

Διευθυντής: Ζαρογιάννης Σωτήριος, Αναπληρωτής Καθηγητής

Διδακτορική Διατριβή

«Investigation of 2-deoxyglucose (2DG) as a modulator of mesothelial and endothelial cell membrane function in Peritoneal Dialysis»

υπό

Ελεάννα Πιταράκη

Βιολόγος, MSc

Υπεβλήθη για την εκπλήρωση μέρους των απαιτήσεων για την απόκτηση Διδακτορικού Διπλώματος στο Τμήμα Ιατρικής του Πανεπιστημίου Θεσσαλίας

Λάρισα, Ιανουάριος, 2024

Η έγκριση της Διδακτορικής Διατριβής από το Τμήμα Ιατρικής της Σχολής Επιστημών Υγείας του Πανεπιστημίου Θεσσαλίας δεν υποδηλώνει αποδοχή των απόψεων του συγγραφέα (σύμφωνα με τις διατάξεις του άρθρου 202, παράγραφος 2 του Ν. 5343/1932).

Εγκρίθηκε από τα Μέλη της Επταμελούς Εξεταστικής Επιτροπής (8η/31-01-2024 ΓΣΕΣ):

1ος Εξεταστής: Ζαρογιάννης Σωτήριος
(Επιβλέπων) Αναπλ. Καθηγητής, Εργαστήριο Φυσιολογίας, Τμήμα Ιατρικής, Σχολή Επιστημών Υγείας, Πανεπιστήμιο Θεσσαλίας

2ος Εξεταστής: Χατζόγλου Χρυσή
Καθηγήτρια, Εργαστήριο Φυσιολογίας, Τμήμα Ιατρικής, Σχολή Επιστημών Υγείας, Πανεπιστήμιο Θεσσαλίας

3ος Εξεταστής: Schmitt Claus Peter
Professor, Pediatric Nephology, Center for Pediatrics and Adolescent Medicine, University of Heidelberg

4ος Εξεταστής: Γουργουλιάνης Κωνσταντίνος
Καθηγητής, Πνευμονολογική Κλινική, Τμήμα Ιατρικής, Σχολή Επιστημών Υγείας, Πανεπιστήμιο Θεσσαλίας

5ος Εξεταστής: Στεφανίδης Ιωάννης
Καθηγητής, Νεφρολογική Κλινική, Τμήμα Ιατρικής, Σχολή Επιστημών Υγείας, Πανεπιστήμιο Θεσσαλίας

6ος Εξεταστής: Ελευθεριάδης Θεόδωρος
Καθηγητής, Νεφρολογική Κλινική, Τμήμα Ιατρικής, Σχολή Επιστημών Υγείας, Πανεπιστήμιο Θεσσαλίας

7ος Εξεταστής: Λιακόπουλος Βασίλειος
Καθηγητής, Β' Νεφρολογική Κλινική, Νοσοκομείο ΑΧΕΠΑ, Τμήμα Ιατρικής, Σχολή Επιστημών Υγείας, Αριστοτέλειο Πανεπιστήμιο Θεσσαλονίκης

ACKNOWLEDGEMENTS

My education is a reflection of the support from my very loving and understanding family. They provided me with encouragement and positive belief in my success that kept me going regardless of the challenges I faced.

I would like to thank each and every member of my Research Committee for their enduring support during my doctoral studies but primarily, the Associate Professor of Physiology and Chair of the Department of Physiology, Dr. Sotirios Zarogiannis. Over the last six years, you were not only my Supervisor of both Master and Doctorate degrees, but also a good friend always keen to help and advise me. Your support and guidance stimulated me to think in a broader scientific way.

To the Professor of Medical Physiology, Dr. Chrissi Hatzoglou, a great thanks for everything, from scientific guidance and discussions to helping me with the lab needs. Your help is always invaluable.

To the Professor of Pediatric Nephrology, Dr. Claus Peter Schmitt, my deepest respect and a heartfelt thank you.

No words will suffice the depth of my gratitude to the Professor of Respiratory, Dr. Konstantinos Gourgoulianis. Thank you for your constant encouragement and support, and the very fruitful scientific discussions that we had.

I would also like to thank the members of my examination committee, Professor of Pathology-Nephrology, Dr. Ioannis Stefanidis and Professor of Nephrology, Dr. Theodoros Eleftheriadis for taking the time to read and assess my PhD Thesis.

Many thanks to the Professor of Nephrology, Dr. Vassileios Liakopoylos not only for the kind gifts of the Peritoneal Dialysis fluids but also for stimulating discussions and inspiration.

Among my mentors, I could not miss the former Postdoctoral researcher Mr. Rajesh Jagirdar. From my very first day at this lab as a naïve new recruit, he aimed to impart all his knowledge to me. We went through good and bad times, but never quit supporting and assisting each other.

Special mention goes to Dr. Erasmia Rouka because apart from her scientific contribution to the completion of my dissertation, she was always a helping hand and a listening ear.

The journey of my PhD is now done!

Eleanna Pitaraki

SHORT CURRICULUM VITAE

Name: Eleanna Pitaraki

Date of Birth: ***

Present Appointment: Biologist, MSc, PhD candidate, Laboratory of Physiology, Faculty of Medicine, School of Health Sciences, University of Thessaly, BIOPOLIS, Larissa, Greece

Research experience	
Date	***Appointment***
Nov 2019 – *present*	**PhD Candidate**, Laboratory of Physiology, Faculty of Medicine, University of Thessaly, Larissa, Greece Title: 'Investigation of 2-deoxyglucose (2DG) as a modulator of mesothelial and endothelial cell membrane function in Peritoneal Dialysis' *Anticipated Defence on February 2024*
Feb 2019 – *present*	**Research Fellow**, Department of Respiratory Medicine, Faculty of Medicine, University of Thessaly, Larissa, Greece Laboratory handling of human biological specimens
Sep 2020 – Mar 2022	**Clinical Study Coordinator**, Department of Respiratory Medicine, Faculty of Medicine, University of Thessaly, Larissa, Greece Pfizer sponsored non-interventional Clinical Study (B0661128) 'Real World data on VTE treatment in Greece - (Venous Thromboembolism Real – VicToRiA study)'
Mar 2021 – Dec 2022	**Research Assistant**, Department of Physiology, University of Thessaly, Larissa, Greece H.F.R.I. Research Proposal PRINCIPLE_3221 'The role of primary cilium in the physiology and pathophysiology of pleural mesothelial cells: Functional and molecular studies in two-dimensional and three-dimensional cell cultures in patients with parapneumonic and malignant pleural effusions'

Teaching experience			
Date	***Subject***	***Course (Supervisor)***	***Department***
Oct 2021 – Feb 2022	Human pathology and pathophysiology	Clinical anatomy (Kotsiou Ourania, Assistant Professor)	Department of Nursing, University of Thessaly, Larissa, Greece
May 2021 – Sep 2021	Care of cardiorespiratory patient	Physiology and Pathophysiology II (Kotsiou Ourania, Assistant Professor)	Department of Nursing, University of Thessaly, Larissa, Greece

Academic degrees			
Date	***Title of Award***	***Subject***	***Awarding Body***
Nov 2019 – *present*	PhD Candidate	Physiology	Faculty of Medicine, University of Thessaly, Larissa, Greece
Oct 2017 – Oct 2018	MSc	Clinical Applications of Molecular Medicine	Faculty of Medicine, University of Thessaly, Larissa, Greece
Oct 2013 – Sep 2017	BSc	Biology	Faculty of Biology, University of Patras, Patra, Greece

Scholarships:

- **02/2019 – 05/2021:** Scientific Society for Respiratory Disorders and Critical Illness, Athens, Greece
- **05/2021 – 09/2021:** Department of Nursing, University of Thessaly, Larissa, Greece

List of Publications:

1. Jagirdar RM, **Pitaraki E**, Rouka E, Papazoglou ED, Bartosova M, Zembekakis P, Schmitt CP, Zarogiannis SG, Liakopoulos V. Differential effects of biocompatible peritoneal dialysis fluids on human mesothelial and endothelial cell 2D and 3D phenotypes. *Artificial Organs*. *In Press*. **IF: 2.6**
2. **Pitaraki E**, Jagirdar R.M, Rouka E, Bartosova M, Sinis S.I, Gourgoulianis K.I, Eleftheriadis T, Stefanidis I, Liakopoulos V, Hatzoglou C, Schmitt C.P, Zarogiannis S.G. 2-Deoxy-glucose ameliorates the peritoneal mesothelial and endothelial barrier function perturbation occurring due to Peritoneal Dialysis fluids exposure. *Biochem Biophys Res Commun*. 2023;693:149376. **IF: 3.3**
3. Giannopoulos AS, Giannakou L, Gourgoulianni N, **Pitaraki E**, Jagirdar RM, Marnas P, Tzamalas P, Rouka E, Livanou E, Hatzoglou C, Gourgoulianis KI, Lupold S, Blackenhorn W, Zarogiannis SG. The effect of cigarette smoke extract exposure on the size and sexual behavior of Drosophila melanogaster. *Environ Toxicol Pharmacol*. 2023;104:104325. **IF: 5.7**
4. Rouka E, Jagirdar RM, Sarrigeorgiou I, **Pitaraki E**, Sinis SI, Varsamas C, Papazoglou ED, Kotsiou O, Lymberi P, Giannou A, Hatzoglou C, Gourgoulianis KI, Zarogiannis SG. Changes in expression of mesothelial BBS genes in 2D and 3D after lithium chloride and ammonium sulphate induction of primary cilium disturbance. *Pharmacol Rep*. 2023;75(5):1230-1239. **IF: 3.9**
5. Jagirdar RM[1], **Pitaraki E[1]**, Kotsiou OS[1], Rouka E, Sinis SI, Varsamas C, Marnas P, Stergiopoulou E, Giannou A, Hatzoglou C, Gourgoulianis KI, Zarogiannis SG. Effects of

pharmacological primary cilium disturbance in the context of in vitro 2D and 3D malignant pleura mesothelioma. *Biochem Biophys Res Commun.* 2023;654:128-135. **IF: 3.3**

6. Faropoulos K, Polia A, Tsakona C, **Pitaraki E**, Moutafidi A, Gatzounis G, Assimakopoulou M. Evaluation of AQP4/TRPV4 channel co-expression, microvessel density and its association with peritumoral brain edema in intracranial meningiomas. *J Mol Neurosci.* 2021;71(9):1786-1795. **IF: 2.8**
7. Jagirdar RM, Papazoglou ED, **Pitaraki E**, Kouliou OA, Rouka E, Giannakou L, Giannopoulos S, Sinis SI, Hatzoglou C, Gourgoulianis KI, Zarogiannis SG. Cell and extracellular-matrix interaction models in benign mesothelial and malignant pleural mesothelioma cells in 2D and 3D in-vitro. *Clin Exp Pharmacol Physiol.* 2021;48(4):543-552. **IF: 2.9**
8. Papazoglou ED, Jagirdar RM, Kouliou OA, **Pitaraki E**, Hatzoglou C, Gourgoulianis KI, Zarogiannis SG. In Vitro Characterization of Cisplatin and Pemetrexed Effects in Malignant Pleural Mesothelioma 3D Culture Phenotypes. *Cancers (Basel).* 2019;11(10):1446. **IF: 5.2**
9. Gerogianni I, **Pitaraki E**, Jagirdar RM, Kouliou O, Giannakou L, Giannopoulos S, Papazoglou E, Hatzoglou C, Gourgoulianis KI, Zarogiannis SG. 2-Deoxy-glucose Enhances the Effect of Cisplatin and Pemetrexed in Reducing Malignant Pleural Mesothelioma Cell Proliferation but Not Spheroid Growth. *Anticancer Res.* 2019;39(7):3809-3814. **IF: 2.0**

Awards:

1. L. Giannakou, A.S. Giannopoulos, E. Rouka, **E. Pitaraki**, R. Jagirdar, C. Hatzoglou, K. Gourgoulianis, S. Zarogiannis. Drosophila melanogaster models of Sestrin-associated human lung diseases: In Silico analysis of the fruit fly Sestrin interactome.
   Best Poster Award. 1st Greek Physiology Society Conference, Athens, Greece, 2022.
2. **Pitaraki E**, Jagirdar R, Roumeliotis S, Hatzoglou C, Liakopoulos V, Zarogiannis SG. Effect of Peritoneal Dialysis Fluids on mesothelial-to-mesenchymal transition of human mesothelial cells.
   Best Oral Presentation Award. 21st National Conference of Nephrology, Delphoi, Greece, 2019.
3. Papazoglou ED, Jagirdar RM, Kouliou OA, **Pitaraki E**, Hatzoglou C, Gourgoulianis KI, Zarogiannis SG. In vitro characterization of cisplatin and pemetrexed effects in malignant pleural mesothelioma 3D culture phenotypes. Cancers *(Basel)* 2019;11(10):1446.
   Award for the Best Publication of the Department of Respiratory Medicine of University of Thessaly for the period 1999-2019. Annual Panhellenic Conference of Pneumonology and Intensive Care, Volos, Greece, 2019.

International Conference Presentations:

Track record (2018-2023): 26

- *1st Author: 4*
- *2nd Author: 3*
- *Other Author position: 19*

Hellenic Conference Presentations:

Track record (2018-2023): 22

- *1st Author: 10*
- *2nd Author: 4*
- *Other Author position: 8*

«Investigation of 2-deoxyglucose (2DG) as a modulator of mesothelial and endothelial cell membrane function in Peritoneal Dialysis»

Ελεάννα Πιταράκη

Πανεπιστήμιο Θεσσαλίας, Τμήμα Ιατρικής, 2024

ΤΡΙΜΕΛΗΣ ΣΥΜΒΟΥΛΕΥΤΙΚΗ ΕΠΙΤΡΟΠΗ

1. **Σωτήριος Ζαρογιάννης**, Αναπληρωτής Καθηγητής, Εργαστήριο Φυσιολογίας, Τμήμα Ιατρικής, Σχολή Επιστημών Υγείας, Πανεπιστήμιο Θεσσαλίας, Λάρισα, Ελλάδα **(Επιβλέπων)**
2. **Χρυσή Χατζόγλου**, Καθηγήτρια, Εργαστήριο Φυσιολογίας, Τμήμα Ιατρικής, Σχολή Επιστημών Υγείας, Πανεπιστήμιο Θεσσαλίας, Λάρισα, Ελλάδα
3. **Claus Peter Schmitt**, Professor, Pediatric Nephology, Center for Pediatrics and Adolescent Medicine, University of Heidelberg, Heidelberg, Germany

Περίληψη

Η Περιτοναϊκή Κάθαρσης μέσω της παρατεταμένης έκθεση στα Υγρά Περιτοναϊκής Κάθαρσης (ΥΠΚ) προκαλεί υπερ-αγγειογένεση και επάγει την ίνωση της περιτοναϊκής μεμβράνης, οδηγώντας τελικά σε απώλεια υπερδιήθησης. Ως εκ τούτου, υπάρχει έντονο επιστημονικό ενδιαφέρον σχετικά με την ανάπτυξη στρατηγικών που θα επιβραδύνουν την έκπτωση της περιτοναϊκής μεμβράνης τόσο σε μορφολογικό όσο και λειτουργικό επίπεδο.

Πρόσφατα δεδομένα υποστηρίζουν ότι τα μεσοθηλιακά κύτταρα που εκτίθενται σε ΥΠΚ υψηλής περιεκτικότητας σε προϊόντα αποικοδόμησης της γλυκόζης (ΠΑΓ) υπόκεινται μεταβολικό επαναπρογραμματισμό προς έναν πιο γλυκολυτικό φαινότυπο που σχετίζεται με τη μεσοθηλιακή-προς-μεσεγχυματική μετάβαση (ΜΜΜ) των κυττάρων. Ωστόσο, προσθήκη 2-δεοξυ-γλυκόζης (2DG) ανέστειλε την παραπάνω διαδικασία. Στην παρούσα μελέτη διερευνήθηκε εάν αυτή η δράση της 2DG εντοπίζεται και σε μεσοθηλιακά κύτταρα που εκτίθενται σε ΥΠΚ χαμηλής περιεκτικότητας σε ΠΑΓ, αλλά και εάν διατηρείται και στα ενδοθηλιακά κύτταρα. Επιπλέον, εξετάστηκε εάν η προσθήκη της 2DG σε διαφορετικούς τύπους ΥΠΚ επιδρά στη διαπερατότητα του μεσοθηλιακού και ενδοθηλιακού φραγμούς της περιτοναϊκής μεμβράνης.

Η αντιϊνωτική δράση της 2DG επιβεβαιώθηκε μέσω της δοκιμασίας συστολής γέλης κολλαγόνου με ενσωματωμένα μεσοθηλιακά (MeT-5A) και ενδοθηλιακά (EA.hy926) κύτταρα, τα οποία καλλιεργήθηκαν στα διαλύματα Dianeal® 2,5% γλυκόζη, BicaVera® 2,3% γλυκόζη και Balance® 2,3% γλυκόζη με ή χωρίς την προσθήκη 0,2mM 2DG. Ανάλογα ευρήματα προέκυψαν και από τα επίπεδα έκφρασης των γονιδίων *αSMA* και *CDH2* για τα οποία εφαρμόστηκε ποσοτική PCR σε πραγματικό χρόνο. Πιο συγκεκριμένα, η συσταλτότητα τόσο των MeT-5A όσο και των EA.hy926 κυττάρων υπό την επίδραση του διαλύματος Dianeal®/2DG μειώθηκε, συνοδευόμενη από αλλαγές στην έκφραση των γονιδίων *αSMA* και *CDH2*. Στην περίπτωση βέβαια των EA.hy926 κυττάρων, η έκφραση του γονιδίου *αSMA* μειώθηκε επίσης υπό την επίδραση του διαλύματος Balance®/2DG.

Αναφορικά με τη δράση της 2DG στη διαπερατότητα κυτταρικών μονοστιβάδων, εκτιμήθηκε μέσω καταγραφής της διαμεμβρανικής αντίστασης (R_{TM}), της παρακυτταρικής μεταφοράς φθορίζουσας δεξτράνης (10, 70kDa) καθώς και των επιπέδων γονιδιακής έκφρασης των *CLDN1*, *CLDN2*, *CLDN3*, *CLDN4*, *CLDN5*, *ZO1*,

SGLT1 και *SGLT2*. Συνολικά, η προσθήκη 2DG μείωσε τις διαταραχές που επάγει στη λειτουργία του μεσοθηλιακού ή/και ενδοθηλιακού φραγμού η χρήση ΥΠΚ, όπως έδειξαν τα επίπεδα R_{TM}, το ποσοστό μεταφοράς δεξτράνης και η έκφραση των γονιδίων *CLDN-1* έως *-5*, *ZO1* και *SGLT2*, με τη δράση της να είναι πιο εμφανής στις μονοστιβάδες MeT-5A κυττάρων. Συνεπώς, ο εμπλουτισμός όλων των τύπων ΥΠΚ με 2DG όχι μόνο μειώνει τη ΜΜΜ αλλά επίσης βελτιώνει τα λειτουργικά χαρακτηριστικά της διαπερατότητας του μεσοθηλιακού και ενδοθηλιακού φραγμού της περιτοναϊκής μεμβράνης.

Abstract

The Peritoneal Dialysis modality with the prolonged exposure to Peritoneal Dialysis Fluids (PDF) induce hyper-vascularization as well as peritoneal membrane thickening and fibrosis, ultimately leading to ultrafiltration failure. Therefore, there is intense scientific interest regarding the development of strategies that would delay the deterioration of the peritoneal membrane at a morphological and functional level.

Recent evidence reported that mesothelial cells exposed to PDF with a high content in glucose degradation products (GDP) undergo metabolic reprogramming towards a more glycolytic phenotype associated with mesothelial-to-mesenchymal transition (MMT). However, addition of 2-deoxyglucose (2DG) inhibited the above process of MMT. In the present study, we investigated whether the 2DG effect is valid in mesothelial cells treated with low GDP PDF, and whether the same stands for endothelial cells as well. Furthermore, the effect of 2DG PDF supplementation was tested with regards to the mesothelial and endothelial barrier function.

The antifibrotic effect of 2DG administration was confirmed through the collagen gel contraction assay with embedded mesothelial (MeT-5A) and endothelial (EA.hy926) cells cultured in Dianeal® 2.5% glucose (CPDF), BicaVera® 2.3% glucose (BPDF) and Balance® 2.3% glucose (LPDF) with or without the addition of 0.2 mM 2DG. Similar findings were obtained by performing qPCR for the *αSMA* and *CDH2* genes. More specifically, the contractility of both MeT-5A and EA926 cells incubated with CPDF/2DG solution was reduced, accompanied by fold changes in *αSMA* and *CDH2* gene expression. In the case of EA.hy926 cells, *αSMA* gene expression was also reduced under LPDF/2DG incubation.

Regarding the effect of 2DG on permeability characteristics of the mesothelial and/or endothelial cell monolayers, it was assessed by monitoring the transmembrane resistance (R_{TM}), FITC-labelled dextran (10, 70kDa) diffusion as well as gene expression levels of *CLDN1*, *CLDN2*, *CLDN-3*, *CLDN4*, *CLDN5*, *ZO1*, *SGLT1* and *SGLT2*. Overall, the addition of 2DG attenuated the PDF-induced perturbations in mesothelial and/or endothelial barrier function, as shown by R_{TM} values, dextran transport rate, and gene expression levels of *CLDN-1* to *-5*, *ZO1*, and *SGLT2*, while its effect was more evident in MeT-5A cell monolayers. Therefore, supplementation of all types of PDF with 2DG

not only mitigates MMT but also improves the functional permeability characteristics of the mesothelial and endothelial barrier of peritoneal membrane.

List of abbreviations

AGE: Advanced glycation end-products

AJ: Adherens junctions

AlaGln: Alanyl-glutamine

APC: Antigen-presenting cells

APD: Automated Peritoneal Dialysis

AQP: Aquaporin

αSMA: Alpha smooth muscle actin

CAPD: Continuous Ambulatory Peritoneal Dialysis

CKD: Chronic Kidney Disease

COL1A1: Collagen type 1 alpha 1 chain

EMT: Epithelial-to-mesenchymal transition

ENaC: Epithelial sodium channel

EndoMT: Endothelial-to-mesenchymal transition

ESKD: End-stage Kidney Disease

FBS: Fetal bovine serum

FN: Fibronectin

GDP: Glucose degradation products

GJ: Gap junctions

GSK-3β: Glycogen synthase kinase-3β

HPMC: Human peritoneal mesothelial cells

HSR: Heat sock response

HUVEC: Human umbilical vein endothelial cells

IFN: Interferon

IL: Interleukin

JAM: Junctional adhesion molecule

KRB: Krebs-Ringer Bicarbonate solution

LiCl: Lithium chloride

MMT: Mesothelial-to-mesenchymal transition

MW: Molecular weight

OD: Optical density

PBS: Phosphate buffered saline

PCR: Polymerase chain reaction

PD: Peritoneal Dialysis

PDF: Peritoneal Dialysis fluids

PM: Peritoneal membrane

RAGE: Receptor for advanced glycation end-products

R_{TM}: Transmembrane resistance

SEM: Standard error of mean

SG: Steviol glycosides

SGLT: Sodium-glucose cotransporter

TER: Transmembrane electrical resistance

TGF: Transforming growth factor

TMD: Transmembrane domain

TNF: Tumor necrosis factor

TJ: Tight junctions

UDG: uracil-DNA glycosylase

UF: Ultrafiltration

UFF: Ultrafiltration failure

VEGF: Vascular endothelial growth factor

ZO: Zonula occludens

2DG: 2-deoxyglucose

3D: 3-Dimensional

Table of Contents

Introduction

The peritoneum is a delicate membrane structure divided into the parietal and visceral layer that line the entire peritoneal cavity and cover the abdominal organs. It performs numerous functions that were gradually identified from the 19th century, beginning with the maintenance of local homeostasis and the protection from frictional damage among abdominal organs [1]. The use of peritoneum as a semipermeable dialyzing membrane in patients with End Stage Kidney Disease (ESKD) requiring renal replacement therapy was the result of its property to clear excess water, solutes, and metabolic waste products during Peritoneal Dialysis (PD) which was established in the 1960s [2].

PD is a home-based renal replacement therapy alternative to hemodialysis (HD). The driving forces defining the exchange of water, solutes and toxins are diffusion and convection across the peritoneal membrane. PD fluids (PDF)-induced osmosis occurs through the highly vascularized peritoneal membrane. Despite its advantages compared to HD such as the quality of life or its cost-effectiveness, PD is applied in a mere 13% of patients suffering from ESKD in Europe and 10% in USA [3,4]. This variance is partially explained by shortcomings of the chronic exposure to PDF. The most pronounced PD-induced alterations are the progressive loss of the mesothelial cell layer lining the peritoneal cavity, also associated with epithelial-to-mesenchymal transition (EMT), the submesothelial thickening and peritoneal vasculopathy as well as the fibrosis.

Standard PDF contain supraphysiological concentrations of glucose at around 10- to 50-fold higher than serum, serving as the osmotic agent that causes removal of water, uremic toxins and electrolytes by ultrafiltration (UF)-associated solvent drag called convection. A lactate or bicarbonate buffer compound is also presented for achievement of metabolic acidosis correction, while the pH ranges from 5.5 to 7.4. Heat sterilization and prolonged storage of PDF promotes glucose to degrade into glucose degradation products (GDP; e.g., methylglyoxal, 3,4-dideoxyglucosone-3-ene) correlated with peritoneal deposition of advanced glycation end-products (AGE) and accelerating peritoneal transport status [5,6]. Altogether, PDF unphysiological composition causes long-term peritoneal membrane deterioration, subsequently leading to ultrafiltration failure (UFF) and ESKD patients must switch to either HD or kidney transplantation.

To this end, many strategies to preserve the peritoneal function and improve the clinical outcome of the modality have been employed, including use of low-GDP PDF as evidence suggested the reduction of detrimental effects on the peritoneal membrane structure, the improve preservation of the barrier function and reduction in the incidence of encapsulating peritoneal sclerosis [7–9]. Several alternative osmotic agents are under investigation, such as xylitol or L-carnitine, albeit confirmation of clinically relevant results is still lacking while the biocompatibility of this solutions remains uncertain [10–12]. Eventually, addition of protective compounds has been taken into consideration to mitigate the negative effects of glucose-based PDF. Alanyl-glutamine or lithium chloride supplementation to either high- or low-GDP PDF reveals promising end-points regarding mesothelium integrity, solute clearance, EMT and angiogenesis but more extended studies are required prior to its establishment [13–15].

Still five decades after PD technique establishment, limited progress regarding biocompatibility of PDF content has been achieved, and glucose-based solutions still predominate [16]. Only recently, the inhibitor of glycolysis, 2-deoxyglucose (2DG), was successfully used to prevent mesothelial-to-mesenchymal transition (MMT) induced by both *in-vitro* and *in vivo* exposure of mesothelial cells in a high-GDP PDF [17]. These findings warrant a rigorous characterization of 2DG effects on the mesothelial and endothelial barrier function in the context of composition of PDF as it could prove a potential candidate for utilization in PD treatment [18].

GENERAL PART

1. Peritoneal anatomy & embryogenesis

Among the human serous membranes, peritoneum is the largest one, with the reported surface area in adults (average value: 1.8 m^2) to be similar to this of human skin. Two layers constitute the peritoneum; the outer one is the parietal peritoneum and lines the inner surface of the abdominal wall, diaphragm and pelvis, and the inner layer is called visceral peritoneum and covers the abdominal organs [19]. Both the parietal and visceral peritoneum are coated with mesothelial cells; however, they are innervated by different nerves. The former receives somatic nerves leading to pressure, temperature and pain sensitivity, and the latter utilizes the same nerve pathways as the visceral organs which render it of low sensitivity to stretch and chemical irritation [20].

The confined area between the two layers is known as the peritoneal cavity and is filled with a small volume of 50-100 ml of peritoneal fluid, relentlessly secreted by mesothelium as a plasma transudate [19,21]. However, in pathological conditions, the balance between peritoneal fluid production and drainage is often disturbed, causing excess accumulation of peritoneal fluid referred to as ascites. Peritoneal fluid contains water, electrolytes, solutes, proteins and various types of immune cells, such as lymphocytes, macrophages, natural killer cells etc. [22]. It primarily facilitates the two peritoneal layers to slide against each other reducing the friction, but it also permits exchange of nutrients between the bloodstream and the peritoneal cavity, pathogen removal and reparative processes [19,23].

Embryonic development of the peritoneum initiates during the gastrulation process, alongside the primitive gut. At this stage, a three-layer flat disc is formed by the innermost endoderm, the outermost ectoderm and the in-between mesoderm, and separates the amniotic cavity and yolk sac [21,24]. Few days later, the mesoderm differentiates into the lateral plate mesoderm, the intermediate and the paraxial mesoderm. The lateral plate mesoderm continues out of the flat disc covering the amniotic cavity (parietal plate) and the yolk sac (visceral plate), while the paraxial mesoderm surrounds the neural tube. Within the next weeks, the initially flat disc curves; the parietal plate together with the ectoderm form the embryonic body wall, including the future parietal peritoneum, and the visceral plate with the endoderm form the embryonic gut wall which later on comprise the visceral peritoneum [21,25].

The above closing process of the primitive gut brings together (ventrally and dorsally to the gut) two opposite layers of peritoneum, known as primitive mesenteries, demonstrating their peritoneal derivation. The primitive gut divides into foregut, midgut and hindgut, and their differentiation occurs simultaneous at each level. Consequently, as the gut differentiates, the mesenteries and the covering peritoneum also develop [26]. At the level of the foregut, the dorsal and ventral mesenteries construct the splenic and hepatic bud, respectively. On the one hand, the dorsal mesentery connected directly to the spleen becomes the splenorenal ligament, and the remnant between the spleen and the stomach is the gastrosplenic ligament. On the other, the ventral mesentery between the forming liver and cavity wall turns into the falciform ligament, while the one between the liver and the stomach is the lesser omentum that contains the biliary tract, hepatic artery, and portal vein. Therefore, both ligaments and lesser omentum can also be considered peritoneal derived structures (**Figure 1**) [26–28].

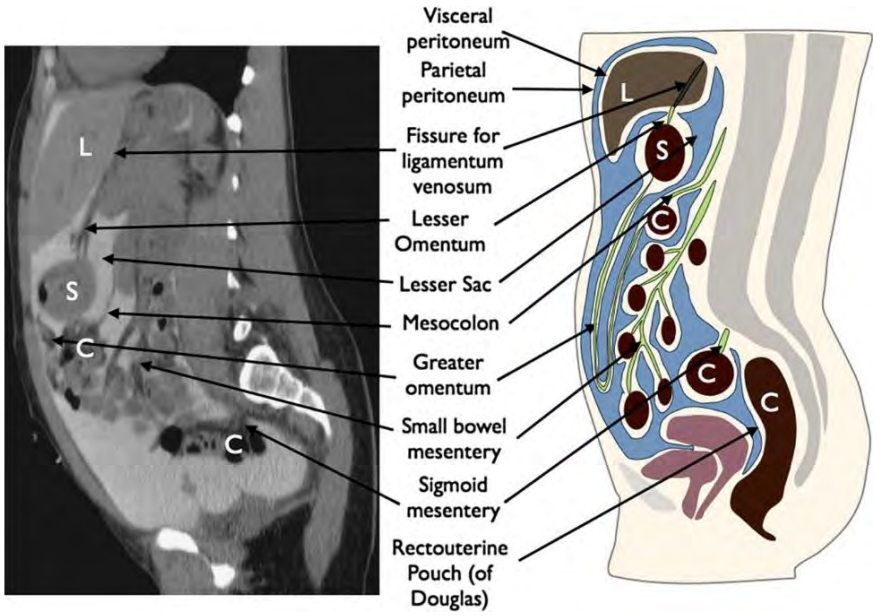

Figure 1: *Sagittal computed tomography image correlated with a schematic diagram demonstrating the peritoneal cavity. C, colon; S, stomach; L, liver [Source: Patel RR, Planche K. Applied peritoneal anatomy. Clin Radiol. 2013;68(5):509-20].*

By the fifth week of gestation, the thickening of parietal peritoneum along with the intermediate mesoderm give rise to the bilateral gonadal ridges and at the six weeks, indifferent sex cords or gonads have been developed through gonadal ridge proliferation

and epithelial cell migration within the underlying mesenchyme. The surface epithelium of the future ovaries or testes will arise from the parietal mesothelium, whereas the subcoelomic intermediate mesoderm constructs the stroma. In males, the parietal layer of the gonads undergoes continuous folding with the developing organs beneath, resulting in the formation a perfectly unified peritoneum. In contrast, in females, the peritoneum forms an open-sac system where the fallopian tubes and ovaries are connected to the peritoneal cavity [21,25].

2. Peritoneal histology

The peritoneum consists of a single layer of predominantly elongated, flattened, squamous-like mesothelial cells, which sits on a basal lamina on top of the submesothelial stroma, a thicker layer of loose connective tissue of varying density (**Figure 2**). This submesothelial domain is mainly composed of fibroblasts, adipocytes, collagen fibrils, blood and lymphatic vessels, and nerves. Therefore, the connective tissue serves not only as a pillar but also as a diffusion barrier allowing the passage of water, electrolytes, oxygen and other nutrients between the intravascular compartment and the peritoneal cavity [24,29].

The most superficial structure, mesothelium, is made up of cells with an approximate diameter of 25 μm, and the presence of numerous microvilli (their density varies depending on peritoneal location) and occasional cilia at their apical surface [30]. Microvilli give more than 20-fold rise to the peritoneal surface and ensure integrity of mesothelium by capturing proteins and serous exudates present in the peritoneal fluid. The functional properties of cilia are reflected in the regulation of surfactant secretion. Both structures adapt to microenvironmental changes, and their localization can be affected under physiological and pathophysiological conditions. In fact, a decrease in their number, as often happens in patients undergoing PD, causes a decrease in the functionality of the peritoneum and indicates cell apoptosis [31,32]. A highly hydrophilic protective barrier, the ‘glycocalyx’, consisting of proteoglycans and glycosaminoglycans, and trapped fluid with various substances is secreted on top of the microvilli. This creates a stagnant fluid layer over the peritoneum protecting its serosal surface from frictional damage [33,34].

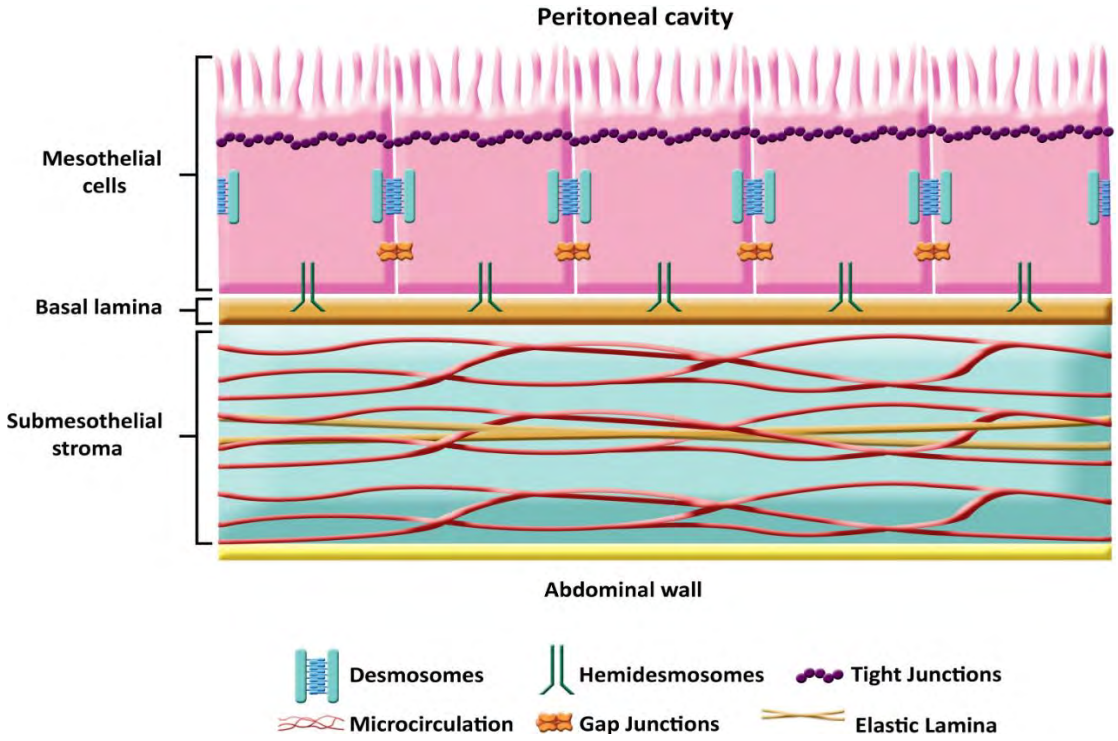

Figure 2: *Schematic representation of the human peritoneum (Source: Kastelein, A.W., et al. Embryology, anatomy, physiology and pathophysiology of the peritoneum and the peritoneal vasculature. Semin. Cell Dev. Biol. 2019;92: 27-36).*

The phenotypic expression of mesothelial cells varies depending on their location or activation state, despite their morphologic resemblance with epithelial cells [35]. They possess apical/basal polarity, junctional complexes and other epithelial features, though they derive from the mesoderm expressing also mesenchymal characteristics including vimentin and desmin [36,37]. This duality could be further exemplified by EMT, a well characterized biologic process following injury or inflammation, enabling a polarized epithelial cell to undergo a series of overlapping events that will differentiate the cell phenotype [38]. A more recent term for this ability of mesothelial cells to be morphologically and functionally transformed upon stimulation is the MMT [31].

Adjacent mesothelial cells are linked together with intercellular junctional complexes such as tight junctions (TJ), adherens junctions (AJ), and desmosomes, while they also exhibit gap junctions (GJ). Lymphatic stomatal openings of a diameter of 3-12 μm are traced in areas containing also cuboidal mesothelial cells, like on the peritoneal side of the diaphragm or over the omental milky spots, enabling uptake and movement of cells from the peritoneal cavity into the lymphatic system [21,39]. TJ are internally connected

to the cytoskeleton of mesothelial cells, located at the most apical region of cell-cell contacts. They anatomically appeared as a series of appositions in such a close proximity to form a continuous seal that are also referred as “kissing points” between the exocytoplasmic surfaces of the lateral membranes. TJ are recognized to have a dual role of maintaining cell polarity (fence function) and determining the paracellular permeability (gate function). Acting as a fence within the cell membrane, TJ restrict intermixing of apical and basolateral domains and mechanically restrain diffusion of proteins and lipids into lipid bilayer. At the same time, they form a semi-permeable barrier preventing unregulated leakage of water-soluble molecules across intercellular space [40].

The molecular composition of TJ has been extensively investigated and the initial theory that the strands are composed by a purely lipid organization inverted cylindrical micelles has collapsed throughout the years [41]. Instead, biochemical characterization has revealed the participation of a protein complex composed of 2 major transmembrane protein groups: membrane-spanning proteins that mediate cell-cell adhesion, and cytoplasmic proteins forming a ‘plaque’ for attachment of the former to the cytoskeleton. The first group includes the protein family of claudins, occludins, junctional adhesion molecules (JAM), tricellulin and their extracellular domains while the latter group is further divided into 3 main categories: scaffolding proteins comprised of the zonula occludens (ZO) protein family and cingulin that link TJ to the actin cytoskeleton, signalling proteins that control junction assembly and function, and transcriptional and post-transcriptional regulators capable of dissociating from the anchored TJ and penetrate the cell nucleus to modulate gene expression [41,42].

The main components of AJ are the E-cadherin protein as well as members of the catenin family, such as p120-catenin, β-catenin and α-catenin; however, several transmembrane glycoproteins of the classical cadherin superfamily are also included. Multiple key functions of AJ including cell-cell adhesion initiation and stabilization, actin cytoskeleton regulation, intracellular signalling and transcriptional regulation are controlled by interactions among the above protein members. For example, E-cadherin is required not only for signalling pathways but also for binding and localization of the cytoplasmic catenins which in turn, link the cadherin complex with the actin cytoskeleton [43].

Furthermore, GJ are responsible for chemical and electrical intercellular communication, thus critical in coordination of cell functions in multicellular organisms [44]. The mesothelial cells synchronously respond to a ligand or differentiate together during developmental stages through GJ-mediated communication compartments. GJ are composed of membrane proteins that form aqueous channels allowing exchange of ions and low molecular weight hydrophilic compounds, including second messengers (e.g. Ca^{2+}), inositol triphosphate (IP_3), and cyclic nucleotides and oligonucleotides [45]. Two protein families, chordate connexins and pre-chordate innexins, are known to form GJ in vertebrates and invertebrates, respectively. However, a more recently discovered category in vertebrates is this of pannexins, related to invertebrate innexins based on gene and expressed transcripts similarity. Although both connexin and innexin are tetraspan transmembrane proteins, no amino acid sequence similarity has been found between them. Connexins are categorized into five subgroups (α, β, γ, δ, ε) based on their degree of sequence identity and length of the cytoplasmic loop. The most commonly used abbreviation for each protein is the 'Cx' followed by the number of its predicted molecular weight (MW) in kDa (e.g., Cx43 for connexin of MW equal to 43 kDa), while the corresponding genes are identified with 'GJ' and sequenced based on the order of their discovery (e.g., GJα1 refers to the first connexin of α group) [46].

Desmosomes of 0.1 to 0.5 μm are attached to intermediate filaments of two neighbour mesothelial cells to mechanistically bind them with each other [47]. They appear in the electron microscope as disc-shaped organelles and constitute multiprotein complexes notably present in cells originating from ectodermal lineages. These junctions play a crucial role in preserving tissue cohesion, particularly in organs subjected to significant mechanical stress, such as the heart but also in peritoneum surrounding all the abdominal organs [48]. Cell-cell adhesion is considered to primarily occur through heterophilic interactions involving transmembrane glycoproteins, members of cadherin family, especially in metazoan epithelia. Desmosomes still use cadherin receptors for adhesion, but they connect intermediate filaments rather than actin, facilitated by members of plakoglobin, plakophilin and desmoplakin families [49]. Another tetraspan membrane component, Perp, has been also identified originally as a target associated with apoptosis and regulated by the p53 tumor suppressor, and later correlated with severe skin fragility disorder but its precise function in desmosomes remains poorly studied [48,50].

Hemidesmosome structural component is also a hallmark feature of junctional mesothelium, named by morphological resemblance to desmosomes under the electron microscope, but functionally distinguishable. When these junctions were first identified were considered to be associated with intermediate filaments and involved in cell-cell adhesion while hemidesmosomes are protein complexes responsible for binding keratin attached to the inner plaque of stratified mesothelial cells to the collagen fibrils and other extracellular matrix (ECM) components of the basal lamina [51]. Despite linking to the intermediate filament system, hemidesmosomes contain a specialized set of proteins consisted of the cytoplasmic plaque proteins HD1/plektin and BP230, and the transmembrane proteins $\alpha_6\beta_4$ integrin and BP180, instead of desmosomal proteins such as desmoplakin [52,53].

3. Peritoneal physiology

Traditionally, the main function attributed to the peritoneum is the mechanical protection of abdominal organs also providing a slippery, non-adhesive interface for their free movement. However, over the last two decades, additional physiological properties of the peritoneum have been discovered including fluid transport, initiation and resolution of inflammation, tissue repair, antigen presentation, and tumor dissemination or development of pathological conditions such as endometriosis, malignant mesothelioma and peritoneal carcinomatosis [21].

3.1 Peritoneal cavity homeostasis

A small amount of peritoneal fluid fills the peritoneal cavity between the parietal and visceral peritoneum. It is essential for lubricating the surfaces of the two layers and preventing them from adhere to the internal organs [19]. Typically, 50-100 ml are found to healthy adults with a slight increase in females during ovulation phase of the menstrual cycle, while a 5-ml turnover occurs every 24 hours [54]. In some clinically pathological conditions, a rise in peritoneal fluid volume is detected, which is often not apparent until accumulation of more than 500 ml [55]. Either an elevation in fluid formation or a decrease in fluid removal can be responsible for the accumulation (ascites). The former

is caused by the over-increase of the hydrostatic pressure gradient, or the decline of the colloid osmotic pressure, or increased vascular permeability [56]. Normally, the peritoneal fluid is characterised by 1.01 to 1.02 specific gravity, whereas out of the border values are used for ascites classification as transudative or exudative, respectively. The pressure and flow characteristics of gas and fluid within the peritoneal cavity are relevant to localization of abdominal accumulation. For example, in ascites, the specific gravity of peritoneal fluid provokes upward floating of the gas-filled bowel loops, but it turns into downward when gas is introduced under pressure at laparoscopy [57].

3.2 Fluid transport

The exchange of water and solutes between peritoneal capillary plasma and the fluid into the peritoneal cavity happens as it traverses through endothelium lining the peritoneal blood vessels, interstitium and eventually, mesothelium. Hence, the primary barrier should be penetrated is the endothelial cells, which appears to be the rate-limiting impediment, constraining the transport to less than 0.01% of the total surface area. It provides a remarkable pathway for removal of waste products by the means of simple and facilitated diffusion as well as secondary active transport like the glucose transporter 1 (GLUT1) or the lactate/H^+ and lactate/Na^+ cotransporters. Computer stimulations propose that the endothelium could be effectively described by mathematical models such as the 'Three-pore Model' and the 'Distributive Model' [58,59].

In the context of the Three-pore model, the so-called "large pores" of radius 200-300 Å mediate the pathway for macromolecular leakage (e.g. albumin) from the plasma into the peritoneal cavity driven by hydrostatic pressure. The number of large pores is extremely limited (<0.5% of the total pore area), whereas the vast majority of the total exchange area (99.5%) and the total peritoneal UF coefficient (L_pS; approximately 90%) is consisted of inter-endothelial clefts denoted as "small pores" of 40-55 Å. They have been associated with the principal route for diffusive transport of small water-soluble molecules like urea, creatinine and glucose. Despite, their characterization as protein-restrictive pores, albumin can to some extent diffuse across them [60,61]. The last pathway of the Three-pore model holds for ~2% of L_pS and is identified by the

"ultrasmall pores" (<3 Å) that solely account for water transport through osmotic gradient. Numerous studies have shown that the water-specific membrane channel, aquaporin (AQP)-1, is corresponded to the ultrasmall pores of endothelial cells [62,63]. The transport mechanisms across all the three types of pores are operated by Starling forces that ensure an equilibration between the transcapillary hydrostatic pressure and the counteracting effective colloid osmotic pressure [64].

The interstitium comprising collagen bundles within a mucopolysaccharide hydrogel and an intricate network of capillaries is potentially the second barrier [65]. Proteoglycan fibrils intertwine with each other and form a fine meshwork that fills the space between collagen fibers. The interstitial fluid in these areas allows the free movement of electrolytes and solutes, and consequently, a non-impaired resistance in fluid transport is considered in several studies [66,67]. However, other scientists refer that the interstitium could alter small solute transport by approximately 20-30% of the overall diffusion [68]. The anatomically last barrier to fluid and solute transport is the mesothelium, whose role is important in terms of the structural and functional preservation of the peritoneum and thus, it will be extensively studied below [69].

One the other hand, the mathematical distributed model has been explicitly developed to investigate the transport of fluid and solutes across microvessels and interstitial tissue, while it also predicts concentration gradients within multiple spots of the peritoneal cavity [59].

3.3 Initiation and resolution of inflammation

All three serosal membranes are prone to bacterial invasion; therefore, the inflammatory response of the peritoneum is critical in protecting against PD-related cases of peritonitis whose pathogenesis may be contamination of the PD catheter or its connections by coagulase-negative staphylococcal species (e.g. *Staphylococcus epidermidis* or *St. aureus*), or exit-site and tunnel infections [70]. Peritoneal injury can be also derived from surgery, inflammation, or ischemia. Peritoneal stromal fibroblasts and mesothelial cells play a crucial role in immune defense. They respond by enhancing vascular perfusion, accumulating macrophages and other immune cells, and secreting a variety of pro-, anti- and immunomodulatory mediators [71]. Entry of a foreign material causes leukocytes

recruitment, while the initiation of cytokine production [interleukin (IL)-1β, interferon (IFN)-γ, tumor necrosis factor (TNF)-α] by monocytes subsequently activate the mesothelial cells to release prostaglandins, chemokines, nitric oxide, reactive nitrogen and oxygen species, cytokines, growth factors and ECM components [72]. Serosal inflammation is likely initiated on the apical surface of mesothelial cells, where the glycocalyx interacts with recruited immune cells, driven by a chemotactic gradient [73].

3.4 Tissue repair

Numerous studies have shown that the mesothelial cells possess the ability to release a diverse range of growth factors and ECM components associated with inflammation and tissue repair. Normally, there is a delicate equilibrium between formation and breakdown of peritoneal surface adhesions. In cases of injured or inflamed peritoneum, inflammatory cells accumulate and the cell surface tissue factor, responsible for coagulation is released by mesothelial cells, but the activated fibrinolytic system breaks down this fibrin precipitation [74]. However, unregulated adhesion formation occurs when there is an imbalance of the aforementioned mechanisms, leading to the attraction of ECM molecules that consolidate fibrin depositions with fibroblasts, macrophages and multinucleated cells, adhering to both peritoneal surfaces [75].

Apart from secreting proinflammatory mediators, and participating in coagulation and fibrinolysis, the plasticity of mesothelial cells allows for their transdifferentiation into a mesenchymal phenotype through a process known as MMT, akin to EMT. This procedure is the key event in tissue repair, and stabilization of peritoneal microenvironment as well as in fibrosis, and tumor growth and invasion. The mesothelial cell obtained myofibroblastic phenotype is characterized by an invasive, migratory behavior accompanied by progressive loss of intercellular junctions and cell polarity as well as cytoskeleton reorganization [76]. They also demonstrate decline or complete lack of E-cadherin expression, and diminished cytokeratin but elevated expression of vimentin and AGE receptors [31]. To initiate MMT, transforming growth factor (TGF)-β1, IL-1β and other cytokines are required [77]. In some cases, the contractile abilities of myofibroblastic cells, in addition to producing stromal components or expressing inflammatory mediators, may also induce fibrosis even if their role in peritoneum is not

fully clarified yet. However, in many studies, contractility is estimated by the expression of α smooth muscle actin (αSMA) as a marker for transformed mesothelial cells [78].

3.5 Antigen presentation

The contribution of mesothelial cells in the immune defence is mainly regulated by their antigen-presenting function. T-helper cells identify foreign materials by interacting with molecules of the major histocompatibility complex II, which are demonstrated by antigen-presenting cells (APCs) such as dendritic cells, macrophages, monocytes or B cells. This ability of APCs to display fragments of antigens on their surface is also found in mesothelial cells as evidenced by previous studies conducted on human peritoneal mesothelial cells (HPMC) that provided data about tetanus toxoid, purified protein derivates or *Candida albicans* bodies [79,80]. Additionally, it has been demonstrated that the IFN-γ activation of mesothelial cells induces IL-15 secretion which stimulates T-cell growth and cooperates with IL-2. Elevated levels of these molecules have been found in the effluent of patients suffering from peritonitis [80,81].

3.6 Tumor growth and dissemination

Several studies have provided evidence that sites distal to an injury is a preferred localization for tumor growth while many epithelial malignancies (e.g., ovarian cancer) spread to the peritoneum. The precise mechanisms through which metastatic cancer cells adhere to the parietal or visceral peritoneal surfaces is unknown; however, integrins and cell surface glycoprotein receptors, which are expressed in abundance by both cancer and healthy mesothelial cells, may be the primary adhesion molecule whose ligands account for many ECM components. Moreover, fibroblasts associated with cancer in the tumor stroma influence its growth and invasion behaviour, and it’s of outstanding interest that these fibroblasts in peritoneal metastasis originate from mesothelial cells through MMT, which also enhances integrin-dependent adhesion [82,83].

4. Peritoneal membrane permeability via paracellular and transcellular pathways

An extensive mesothelial cell monolayer residing on a basal lamina lines the peritoneal cavity and internal organs while an endothelial cell monolayer lines the subsequent blood vessels, as previously reported. Both the mesothelium and endothelium are size- or charge-selectively permeable forming a barrier that prevents uncontrolled diffusion and solute convection and governs fluid homeostasis within the peritoneal cavity, while the negative charge of PM constitutes an additional factor of selective permeability [24,84].

Two routes regulate the fluid and solute exchange across the mesothelial and endothelial barriers, one transcellular and one paracellular transport pathway. The former is referring to the passage through a cell either passively or actively, as a result of the applied hydrostatic or osmotic pressure or even by diffusion, while in some cases macromolecules such as albumin are transferred by means of the vesicular-mediated endocytosis, transcytosis across the cell and finally, exocytosis. Therefore, the transcellular pathway requires the presence of ion channels and pumps in the apical and basolateral cell membranes, and/or energy [85]. On the other hand, solute transport via the paracellular pathway is exclusively determined by the electrochemical gradient across mesothelium or endothelium and thus, it is referring to the passive diffusion through the interstitial space of adjacent cells. Among the structures that connect adjacent cells, TJ primarily restrict the paracellular permeability in a selective manner, differentiating by charge and size of ions or hydrophilic non-ionic tracers [86]. Based on the contribution of each pathway to solute transport, monolayers are qualitatively characterized as ‘leaky’ or’ tight’ with leaky epithelia like peritoneum to exhibit low resistance concerning paracellular route, in contrast with tight epithelia where resistance is equivalent or even higher than this of transcellular route [87].

Although TJ comprise many protein components, claudins are the major constituent of the paracellular pathway. At least 27 members belong to the human claudin family with the Claudin-1 and -2 to have been identified back in 1998 [88,89]. Claudins are tetraspan proteins with a molecular weight ranging from 21 to 34 kDa that are found in all epithelial and endothelial cells [84,90]. Their structural pattern is described by hydropathy plots as following: N-terminal cytoplasmic domain, transmembrane domain

(TMD)-1, a long extracellular domain (ECL1) with ~50 amino acids, TMD-2, a short intracellular loop, TMD-3, a shorter ECL2 of ~25 amino acids, TMD-4 and, C-terminal cytoplasmatic domain capable of interacting with other intracellular proteins through the PDZ domain that recognize short amino acid motifs located at the C-termini of target proteins (**Figure 3**) [91]. The amino acid similarity among members of the claudin protein family does not exceed 30%, resulting in different properties and expression patterns. In general, their expression is highly specific to each tissue and regulated by MMT-related transcription factors, hormones and cytokines [92,93].

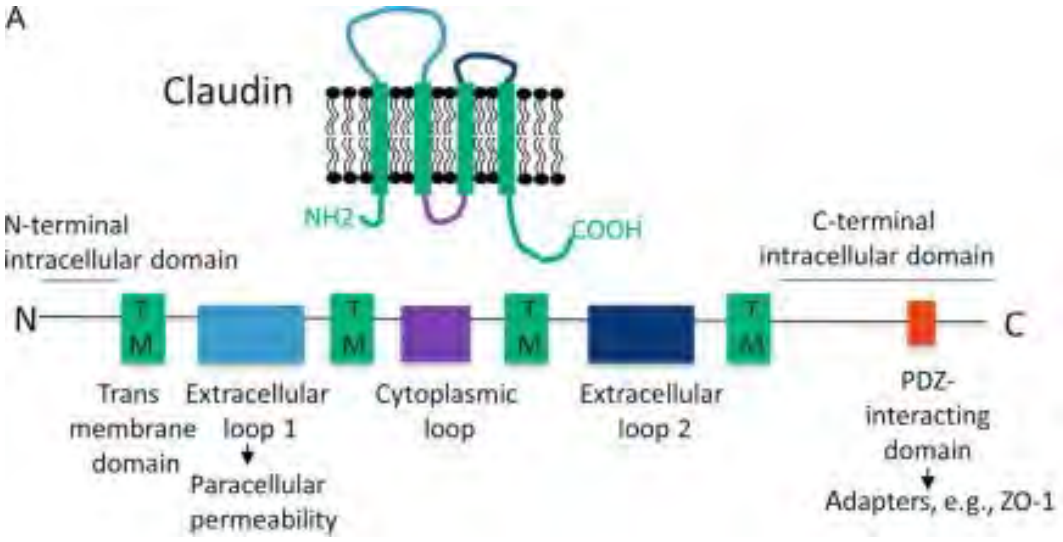

Figure 3*: Structure of claudin proteins (Source: Szaszi K. and Amoozadeh Y. New insights into functions, regulation, and pathological roles of tight junctions in kidney tubular epithelium. Int Rev Cell Mol Biol. 2014;308: 205-71).*

Evidence supporting the involvement of claudins in paracellular transport were based on microscopy (either conventional transmission or freeze-fracture electron microscopic images) and electrophysiology. Recording of resistance values and/or NaCl diffusion voltage in cultured epithelial cells led to the classification of claudins as pore-forming or barrier-forming proteins, while the permeability characteristics of some members depend on their stoichiometry with others [94,95]. In combination with a large array of silencing and overexpression studies, four groups according to claudin's specific properties have arisen as follows:

- pore-forming claudins: CLDN-2, -10a/b, -15, -17

- barrier-forming or sealing claudins: CLDN-1, -3, -5, -11, -14, -19
- claudins with inconsistent function: CLDN: -4, -7, -8, -16
- claudins with unknown function: CLDN-6, -9, -12, -13, -18, -20 to -27 [94,96].

Finally, when assessing ion transport physiologically, the pore-forming claudins are further subdivided into those selectively allowing cations and anions. Certain species also permit non-ionic solute permeation, albeit in a size-dependent manner, particularly for small molecules [97].

5. Peritoneal Dialysis

Chronic kidney disease (CKD) is reported to affect more than 10% of the general population worldwide, while it is about to ascend to the fifth leading cause of global mortality until 2040 [98]. Epidemiological data confirm a constantly growing prevalence of ESKD by 5-8% per year, as a consequence of the increase in population rates of obesity, hypertension, diabetes mellitus and aging [99,100].

The renal replacement therapies that are essential for ESKD patients' survival comprise HD, PD and of course kidney transplantation [101]. Although the latter should ideally be the optimal choice, the disproportion between available transplants and potential recipients as well as the risk of potential rejection of the kidney transplant along with other long-term risks (e.g., hernia, blood vessel and/or urine tube narrowing, heart problems) leaves the vast majority of ESKD patients faced with the other two chronic dialysis therapies [102]. In contrast to extracorporeal blood purification by means of HD that requires 3- to 4-hour sessions in specialized medical centers twice or thrice per week, the PD is a substantially cheaper home-based therapy and thus, more patient friendly providing autonomy and a better quality of life [103]. However, it accounts for the treatment of approximately 11% of patients undergoing dialysis worldwide, due to barriers associated with low-oncome limitations, infectious peritonitis episodes and PDF bio-incompatibility [16,104–106].

The PD modality relies on the PM serving as a dialyzing membrane, and on the subsequent peritoneal blood flow for the excess water and uremic toxins to be removed from the patient's body. This process of fluid efflux from the systemic circulation is achievable thanks to the osmotic gradient produced by the introduction of hyperosmotic

PDF in the peritoneal cavity [107]. To this end, a catheter is inserted to the peritoneum, traversing the abdominal wall and eventually, providing an avenue for the PD exchange procedure. The selection of PD catheter as well as the insertion technique may vary according to the available material resources per geographic region and local provider expertise in placement method, however, there are three catheter types of most common use and equal efficacy, while a profound analysis of insertion procedure after taking into consideration policy changes due to Covid-19 pandemic has been performed on behalf of the European Renal Association [108,109]. The standard Tenckhoff catheters with straight or coiled tips, two polyester cuffs and straight or preformed arc bend intercuff sections comprise the core of devices for attaining access to the peritoneum. A third type of extended two-piece catheter is also widely used, though. This PD catheter consists of a coiled-tip abdominal section with one cuff that attaches to a two-cuff extension part with a preformed arc bend between the cuffs, through a double-barded titanium connector. It is manufactured in such a way that allows remote placement of the exit site on the upper chest, abdominal, or back regions [108].

PD is carried out in the 3 main steps of fill, dwell and drain which constitute the exchange procedure (**Figure 4**). Initially, the patient's peritoneal cavity is filled with the PDF through the PD catheter. Once the PDF has been emptied into the abdomen, the dwell time is initiated. This is the crucial period when dialysis occurs, and the waste products and excess fluid pass from the systemic circulation to the PDF as it remains in the peritoneal cavity. Eventually, the used, saturated PDF is drained from the body into a drainage bag [110]. Although the above steps are the same between the two kinds of PD [Continuous Ambulatory PD (CAPD) & Automated PD (APD)], the exchange schedule differs. In the machine-free CAPD form, a PDF of about 2 liters volume (the exact fill volume is always according to individual patient's needs) is infused in the peritoneal cavity and manually replaced 4 times a day. Usually, the three day dwells last 4 to 6 hours while the nocturnal one lasts 8 to 10 hours [2]. On the other hand, the APD variant is performed by means of an automated cycler, which automatically fills and drains the infused PDF overnight while the patient sleeps. Consequently, it constitutes the optimal choice for patients with an active life absolving them of a manual daytime exchange [111]. Beside the fact that it was developed as an effort to achieve higher clearance of solutes and thus prolong the UF efficacy by using higher dialysate volumes, APD brings a number of advantages over CAPD including reduction of peritonitis episodes and of

complications due to the elevated intraperitoneal pressure (e.g., abdominal hernias, fluid leakage) [112,113].

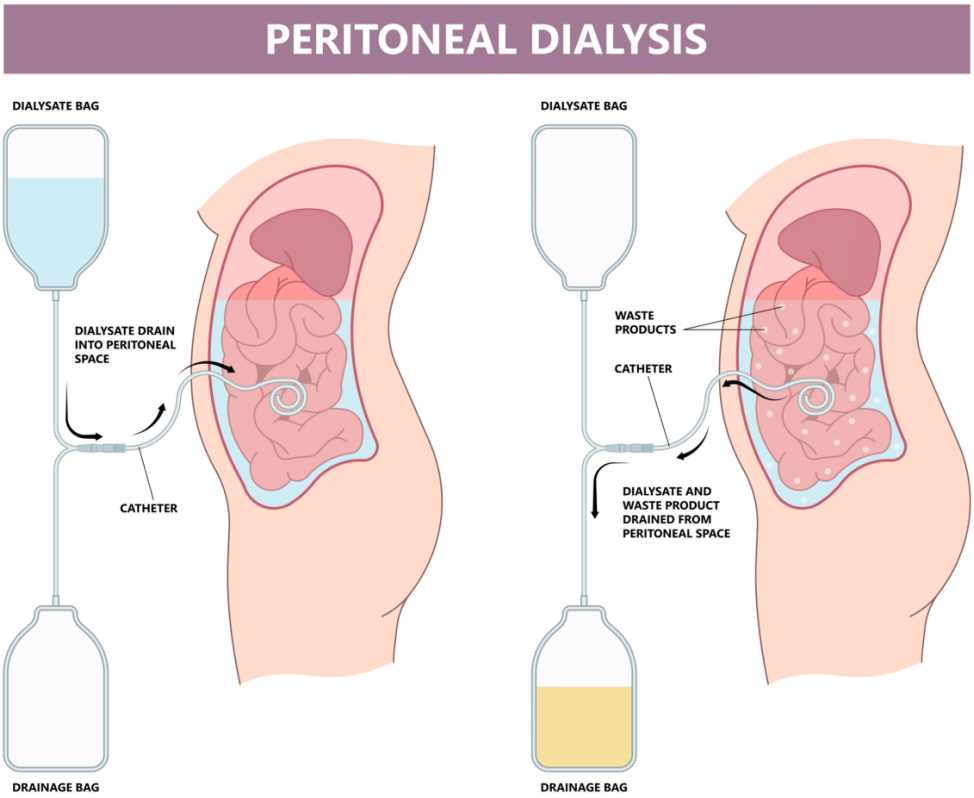

Figure 4: *Peritoneal dialysis (Source: https://www.kidneyhealth.com.sg/peritoneal-dialysis/).*

6. Peritoneal dialysis fluids

Standard single-chamber PDF are composed of high concentrations (>10-50× normal serum levels) of D-glucose (or dextrose) in anhydrous (MW = 180 kDa) or monohydrate form (MW = 198 kDa) as an osmotically active agent of 360-511 mOsm/l, resulting in the excess fluid and solutes removal from the peritoneal capillaries (~280 mOsm/l). The clinical use of glucose in the PD field was established about 50 years ago due to its affordability and straightforward preparation, but also for the reason that it is considered rich in calories and relatively safe with a lack of toxic effects on the systemic circulation. However, prolonged exposure to glucose predisposes to hyperglycemia,

hyperinsulinemia, hyperlipidemia and obesity, while rapid absorption of large amounts through peritoneal membrane leads to loss of UF [114,115].

Moreover, conventional PDF contain low concentrations of selected electrolytes [sodium (Na), potassium (K), chloride (Cl), calcium (Ca) and magnesium (Mg)], and lactate as buffer solution (35-40 mM), while the acidic pH of 5.5 has been chosen to counteract the generation of highly reactive and cytotoxic compounds as well as the glucose caramelization that derive from heat sterilization prior to PDF infusion. During this process, PDF warm up to 37°C and glucose undergoes chemical decomposition resulting in the formation of GDP and AGE that are deleterious for the PM integrity. Absorbed lactate amount from buffer solution has been linked to the formation of GDP, while many studies have shown that NaCl content is further correlated with the PM fibrosis [116,117].

The poor biocompatibility of the aforementioned glucose-based PDF has been a subject of intensive research for more than 3 decades and ultimately, multi-chamber bags were developed. In these bags of the so-called ‘second generation’ more biocompatible PDF, glucose, electrolytes and buffer (lactate, bicarbonate or their combination) contents are separately stored and heat sterilized [118]. Therefore, they allow not only the combined use of lactate- and bicarbonate-buffered solutions or even the replacement of the former by supraphysiological concentrations of the latter, but also the glucose sterilization at an extremely low pH. Consequently, the ready-to-use mixed PDF is characterized by a neutral to physiological pH of 7.0-7.4 and a low concentration of GDP. Still, even the use of low-GDP PDF in due time progressively leads to functional and anatomical PM degeneration, ultimately resulting in UFF [119].

To this end, alternative osmotic agents such as the glucose polymer, icodextrin, or amino acids have been introduced in clinical practice as well. Indeed, icodextrin-based PDF ameliorates UF capacity, however, profound mesothelial cell damage has restricted the PDF type administration once daily [120]. Moreover, increasing evidence points to the use of icodextrin to induce sterile inflammation through bacterial contamination derived from the production process [121,122]. Amino-acid-based PDF are the mainstay treatment for malnourished patients inducing an anabolic response by improvement of amino-acid transport into skeletal muscle, though side effects are also found. Metabolic acidosis and high load of urea in plasma arise from the use of amino acids as a metabolic

substrate [123]. Consequently, none of these two glucose-free PDF could abolish the use of the glucose-based ones.

7. Solute and water transport mechanisms within the Peritoneal Dialysis context

To comprehend the use of PM as a dialyzing membrane in the context of PD therapy, it is crucial to delve into the involved transport mechanisms during a PD exchange. After the PDF infusion, the intraperitoneal fluid volume increases followed by an analogous increase of intraperitoneal hydrostatic pressure. Additionally, a high osmotic pressure between the peritoneal cavity and the underlying tissue bearing blood and lymph capillaries is induced by the PDF hypertonicity. As these forces occur simultaneously, excess water and metabolic waste products enter the dialysate for further removal from the patient's body, whereas solutes including the PDF osmotic agent (glucose) are absorbed [67].

Based on the above, two mechanisms are responsible for the transport of water and solutes in patients undergoing PD, diffusion and convection/UF. The former is governed by the concentration gradient and thus, low-molecular weight substances including electrolytes diffuse from the capillary blood considered as the higher concentration compartment to the lower concentration compartment of peritoneal cavity containing the PDF, after penetrating the semipermeable PM in-between the two compartments. Since diffusion acts to eliminate concentration differences, solute clearance appears to occur in a pretty high rate at the beginning of each cycle when the waste products to be removed are merely detected in patient's blood but not in the dialysate, whereas it gradually decreases as the dwell time approaches the end [124]. To this extent, solute clearance could be maintained by augmenting the frequency of PD exchanges or the volume of the infused PDF. Administration of larger PDF volumes may also optimize the active peritoneal surface area because of the exertion of an even higher pressure on the intra-abdominal organs, while this parameter is also depended on the patient's body position. Furthermore, the molecular weight significantly affects the diffusion rate of solutes while the distance between blood capillaries and mesothelium (equivalent to

PDF) along with the number of pores per unit of surface area determine the endogenous membrane resistance [125–127].

Convective solute transport from the peritoneal capillary blood into the PDF is performed in conjunction with solvent movement by the means of UF as a result of the glucose PDF content which produces crystalloid osmotic pressure in conjunction with the transmembrane hydrostatic pressure [63,128]. This type of transfer is favoured against diffusion for the high-molecular weight solutes while convention rate is proportionally determined by the membrane area as well as its hydraulic permeability [129,130]. The glucose efficacy in facilitating convective water and solute transport is restricted to the resistance applied by the PM for its opposing movement from the peritoneal cavity to the blood microvessels. This resistance is quantified in physiological terms as the osmotic reflection coefficient. By definition, the complete resistance of PM to solute movement is reported with the reflection coefficient equalling 1.00 in contrast to the absence of resistance that equals 0.00. During the PD exchange, the coefficient of glucose variation refers to the mean of each membrane pore type [125,131].

Since the PDF content in electrolytes is of balanced concentration, diffusion plays far less important role in the removal of these molecules from the body than UF. However, it may be the dominant way for their absorption from the body [125,132]. Normally, in the blood capillaries, the hydrostatic pressure is higher than the intraperitoneal one, a condition that is conducive for the UF process and subsequent excess water exit through the small pores and aquaporin (AQP) channels [133,134]. Since the latter pathway is water-specific, the observed solute-free fluid transport during the early phase of an exchange triggered by the glucose-induced increased osmotic pressure, results in dilution of the sodium into the dialysate whereas a relative high concentration remains into the blood compartment. This phenomenon is well-described as *'sodium sieving'* and the most common clinical signs and symptoms that derive from the water rather than sodium removal from the extracellular fluid compartment are hypernatremia, thirst and hypertension [124,135]. During the later stage of the exchange, as a significant amount of glucose has been absorbed and there is a profound decline in UF rate, sodium concentration between the two compartments tends to equilibrate [135,136].

Overall, both diffusion and UF processes depend on specific factors. Conversely, solvent movement and the bulk-flow of solutes across the PM are determined by the exact glucose concentration, the dwell time, and the individual patient's PM characteristics.

With regard to the dissolved molecules, they are constantly moving according to their mass and environmental characteristics as well as the amount of produced thermal energy, which in turn is a function of temperature. Therefore, solute diffusion rate seems to be defined by the following:

- chemical slope
- molecular weight of the transported substance
- active peritoneal surface area
- endogenous membrane resistance
- blood circulation and capillary amount
- temperature of the PDF
- total volume of the PDF per 24 hours
- dwell time [126,127].

Among the above mentioned factors, these that can be optimized to maximize UF capacity in PD are the dialysate volume, the dwell time, and the frequency of exchanges per day [137–139].

8. Structural and functional alterations of the peritoneal membrane during Peritoneal Dialysis

Increasing evidence confirm that the peritoneum of ESKD patients at the time of PD onset already exhibits structural alterations such as submesothelial thickening and hyalinizing vasculopathy, as a result of uremic status, which are further aggravated by comorbidity with diabetes [140,141]. Suffering from inadequate purification capacity for solutes, uremic toxins and water, ESKD patients are already salt-, toxin-, and fluid-overloaded. However, the observed PM transformation is considered as mild-degree compared to the subsequent PD-related changes that are derived over time [142,143].

The invasion of pathogens (e.g., *Staphylococcus epidermidis*, *St. aureus*, *Escherichia coli*) in body tissue through the exit site of the catheter leads to serious damage of the peritoneum, a situation named peritonitis [144]. Given that infections are followed by activation of immune system as well as recruitment of inflammatory cells, the impact of bacterial peritonitis in the PM fibrosis is well established, and therefore peritonitis has

been traditionally considered a major complication during PD that results in considerable mortality and health care costs [145]. In such situations, several cytokines are elevated accompanied by subsequent production of certain chemokines after activation of mesothelial cells. Variations in chemokine profile of PD patients among different stages of infection have been found in effluents [146]. In this respect, the diagnostic value of specific molecules such as TNF-α and IL-1 has been suggested in the early diagnosis of peritonitis [147,148]. Another important aspect of peritonitis is related to functional PM alterations, since the accomplishment of neutrophils transmigration across endothelium entails the participation of adhesion molecules and reorganization of the intracellular junctions and the cytoskeleton [149]. Ultimately, recurrent inflammation episodes due to peritonitis increase the D/P of creatinine and diminish the UF capacity [144].

On the other hand, recent studies suggest that the main culprits of PM deterioration are the PD modality and the prolonged exposure to PDF [119]. PDF are infused multiple times per day into the abdominal cavity with glucose being the predominant osmotic agent, while many PDF have an acidic pH and high GDP content. Their supraphysiological composition is deleterious for the PM integrity, gradually affecting its functionality until UF failure (UFF) arises at approximately 5 to 6 years post-PD onset [150]. In order for the loss of the osmotic gradient to be counterbalanced, an additional glucose load is required that in a vicious circle exacerbates the PM degeneration and inevitably leads to PD dropout, and patients need to transfer to HD or undergo kidney transplantation [151,152].

The above outcomes are related to the development of anatomic alterations of PM. Long-term exposure to the high glucose and GPD content of conventional PDF along with AGE inhibit cell proliferation while induce apoptosis and necrosis of mesothelial cells as well as local production of inflammatory cytokines [153]. The progressive denudation of peritoneum of mesothelial cells is closely associated with MMT process which is strongly believed to constitute an additional source of myofibroblasts, apart from the presence of mesothelial progenitor cells [154]. The derived accumulation of collagen and myofibroblasts in the submesothelial zone causes a profound thickening of the area that, along with the loss of mesothelial cells and the chronic cytokine-induced inflammation promote PM fibrosis [76]. Elevated expression levels of specific cytokines such as TGF-β1 have been also shown to impair the viability and proliferation of cells.

Therefore, blockade of TGF-β1 has been proposed to prevent PM damage occurring due to PDF cytotoxicity [155,156].

However, damage on the PM function arises also from neoangiogenesis, a massive increase in blood vessel density that subsequently increases the surface area available for solute diffusion. In combination with the submesothelial thickening which enhances water flux resistance, the PM functional attributes are significantly altered, ultimately leading to UFF [142]. To this end, studies in peritoneal specimens collected from individuals with uremia have shown that vascular changes such as hyalinization of blood vessels and vasculopathy are more noticeable in patients in PD for over 4 years compared to uremic non-PD patients [142,157]. Additionally, increased synthesis of vascular endothelial growth factor (VEGF), a low molecular glycoprotein also known as vascular permeability factor, significantly stimulates vascular endothelial cell proliferation and vascularization, and thus contributes to peritoneal neoangiogenesis [158,159].

There is emerging evidence that the VEGF expression in the peritoneum and its levels in dialysate are correlated with peritoneal transport rates, since it has been repeatedly noted that cells undergone MMT and acquired a fibroblastic phenotype synthesize significant more VEGF, and a high production affects to increased PM permeability to small solutes and declined UF capacity [160–162]. Apart from the role of VEGF in PM deterioration, these findings also highlight the significance of mesothelial cells in the vascular changes during PD, an observation that was further amplified by studies in human umbilical vein endothelial cells (HUVEC) showing that supernatant derived from either receptor for AGE (RAGE)-stimulated mesothelial cells, or co-culture of HUVEC with RAGE-stimulated mesothelial cells induces equivalent capillary tube formation and thus, there may be a direct communication or cross-talk between mesothelial and endothelial cells [163].

All the above histological changes are linked to profound alterations in PM barrier function [164,165]. Both high glucose PDF content per se and glucose derivatives (GDP, AGE) have been incriminated to significantly decrease the expression of molecular mediators of paracellular permeability such as Claudin-1, Occludin, and ZO-1, while the impact of glucose is time- and dose-depended [164–167]. Similar findings have been recapitulated in HPMC isolated from PD effluents where a decline in transmembrane electrical resistance (TER) was observed. Given that TER measurements are used to characterize barrier properties, the results are linked to respective alterations in Claudin-

1, Occludin, and ZO-1 [168,169]. Moreover, there are data stemming from studies on retinal endothelial cell permeability in response to hyperglycaemia that have shown reduction of Claudin-5, Occludin, ZO-1 and JAM-A [170,171]. Contrary, hyperglycaemia has been found in both epithelial and endothelial cells to increase the expression of transcellular water and ion channels such as AQP1, epithelial sodium channel (ENaC) and of course the sodium-glucose cotransporters SGLT1 and SGLT2 [172–175]. Human parietal peritoneum is also prone to ENaC inhibition by amiloride and thus, modulation of the peritoneal membrane permeability [176]. Still, although there is a clear relationship between exposure of cells in high levels of glucose and PM permeability in PD, there is a substantial lack of data with respect to changes in mesothelial or endothelial cell monolayer permeability caused by commercially available PDF.

PD vintage, high glucose, GDP, and AGE concentrations are responsible for the interstitial fibrosis and UFF, and therefore introduction of neutral-pH, low-GDP PDF raised hopes regarding the prevention of long-term PM degeneration. Initially, *in vitro* and *in vivo* studies showed promising results such as improvement in local host defence, mitigation of mesothelial cell damage and MMT, reduction of GDP and AGE peritoneal deposition, and less angiogenesis and TGF-β, VEGF signalling; altogether indicating less fibrosis and better preservation of PM UF capacity [177–182]. However, not all subsequent clinical trials were consistent demonstrating differential results in terms of morphological alterations of PM, small solute transport rate and UF capacity [150,183]. In the study of *Schaefer et al.* (2018) in which 82 biopsies of children on PD with low-GDP PDF were analysed, results revealed an intense increase in both density and count per unit length of peritoneal blood capillary, while vascular alterations were accompanied by induction of SMAD phosphorylation due to TGF-β and VEGF release, MMT as well as inflammatory cell invasion [184].

9. Strategies for improving Peritoneal Dialysis fluid biocompatibility

Besides icodextrin and amino acids, other alternative compounds have been systematically investigated to either fully or partially substitute glucose which is linked

to PM degeneration that subsequently affects its functionality during PD therapy. More than a decade ago, the potential of 2-aminoethane sulfonic acid, taurine, that exists freely in the intracellular fluid and is involved in multiple cell functions including osmoregulation, antioxidation and cell membrane stabilization, was explored in terms of UF capacity and biocompatibility using a rat PD model [185–187]. Preliminary data on assessment of net UF as well as mesothelial and fibroblast-like cell proliferation indicated that the efficacy of taurine as an osmolyte is equivalent to that of glucose accompanied by a better biocompatibility with respect to PM preservation [185].

Moreover, partial replacement of glucose by xylitol, a five-carbon sugar alcohol derived by D-xylulose reduction, and L-carnitine, an amino-acid synthesized in human body from lysine and methionine, was investigated performing *in vitro* experiments on human endothelial and mesothelial cells. Findings suggested that the tested PDF does not significantly induce nitro-oxidative stress and inflammation while preserves mesothelial and endothelial cell viability and thus, it is less cytotoxic compared to the standard PDF [12,188]. The first clinical trial of the above experimental PDF was performed for a 4-week duration in 10 ESKD patients receiving CAPD, and the preliminary results indicated a good tolerance with absence of adverse safety signals and stable fluid status, diuresis and dialysis adequacy [189].

More recently, *in vivo* studies in rats were performed to test the effect of PDF containing d-glucose partially replaced by a rare monosaccharide found in the leaves of the African shrub *Protea rubropilosa* that is called d-allose [190,191]. Results indicated that d-allose mitigated peritoneal injury as indicated from immuno-histological staining and peritoneal equilibration test. More specifically, a better viability was achieved in rat peritoneal mesothelial cells, accompanied by decreased cytokine production and oxidative stress despite the absence of significant changes in osmolality of the two tested PDF (PDF containing 4% d-glucose or 3.6% d-glucose along with 0.4% d-allose). In direct administration to rats, a similar positive effect was observed through the suppression of peritoneal thickness and blood d-glucose levels [190]. However, there are no other clinical trials whatsoever regarding the use of d-allose in PD patients to compare these promising findings.

Steviol glycosides (SG) are active compounds found on the leaves of *Stevia rebaudiana*, a plant that is worldwide commercially used as a natural herbal sweetener [192]. However, beyond their sweetening value, SG have multiple medicinal applications by

lowering blood sugar levels and consequently, are used against cancer, cystic fibrosis, kidney damage, inflammation, dental caries etc [193,194]. Based on these characteristics, a pure extract of the plant *stevia rebaudiana* composed of ≥95% SG was tested as an alternative osmotic agent in PDF. Comparisons of the experimental SG-based PDF with a conventional high-GDP, low-pH PDF of 4.25% glucose and a more biocompatible low-GDP, physiological-pH PDF of 2.3% glucose showed a similar trend in mice for weight gain and urea clearance, but significant differences in cell viability and MMT performing both *in vivo* and *in vitro* experiments [195].

Novel therapeutic strategies focus on the supplementation of currently available PDF with small cytoprotective additives that would maintain the PM integrity without affecting its functional characteristics or at least delay the PM degeneration due to PDF bio-incompatible composition [150]. Such an example is the dipeptide alanyl-glutamine (AlaGln) which has been shown to increase the cytoprotective stress proteome of mesothelial cells treated with the standard 3.86% glucose-based PDF and thus, to ameliorate the resistance to the PDF-induced cell damage possibly associated with inadequate levels of glutamine [196]. Most importantly, though, these findings were verified in a first-in-man clinical trial with 20 participants receiving the above PDF with or without the addition of 8 mM AlaGln as well as in a phase 2 randomized controlled trial, while a similar effect was evident also with regards to vascular damage of endothelium [13,197,198]. Other studies have shown AlaGln to attenuate the immune response dissipation of the peritoneal cavity, while increased potassium and phosphate removal that are considered clinically relevant outcomes [199,200]. Since the principles of PD therapy are based on the use of the PM as a semipermeable dialyzing membrane, the impact of AlaGln has been also investigated in the context of endothelial barrier function by assessment of TJ components expression levels and localization which indicated a sealing effect [14,201].

Furthermore, significant cytoprotective effects by lithium chloride (LiCl) addition to two PDF of different composition (conventional PDF of 3.86% glucose content and low pH, icodextrin-based PDF) have been shown in *in vitro* experiments using a human mesothelial cell line and HPMC isolated from PD effluents of uremic patients [202]. Based on the hypothesis that PDF exposure activates the glycogen synthase kinase-3β (GSK-3β), a serine-threonine protein kinase involved in several signaling pathways that negatively regulates the cell survival partly by suppression of the protective heat sock

response (HSR), Rusai *et al.* assessed the impact of GSK-3β inhibition by LiCl on the activation of the heat shock transcription factor 1 (HSF-1) and the production of the heat sock protein Hsp72 as the main HSR effectors [196,202,203]. The attractive cytoprotective results of reduced cell injury after LiCl PDF supplementation were later enriched by transcriptomic and proteomic analysis in both *in vitro* and *in vivo* studies in HPMC and mice, respectively. Exploring the hypertonicity-induced cytotoxicity, the addition of LiCl to the icodextrin-based PDF was tested with regards to counter-regulation of αB-crystallin, a mesothelial cell protein that triggers a fibrotic phenotype under overexpression conditions, and the results confirmed a better mesothelial cell survival by mitigating PM fibrosis and angiogenesis [15].

2DG is a glucose analog that deters glycolysis by inhibiting the function of hexokinase, firstly reported in 1954 [204]. Recently, Si *et al.* demonstrated that high-GDP PDF induce cell metabolic reprogramming to a more glycolytic phenotype in order to produce the energy needed, so-called hyperglycolysis, while this increase in glucose uptake and metabolism was further associated with peritoneal fibrosis [17,205]. In this context, 2DG was successfully used to prevent PDF-induced hyperglycolysis performing both *in vitro* (MeT-5A cells and HPMC) and *in vivo* (chronic PD mouse model) experiments [17]. Along with our previously published data regarding the safe use of 2DG in mesothelial cells in a concentration range up to 0.5 mM, the 2DG antifibrotic, promising effect warrant an extensive characterization of its potential as a cytoprotective PDF additive targeting MMT and subsequent fibrogenesis [18].

10. 2-deoxyglucose as an anti-fibrotic agent in Peritoneal Dialysis

Peritoneal damage and inadequate UF capacity are relevant to glucose-based PDF-induced fibrosis [160]. During the development of inflammation and angiogenesis, MMT subsequently takes place enabling the mesothelial cells to excessively proliferate and migrate in the context of repair of the mesothelium [31]. The process of MMT comprises multiple biochemical changes including the suppression of adhesive and TJ protein expression that subsequently leads to mesothelial cell loss which in turn, is further aggravated by prolonged exposure to PDF bio-incompatible content [76]. The

resultant denuded basement membrane induces fibrogenesis by activating resident fibroblasts, and recruiting inflammatory cells [206]. Furthermore, mesenchymal cells derived from MMT have been proposed to be the primary source of myofibroblasts, strictly correlated with peritoneal fibrosis and transport failure during PD [207,208]. Despite the glucose-related side effects of PD therapy, methods that would prevent or delay the peritoneal fibrosis are lacking, and so far no effective therapeutic anti-fibrosis strategy is available [209].

The Warburg effect is a switch of metabolism from oxidative phosphorylation to aerobic glycolysis that has been documented for almost a century and extensively studied over the past 10 years [210]. Experiments in mouse kidneys subjected to unilateral ureter obstruction surgery or in TGF-β-treated renal interstitial fibroblasts have demonstrated that Warburg effect is apparent in renal fibroblasts, and this constitutes a key aspect of fibroblast activation in renal fibrosis. Despite the fact that aerobic glycolysis, as indicated by increased glucose absorption and lactate production, can remarkably induce myofibroblast activation, inhibition with 2DG, a glucose analog that deters glycolysis by the inhibition of the function of hexokinase, attenuates these affects [211]. In line with this, treatment of CKD with aerobic glycolysis inhibitors may be a reliable anti-fibrotic method.

Recently, it was shown that conventional high-GDP PDF induce hyperglycolysis and MMT both in MeT-5A and primary cells as confirmed by the increased fibronectin (FN) 1, collagen type 1 alpha 1 chain (COL1A1), αSMA protein expression and the decreased E-cadherin expression [17]. Hyperglycolysis is the cell metabolic reprogramming to a more glycolytic phenotype in order to produce the energy needed [212]. The above results were recapitulated also *in vivo* in mice. In all cases, the same findings were also derived from TGF-β1 stimulation, a known pro-fibrotic growth factor in PD. However, the addition of 2DG was again successfully used as a tool to prevent hyperglycolysis-mediated MMT and subsequent peritoneal fibrosis [17]. There are no data regarding the anti-fibrotic effects of 2DG in mesothelial cells under the influence of biocompatible, low in GDP PDF with a more physiologic pH, which would be of importance since they are the most widely used PDF.

SPECIAL PART

11. Aim of the study

The effective PD treatment in patients with ESKD relies on the proper function of the peritoneal membrane as a dialyzing membrane for the removal of excess water and uremic toxins from the systemic circulation. One of the main barriers to the wider use of PD is the PDF bio-incompatibility. Depending on the type, PDF contain high or low levels of GDPs and low-to-neutral pH. Prolonged exposure of the PM to PDF content aggravates MMT, submesothelial fibrosis and hyalinizing vasculopathy, eventually leading to UF at approximately 6 years post-PD onset.

Novelties in the therapeutic approaches for ESKD focus on PDF supplementation with agents that could delay or reverse the degeneration of the PM while maintaining its barrier function. Recently, the inhibition of hyper-glycolysis in mesothelial cells by the administration of 0.2 mM of 2DG along with the conventional PDF was shown to mitigate MMT process and PM fibrogenesis. We have also published that 2DG could be safely used in a concentration range up to 0.5 mM without affecting the mesothelial cell viability thus, suggesting the further investigation of the potential of this agent in terms of functional effects to the PM, such as paracellular and transcellular permeability.

Based on the above, our aim was to initially evaluate whether the beneficial effects of 2DG with respect to mesenchymal transition are valid in three commercially available PDF of different composition in both mesothelial and endothelial cells, performing an *in vitro* functional MMT assay and evaluating gene expression changes in mesenchymal markers. Subsequently, we sought to test whether the addition of 2DG would affect the mesothelial, endothelial and their combined permeability, conducting electrophysiological, biophysical, and molecular experiments.

Overall, we aimed at providing a comprehensive understanding of the PDF-induced hyper-glycolysis effects both in terms of PM fibrosis and barrier function that could be of use in the clinical practice, by elucidating the following questions:

i. Does the 2DG addition have antifibrotic effects in mesothelial and/or endothelial cells exposed to PDF of different composition?

ii. Does the 2DG addition alter the permeability of mesothelial and endothelial monolayers or their combined co-culture model?

iii. Is there a differential effect depending on the solution or cell type used?

iv. Do the previous permeability findings after 2DG addition correspond to corresponding alterations in gene expression levels of components of paracellular and transcellular solute clearance?

12. Materials & Methods

12.1 Cell culture

Two human immortalized cell lines, MeT-5A (benign mesothelial cells; kindly gifted by Prof. Ioannis Kalomenidis, National & Kapodistrian University of Athens, Athens, Greece) and EA.hy926 (endothelial hybrid cells derived from fusion of human umbilical vein endothelial cells with the human lung carcinoma cell line A549; kindly gifted by Prof. Claus Peter Schmitt, Universitätsklinikum Heidelberg, Heidelberg, Germany) were used in the present study. The cell cultures were propagated in Gibco™ RPMI 1640 medium (42401018, ThermoFisher) supplemented with 10% v/v fetal bovine serum (FBS; F0804-500, Sigma), 1% v/v L-glutamine (2 mM; G7513, Sigma), 1% v/v antibiotic additives [Penicillin (100 U/ml) - Streptomycin (100 μg/ml); P4333, Sigma] and 0.2% v/v Plasmocin® prophylactic (2.5 mg/mL; ANT-MPP, InvivoGen) at 37ºC in a humidified incubator (95% air and 5% CO_2). During cell culture, the medium was replenished every 48 hours after a gentle wash with phosphate buffered saline (PBS) solution containing Ca^{2+}, Mg^{2+} (**Table 1**).

For synchronizing purposes, cell lines were treated with 0.5% FBS-RPMI for 24 hours. Confluent culture in T-75 flasks (156499, ThermoFisher) for passaging or experimental setup were washed with PBS followed by the addition of 3 mL of trypsin (T4049, Sigma) for 5 min at 37 ºC, and quenching with 4 mL of 10% FBS-RPMI. Trypsin was removed by sedimentation of the cells by centrifugation at 1,000 rpm at 4 ºC for 2.5 min, and the cell pellets were resuspended in cell culture medium for further use.

For cell counting purposes, the cells were mixed in a 1:10 dilution with 0.04% w/v of trypan blue (T6146-25G, Sigma) in PBS and 10 μL of this mixture was placed on a Neubauer counting slide and examined under an inverted microscope (Nikon Eclipse TS100) at 100x magnification.

***Table 1**: Phosphate buffered saline (PBS) solution composition per liter.*

Final volume: 1 lt, pH = 7.4	**Phosphate Buffered Saline (PBS)**	
	NaCl	137 mM
	KCl	2.7 mM
	Na_2HPO_4	10 mM
	KH_2PO_4	1.8 mM
PBS with Ca^{2+}, Mg^{2+}	$CaCl_2$	1 mM
	$MgCl_2*6H_2O$	0.5 mM

12.2 Peritoneal dialysis fluids and 2-deoxyglucose

Contents of the pack and other information about PDF used in the study are given in **Table 2**. Briefly, three PDF of different composition were tested without or with the addition of 0.2 mM of 2DG (D8375-1G, Sigma) at a concentration of 0.2 mM. The conventional PDF (CPDF) Dianeal® 2.5% dextrose (Baxter Healthcare) was a ready-to-use single-chamber solution, while the double-chamber-bag solutions BicaVera® 2.3% glucose [bicarbonate buffered PDF (BPDF) from Fresenius Medical Care] and Balance® 2.3% glucose [lactate buffered PDF (LPDF) from Fresenius Medical Care] were mixed according to the instructions of manufacturers about volume of each chamber.

***Table 2**: Composition per litre of the used PDF.*

Solution (manufacturer)	**Dianeal (Baxter Healthcare)**	**BicaVera (Fresenius Medical Care)**	**Balance (Fresenius Medical Care)**
Osmotic agent (% w/v)	Dextrose (2.5%)	Glucose (2.3%)	Glucose (2.3%)
Bag	Single chamber	Double chamber	Double chamber
pH	5.0-6.5	7.4	7.0
Osmolarity (mOsm/L)	396	401	401
Buffer solution (mmol/L)	Lactate (40)	Bicarbonate (34)	Lactate (35)

Ca^{2+} (mmol/L)	1.75	1.75	1.75
Na^{+} (mmol/L)	132	134	134
Mg^{2+} (mmol/L)	0.25	0.5	0.5
Cl^{-} (mmol/L)	96	104.5	101.5
Glucose (mmol/L)	126	126.1	126.1

12.3 Gel contraction assay

Synchronized MeT-5A or EA.hy926 cells maintained in 0.5% FBS-RPMI for 24 hours were used to perform the gel contraction assay. For experimental procedures, all reagents were maintained on ice. PDF were mixed with 10% FBS-RMPI at a 1:1 dilution, followed by extra FBS addition to maintain serum levels at a final concentration of 10%, and 2DG supplementation where appropriate. Then, collagen (1.2 mg/mL) extracted from white Norwegian Sprague-Dawley rat tails was added in 1:6 ratio and the mixtures were neutralised by adding 0.5 M NaOH prior to cell embedding (10^6 cells/mL). The collagenous mixtures were thoroughly vortexed and dispensed in 0.6 mL volume in a 24-well plate. The plate was transferred in a 5% CO_2 incubator at 37 ºC for approximately 20-30 min for the gels to polymerize and then, manually separated from the well plate walls by scraping a pipette tip around the perimeter of the well. Additional 0.6 mL of respective treatment was added in each well. During the assay, the plate was maintained to the incubator for a total of 72 hours and imaged on a flatbed HP Deskjet scanner every 24 hours. The scanned area of polymerized gels was measured by ImageJ software using the circular or polygon lasso tool. Contractility index (CI) was calculated as follows:

$$CI = (\text{Well area} - \text{Gel area}) / \text{Well area}$$

At the end of the assay, the polymerized gels were transferred to eppendorf tubes and centrifuged at 9,000 rpm for 15 min. The supernatant was carefully removed with a pipette, and the pellet was resuspended in 250 μL of TRIzol™ reagent (15596-026,

Invitrogen) for total RNA extraction. All samples were thoroughly vortexed until collagenous material break.

12.4 Mesothelial or endothelial cell monolayer model

To develop an *in vitro* model of mesothelial or endothelial monolayer, MeT-5A or EA.hy926 cells respectively, were seeded in Snapwell™ or Transwell® permeable supports. Six Snapwell™ inserts with polycarbonate membranes (diameter: 12 mm, pore size: 0.4 μm, pore density: 1×10^8 pores/cm^2, cell growth area: 1.12 cm^2) supported by a detachable ring were supplied preloaded into 6-well plates (Corning® Costar® 3407, Sigma-Aldrich) while twelve Transwell® inserts with polyester membranes (diameter: 6.5 mm, pore size: 0.4 μm, pore density: 2×10^6 pores/cm^2, cell growth area: 0.33 cm^2) supported by a non-detachable ring were supplied preloaded into 24-well plates (Corning® Costar® 3470, Sigma-Aldrich). A cell suspension of 2.5×10^5 cells in 0.5 mL of medium was added to each Snapwell™ insert, while in Transwell® inserts were cultured 0.5×10^5 cells in 0.2 mL of medium. The basolateral compartment of Snapwell™ or Transwell® plates was containing 10% FBS-RPMI at a volume of 3 or 1 mL, respectively. The plates were maintained at 37 °C in a 5% CO_2 incubator until cell confluence. The culture media was replenished every 2 days and the TER was monitored daily by an EVOM voltohmmeter equipped with a SXT-2 “chopstick” electrode pair (World Precision Instruments, Sarasota, FL34240-9258, USA). The final TER of each cell monolayer was calculated in units of Ω•cm^2 as follows:

$$\text{TER } (\Omega\bullet\text{cm}^2) = [\text{TER}_{\text{CELLS}}\ (\Omega) - \text{TER}_{\text{BLANK}}\ (\Omega)] \times \text{M}_{\text{AREA}}\ (\text{cm}^2)$$

where $\text{TER}_{\text{CELLS}}$ value is obtained by the resistance across the cell layer and $\text{TER}_{\text{BLANK}}$ value by the background resistance of a blank filter without cells. M_{AREA} is referring to cell growth area of the inserts, which is equal to 1.12 cm^2 for the Snapwell plates and 0.33 cm^2 for the Transwell plates.

12.5 Mesothelial and endothelial cell co-culture model

To better simulate the *in vivo* conditions, a second *in vitro* co-culture model of the mesothelial barrier on the upper compartment and the endothelial barrier on the lower compartment was also established. Initially, EA.hy926 cells (2.5×10^5 cells/Snapwell™ insert in 100 μL of 10% FBS-RPMI or 0.5×10^5 cells/ Transwell® insert in 50 μL of 10% FBS-RPMI) were seeded upside-down on the filters and incubated at 37 °C in 5% CO_2 conditions for approximately 4 hours in order to adhere. Within this period, the filters were monitored regularly whether any culture medium addition was required for the cell surface to be maintained wet. At the end of the 4-hour period, the filters were gently inverted, and the EA.hy926 cells were cultured for another 2 days prior to regular cell seeding of MeT-5A cells (2.5×10^5 cells/Snapwell™ insert in 0.5 mL of medium, 0.5×10^5 cells/Transwell® insert in 0.2 mL of medium) on the apical side of the inserts. The TER was daily monitored during the whole procedure as described above.

12.6 Ussing chamber experiments

After 5 or 7 days in culture (for single cell type or co-culture model, respectively), when monolayers were fully formed as evidenced by a plateau in the TER, the Snapwell™ permeable supports were detached and carefully mounted in Ussing chambers (Dipl.-Ing. K. Mussler Scientific Instruments, Aachen, Germany) with an opening surface area of 1.12 cm^2, part of an apparatus for continuous readings of the barrier resistance (R_{TM}) across cell monolayers. The cell monolayers were bathed with 4 mL of Krebs-Ringer bicarbonate solution (KRB; **Table 3**) on each side, balanced at pH 7.4 and continuously oxygenated with 95% O_2-5% CO_2 circulated by gas lift. The chambers were maintained at 37 °C and two pairs of Ag/AgCl electrodes were emerged monitoring the R_{TM} ($\Omega\bullet cm^2$) under open circuit conditions. After an equilibration period of approximately 20 to 30 min, KRB of the clinically relevant side of each monolayer was replaced by 4 mL of proper treatment (PDF supplemented or not with 0.2 mM of 2DG). As clinically relevant sides are considered the apical side for the mesothelial or co-culture monolayers, and the basolateral side for the endothelial monolayers given that upon PDF introduction to the peritoneal cavity of patients, the apical side of the PM mesothelium is directly exposed to PDF, which encounters the basolateral side of capillary walls once it penetrates the

peritoneum. In all cases, R_{TM} measurements were registered in a personal computer (software Clamp v.2.14, Scientific Instruments, Aachen, Germany) for a 4-hour incubation period. At the end of the recording time, the cell monolayers were lysed with 250 μL of TRIzol™ reagent for total RNA extraction.

***Table 3**: Krebs solution composition per litre.*

Krebs solution	Final volume: 1 lt
NaCl	6.866 gr (117.5 mM)
NaH_2PO_4	0.158 gr (1.15 mM)
$NaHCO_3$	2.099 gr (24.99 mM)
KCl	0.421 gr (5.65 mM)
$MgSO_4$	0.239 gr (1.18 mM)
$CaCl_2$	0.37 gr (2.52 mM)
Glucose	1 gr (5.55 mM)

12.7 Paracellular permeability assay

The paracellular permeability of the mesothelial and endothelial barrier or their collective behaviour under the effect of PDF with/without 2DG was also assessed by the diffusion of a fluorescent marker. On the 5^{th} or 7^{th} day (for single cell type or co-culture model, respectively) when MeT-5A and/or EA.hy926 cell monolayers grown in Transwell filters were fully confluent, fluorescent isothiocyanate-labelled (FITC) dextran with molecular weight of 10 kDa (FD10S-250MG, Sigma-Aldrich) or 70 kDa (R9379-100MG, Sigma-Aldrich) diluted in PDF supplemented or not with 0.2 mM of 2DG was added in the apical compartment. An equimolar amount of unlabelled dextran from Leuconostoc mesenteroides with molecular weight of 9-11 kDa (D9260-10G, Sigma-Aldrich) or 64-76 kDa (D8821-10G, Sigma-Aldrich), accordingly, was diluted in 10%FBS-RPMI and added to the basolateral compartment to maintain an isotonic condition. All dextran solutions were prepared in a 100X stock and diluted at a final concentration of 1 mg/mL. The paracellular permeability of mesothelial and/or endothelial monolayers was assessed by calculating the flux of the FITC dextrans from

the apical to basolateral side of Transwell inserts after 4 hours of incubation with the appropriate treatment. At the end of the assay, a sampling of 100 μL volume of each apical compartment (to serve as baseline fluorescence) and basolateral compartment was loaded in a 96-well plate (655180, Griener Bio-one). The plate was rapidly protected from light by covering with aluminium foil and stored at 4 °C until. The next day, the optical density (O.D.) was measured using a multimode plate reader (EnSpire®, PerkinElmer; excitation: 490 nm, emission: 520 nm).

12.8 RNA isolation

Total RNA was isolated with TRIzol® (15596-026, Invitrogen) from collagen gel contraction experiments with embedded MeT-5A or EA.hy926 cells or Snapwell filters used in Ussing chamber experiments. The collected samples were subjected to purification by the addition of 50 μL of chloroform (C2432-1L, Sigma-Aldrich). The aliquots were vigorously shaken by hand and incubated at room temperature for 10 min. After spinning at 9.000 rpm for 15 min at 4 ºC, the aqueous phase was transferred to fresh eppendorf tube and 50 μL of isopropyl alcohol along with equal total volume of 4 M LiCl were added. The tubes were incubated at -20 ºC for 1 hour and then centrifuged at 9,000 rpm for 10 min at 4 ºC. Supernatant was discarded and the pellet was resuspended in 200 μL of 95% ethanol, and incubated at -20 ºC for 1 hour followed by centrifugation at 9,000 rpm for 10 min at 4 ºC. The pellet was finally allowed to dry at room temperature for 30 min and resuspended in 100 μL of Ambion™ nuclease-free water (AM9930, Invitrogen). The purified samples were quantified using a Quawell Q3000 UV spectrophotometer.

12.9 Quantitative Real-Time PCR

Gene specific primer pairs for the human *CLDN1*, *CLDN2*, *CLDN3*, *CLDN4*, *CLDN5*, *ZO1*, *SGLT1*, *αSMA* and *CDH2* transcripts were designed using the NCBI Primer-BLAST tool (**Table 4**) whereas primers for the *SGLT2* transcript were used as previously reported [213,214]. A 200 ng quantity of purified RNA aliquots was reverse transcripted into cDNA using the SuperScript™ III first-strand synthesis system (18080044,

Invitrogen), followed by 1:5 dilution in Ambion™ nuclease-free water. Amplifications were performed with the PowerUP™ SYBR™ Green Master Mix (A25742, Applied Biosystems) and *β-actin* was used as the reference gene. A reaction volume of 20 μL with 0.4 μM of the appropriate primer pair was composed on the ABI 7300 sequence detection system v1.4 (Perkin-Elmer Applied Biosystems) at standard thermal cycling mode for primer $T_m \geq 60$ °C: uracil-DNA glycosylase (UDG) activation at 50 °C for 2 min, Dual-Lock™ DNA polymerase at 95 °C for 2 min, 40 cycles of denaturation at 95 °C for 15 sec, 40 cycles of annealing at 60 °C for 1 min.

***Table 4**: Primer pairs used for Real-Time PCR.*

Genes	Primer	Sequence (5'-3')	T_m (°C)	Product size (bp)
CLDN1	Forward Reverse	CTGAATCTGAGCAGCACATTG TACACTTCATGCCAACGGTG	63.6 64.6	103
CLDN2	Forward Reverse	AATCCCGAGCCAAAGACAGA GTGGTGAGTAGAAGTCCCGT	65.9 60.6	123
CLDN3	Forward Reverse	CATCGGCAGCAACATCATCA GAGTCGTACACCTTGCACTG	68.3 61.0	102
CLDN4	Forward Reverse	ATGGGGCTACAGGTAATGGG AATGTTGCTGCCGATGAAGG	64.6 67.2	111
CLDN5	Forward Reverse	TTCCTGGACCACAACATCGT CCAGCACCGAGTCGTACA	65.5 63.8	112
ZO1	Forward Reverse	ACCAGAAATACCTGACGGTGC GATGGCGTTACCCACAGCTT	60.34 60.68	100
SGLT1	Forward Reverse	ACCCACGAGCTCATTCGCAA GATTGGTGGAAAACATAGCCCACA	62.45 61.59	100
SGLT2	Forward Reverse	TTCAGTCTCCGGCATAGCAAG CATCTCCATGGCACTCTCTGG	60.13 60.20	108
αSMA	Forward Reverse	CTATGAGGGCTATGCCTTGCC GCTCAGCAGTAGTAACGAAGGA	66.7 62.4	122
CDH2	Forward Reverse	TGCGGTACAGTGTAACTGGG GAAACCGGGCTATCTGCTCG	63.6 67.9	123

12.10 Statistical analysis

All experiments were performed 3 to 6 times. Data obtained were analysed with Prism v.9.0 software for Windows (GraphPad Software Inc., San Diego, CA, USA), and presented as mean ± standard error of mean (SEM). Prior to each statistical analysis,

data were checked for normality with D' Agostino-Pearson or Shapiro-Wilk test where appropriate. Values of $p < 0.05$ were deemed as statistically significant.

Gel contraction assay was carried out 4 times for the MeT-5A cell line and 3 times for the EA.hy926 cell line, in 5 to 6 replicates. The average of the replicates of each experimental set was used in the final analysis for a total N = 4 or N = 3, respectively. A 2-Way ANOVA with post hoc Dunnett's multiple comparison test was performed to assess differences within the experimental timepoints (24, 48 and 72 hours) or among treatments. The Ussing chamber experiments were carried out 3-6 times. A 2-Way ANOVA with post hoc Sidak's multiple comparison test was performed to assess statistically significant differences in the mesothelial and/or endothelial R_{TM} before and after treatment with PDF supplemented or not with 2DG, while the same statistical test was also applied in the dextran data sets obtained from the paracellular permeability experiments. Finally, the RT-PCR experiments were carried out 3-4 times in different biological replicates with 2 to 3 technical replicate each. The relative quantification in gene expression was evaluated with the $2^{-(\Delta\Delta Ct)}$ method as previously described [215] based on the averaged Ct (cycle threshold) values. The fold changes in the gene expression levels under the effect of 2DG were calculated using the $\log_2 2^{-(\Delta\Delta Ct)}$ values. A False Discovery Rate (FDR) approach applying multiple unpaired t-tests was used for comparisons between PDF per se and PDF supplemented with 2DG.

13. Results

13.1 Effect of PDF exposure of MeT-5A cells in mesothelial-to-mesenchymal transition (MMT) process

The neutralized collagen gels with embedded MeT-5A cells were left to polymerize over 3 days and the effect of 3 different types of PDF (CPDF, BPDF, LPDF) on cell contractility was assessed by measuring the decrement in size of the surface gel areas at 24, 48 and 72 hours. Comparing the kinetics of cell-induced contraction in each group, a continuous augmentation in CI was ubiquitously evident in all cases (Control: CI_{24h}: 0.66 ± 0.02, CI_{48h}: 0.72 ± 0.01, CI_{72h}: 0.75 ± 0.02, $p < 0.001$; CPDF: CI_{24h}: 0.73 ± 0.01, CI_{48h}: 0.76 ± 0.01, $p < 0.05$, CI_{72h}: 0.81 ± 0.00, $p < 0.001$; BPDF: CI_{24h}: 0.71 ± 0.01, CI_{48h}: 0.74 ± 0.02, $p < 0.05$, CI_{72h}: 0.79 ± 0.01, $p < 0.001$; LPDF: CI_{24h}: 0.70 ± 0.01, CI_{48h}: 0.75 ± 0.02, $p < 0.05$, CI_{72h}: 0.78 ± 0.02, $p < 0.001$) as shown in **Figure 3A**. Assessment of potential differences between the control group and the PDF at the end of the assay (72 hours), revealed a significant higher CI ($p < 0.05$) in CPDF group, accompanied by alterations in gene expression of *αSMA* (4.64 ± 0.55, $p < 0.01$) and *CDH2* (0.44 ± 0.09, $p < 0.05$) defined as fold changes in comparison with control values set as baseline. An increase of *αSMA* mRNA (3.30 ± 0.19, $p < 0.001$) was also apparent in LPDF conditions (**Figure 3B**).

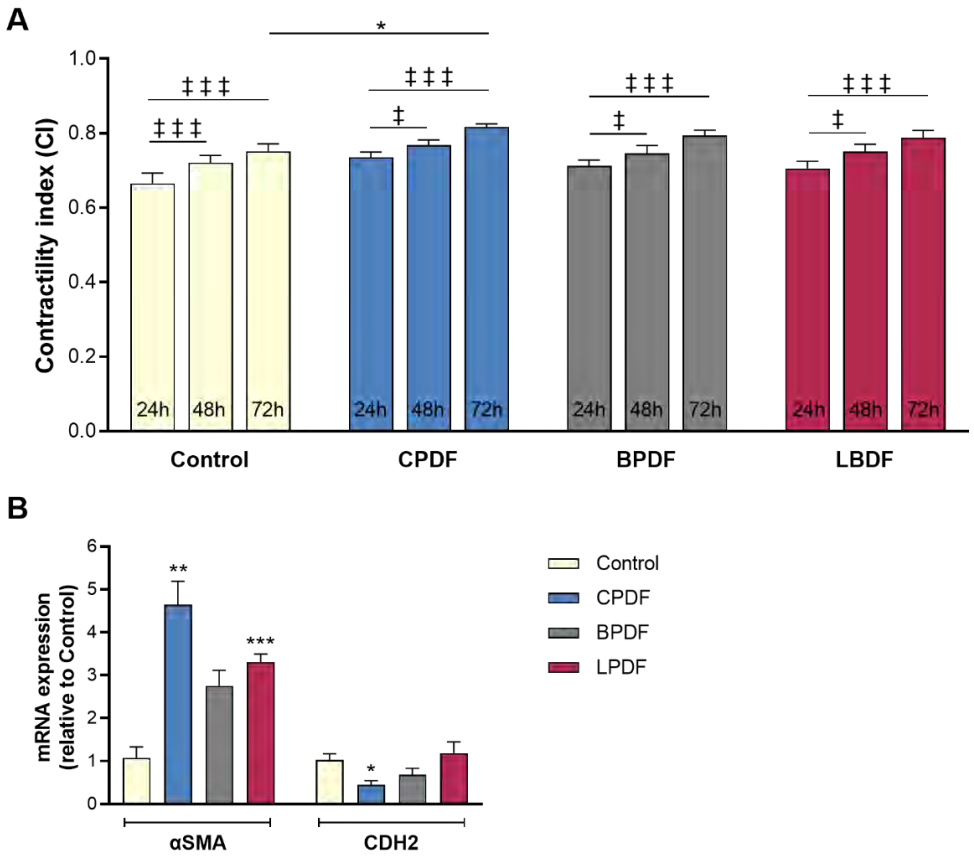

Figure 3: *Contractility index (CI) of* ***(A)*** *MeT-5A embedded gels in cell culture medium (Control) or PDF (CPDF, BPDF, LPDF) after 24, 48, 72 hours of incubation, and* ***(B)*** *mRNA expression levels of αSMA, CDH2 under exposure to the PDF expressed as fold change relative to Control. ‡ Indicates differences compared to 24 hours (‡$p < 0.05$, ‡‡‡$p < 0.001$) while * indicates comparisons with the Control (*$p < 0.05$, **$p < 0.01$, ***$p < 0.001$); $n = 4$. Data demonstrated as mean ± SEM.*

13.2 Alterations in MMT process of MeT-5A cells after exposure to PDF supplemented with 0.2 mM of 2DG

When the 2DG addition in each group was tested, a significant decline in CI ($p < 0.05$) was found in CPDF at all timepoints (CI_{24h}: 0.65 ± 0.02, CI_{48h}: 0.70 ± 0.01, CI_{72h}: 0.75 ± 0.01, $p < 0.05$; **Figure 4B**) which was not the case for control (CI_{24h}: 0.61 ± 0.01, CI_{48h}: 0.66 ± 0.01, CI_{72h}: 0.71 ± 0.02; **Figure 4A**) and LPDF groups (CI_{24h}: 0.65 ± 0.02, CI_{48h}: 0.71 ± 0.03, CI_{72h}: 0.75 ± 0.03; **Figure 4D**) while in BPDF group, a similar decrease was evident only up to 48 hours (CI_{24h}: 0.66 ± 0.00, CI_{48h}: 0.70 ± 0.00, CI_{72h}: 0.75 ± 0.01;

Figure 4C). Furthermore, 2DG addition in CPDF accordingly decreased the gene expression of *αSMA* (0.17 ± 0.03, $p < 0.01$) while increased the gene expression of *CDH2* (2.92 ± 0.29, $p < 0.001$; **Figure 4E, F**) thus, indicating a less contractile behaviour of MeT-5A cells after CPDF supplementation with 2DG.

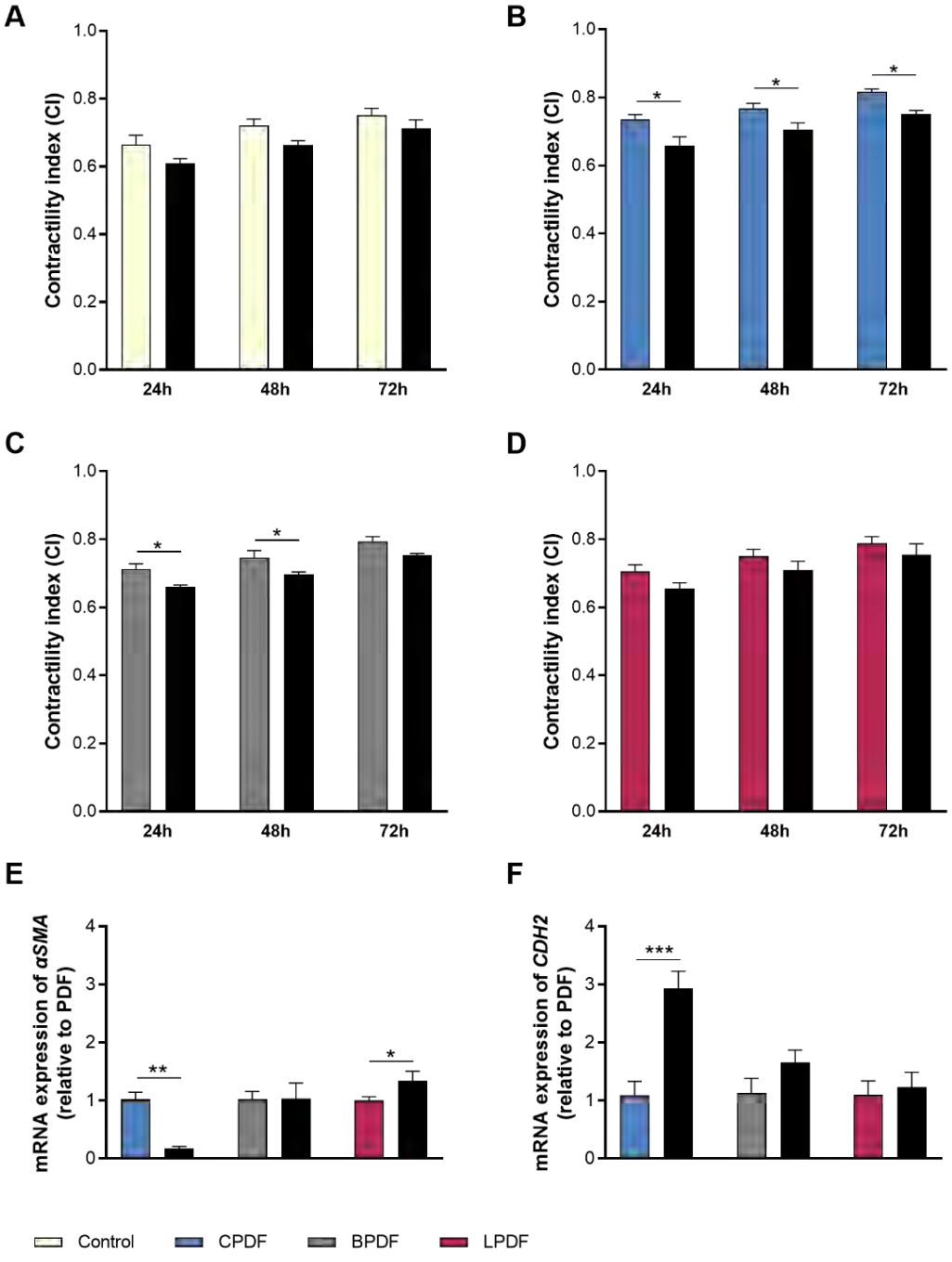

Figure 4: *Effect of 2DG in the CI of MeT-5A cells in* ***(A)*** *Control,* ***(B)*** *CPDF,* ***(C)*** *BPDF,* ***(D)*** *LPDF groups at 24, 48, 72 hours and mRNA expression levels of* ***(E)*** *αSMA,* ***(F)*** *CDH2. *p < 0.05, **p < 0.01, ***p < 0.001; n=4. Data demonstrated as mean ± SEM.*

13.3 Effect of PDF exposure of EA.hy926 cells in endothelial-to-mesenchymal transition (EndoMT) process

The neutralized collagen gels with embedded EA.hy926 cells were left to polymerize over 3 days and the effect of 3 different types of PDF (CPDF, BPDF, LPDF) on cell contractility was assessed by measuring the decrement in size of the surface gel areas at 24, 48 and 72 hours. Comparing the kinetics of cell-induced contraction in each group, a time-dependent increase in CI was found in control conditions (CI_{24h}: 0.51 ± 0.04, CI_{48h}: 0.59 ± 0.02, $p < 0.05$; CI_{72h}: 0.63 ± 0.01, $p < 0.01$), while incubation with the PDF increased the CI only at 72 hours (CPDF: 0.71 ± 0.01, $p < 0.05$; BPDF: 0.65 ± 0.02, $p < 0.05$; LPDF: 0.72 ± 0.01, $p < 0.01$) compared to 24 hours (CPDF: 0.63±0.03, BPDF: 0.58 ± 0.02, LPDF: 0.63 ± 0.03). Comparisons between control group and PDF at the end of the assay (72 hours) revealed a significant higher CI ($p < 0.05$) under CPDF and LPDF exposure (**Figure 5A**). Furthermore, incubation of EA.hy926 cells with CPDF increased the gene expression levels of *αSMA* (3.12 ± 0.27, $p < 0.05$) and decreased *CDH2* (0.11 ± 0.02, $p < 0.001$) levels compared to control, while an increase in *αSMA* (3.35 ± 0.10, $p < 0.05$) was also evident in LPDF group (**Figure 5B**).

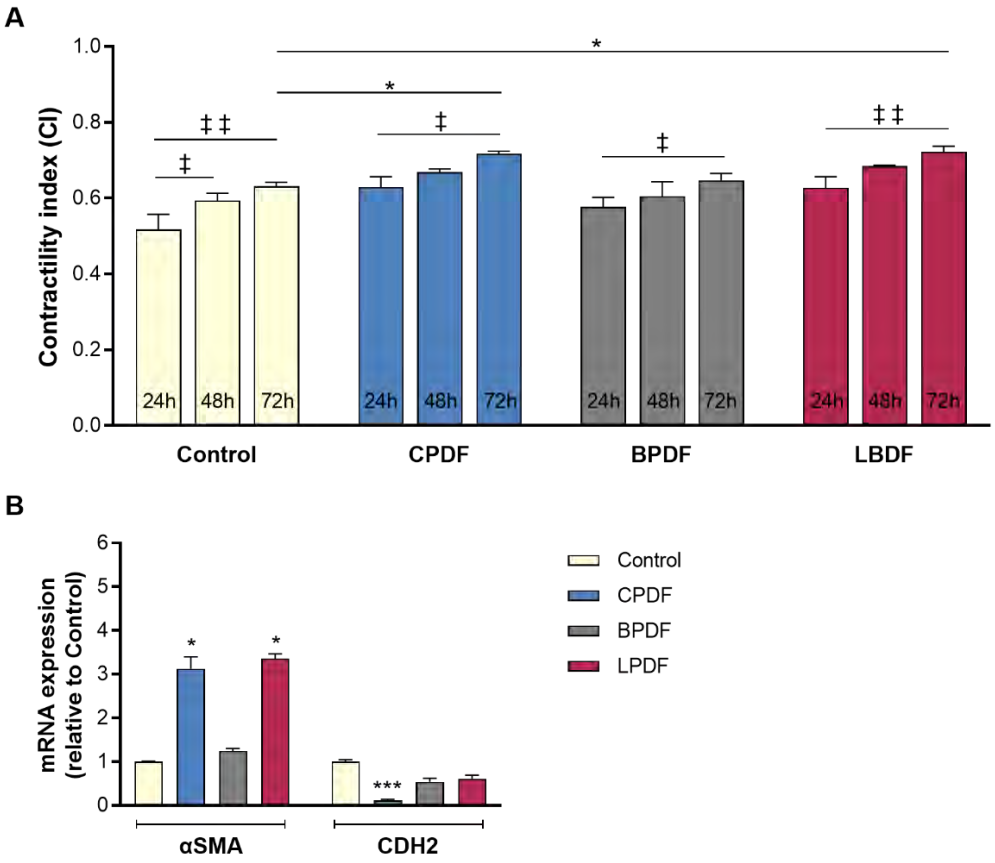

Figure 5: *Contractility index (CI) of* ***(A)*** *EA.hy926 embedded gels in cell culture medium (Control) or PDF (CPDF, BPDF, LPDF) after 24, 48, 72 hours of incubation, and* ***(B)*** *mRNA expression levels of αSMA, CDH2 under exposure to the PDF expressed as fold change relative to Control. ‡ Indicates differences compared to 24 hours (‡$p < 0.05$, ‡‡$p < 0.01$) while * indicates comparisons with the Control (*$p < 0.05$, $p < 0.01$); $n = 3$. Data demonstrated as mean ± SEM.*

13.4 Alterations in EndoMT process of EA.hy926 cells after exposure to PDF supplemented with 0.2 mM of 2DG

When the 2DG addition in each group was tested, a significant decreased CI at 24 hours was ubiquitously observed in all PDF (CPDF: 0.54 ± 0.02, $p < 0.01$; BPDF: 0.45 ± 0.03, $p < 0.05$; LPDF: 0.49 ± 0.03, $p < 0.01$; **Figure 6B-D**) in contrast to the other timepoints (48, 72 hours) where no significant difference was detected due to 2DG PDF supplementation (CPDF: CI_{48h}: 0.64 ± 0.01, CI_{72h}: 0.68 ± 0.02; BPDF: CI_{48h}: 0.58 ± 0.02, CI_{72h}: 0.61 ± 0.03; LPDF: CI_{48h}: 0.63 ± 0.01, CI_{72h}: 0.66 ± 0.03). The above findings

were accompanied by changes in the expression of *αSMA* and *CDH2* genes. More specifically, 2DG decreased the *αSMA* mRNA levels under CPDF (0.19 ± 0.05, $p < 0.001$) or LPDF incubation (0.42 ± 0.02, $p < 0.05$; **Figure 6E**), while *CDH2* was increased (2.60 ± 0.15, $p < 0.001$; **Figure 6F**) by CPDF. Despite the effects of 2DG addition in the PDF, no significant changes whatsoever were found in control conditions (**Figure 6A**).

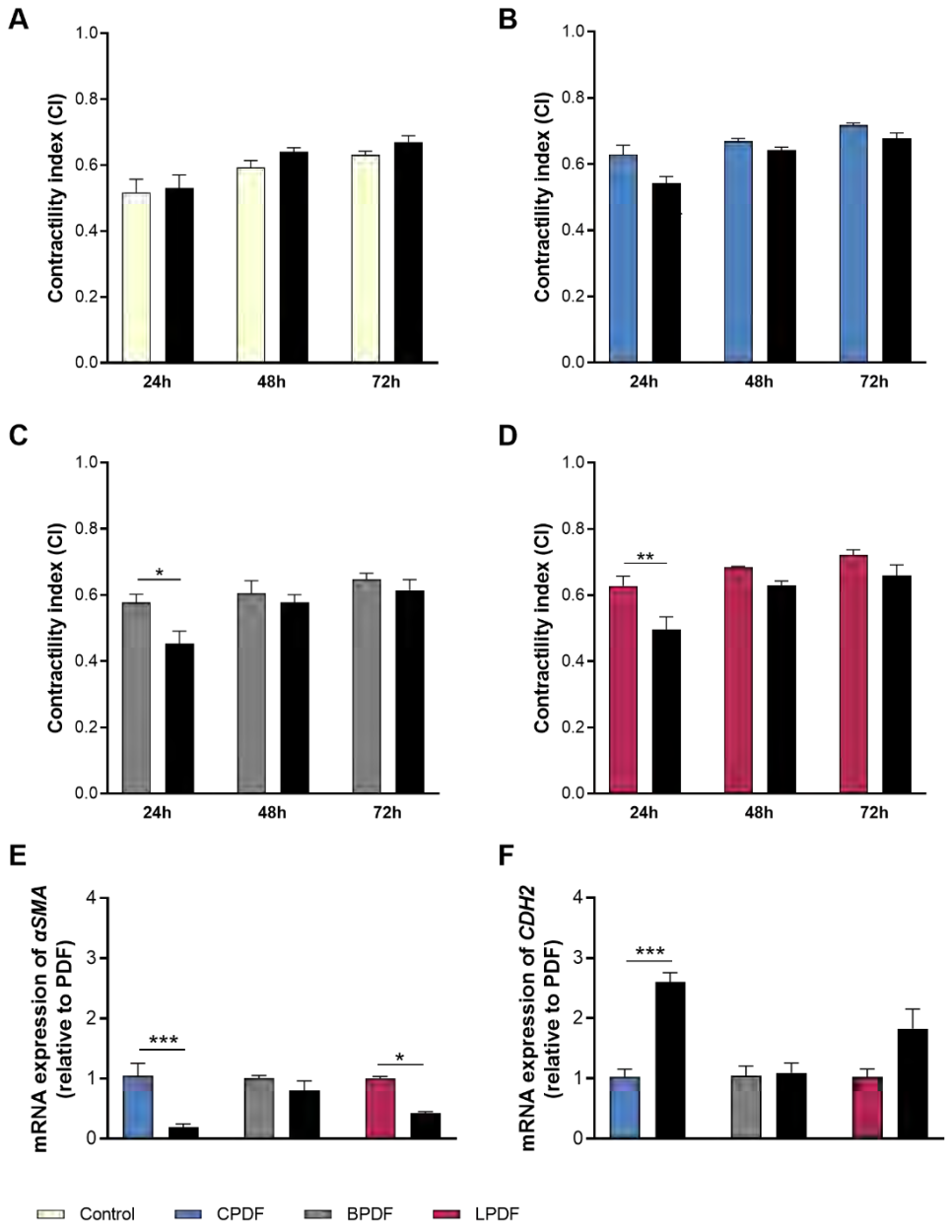

Figure 6: *Effect of 2DG in the CI of EA.hy926 cells in* ***(A)*** *Control,* ***(B)*** *CPDF,* ***(C)*** *BPDF,* ***(D)*** *LPDF groups at 24, 48, 72 hours and mRNA expression levels of* ***(E)*** *αSMA,* ***(F)*** *CDH2. *p < 0.05, **p < 0.01, ***p < 0.001; n=3. Data demonstrated as mean ± SEM.*

13.5 Transmembrane electrical resistance (TER) of MeT-5A and EA.hy926 cell monolayers or mesothelial and endothelial co-culture model

To assess the growth of mesothelial and endothelial cell monolayers or their combined co-culture *in vitro* model in filters, the TER was daily measured. As shown in **Figure 7**, there was a steady increase in TER values of mesothelial (day 1: 4.38 ± 0.23, day 2: 8.42 ± 0.25, day 3: 13.19 ± 0.35, day 4: 17.97 ± 0.30) or endothelial cell monolayer (day 1: 3.50 ± 0.18, day 2: 5.72 ± 0.22, day 3: 8.79 ± 0.36, day 4: 12.35 ± 0.43) over a period of about 4 days, when a gradual stabilization started happening and the TER reached a plateau at day 5 (MeT-5A: 18.48 ± 0.24, EA.hy926: 12.49 ± 0.42). When the two cell lines were cultured concomitantly in each side of the Snapwell/Transwell filter to mimic the two barriers in series as found on the PM, the TER tended to a plateau and quit climbing at day 7 (day 1: 3.12 ± 0.22, day 2: 5.90 ± 0.45, day 3: 12.75 ± 0.33, day 4: 16.11 ± 0.28, day 5: 19.44 ± 0.26, day 6: 21.03 ± 0.42, day 7: 21.34 ± 0.45). In all cases, the stabilization of TER indicated that the monolayers were fully formed. Comparing the TER values upon plateau establishment among the three different cell culture models, the co-culture model displayed a significantly higher TER value compared to the one of the mesothelial monolayer ($p < 0.001$) as well as the one of the endothelial monolayer ($p < 0.001$). Moreover, the TER of the mesothelial monolayer was higher than this of the endothelial monolayer ($p < 0.001$).

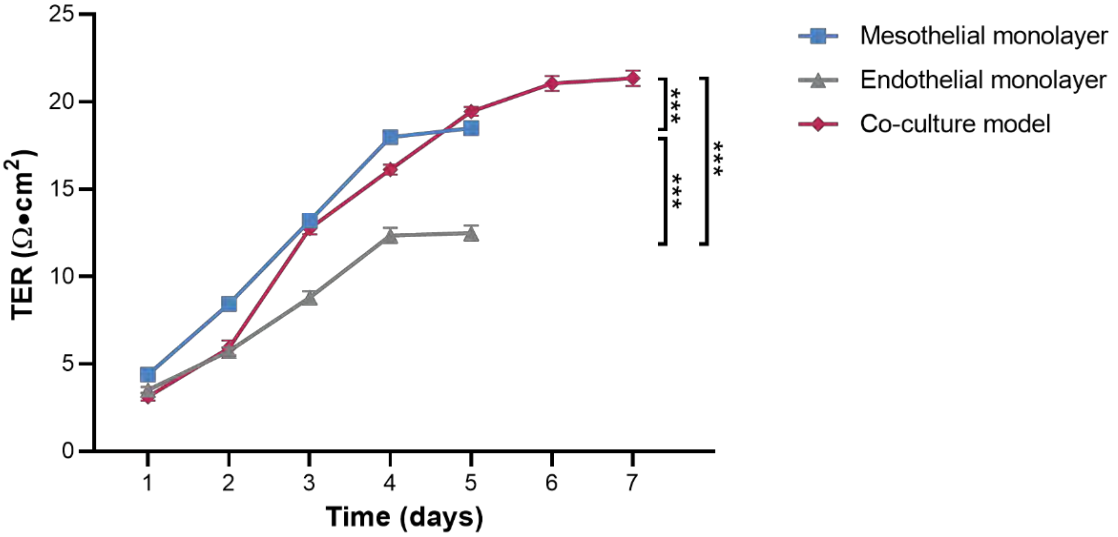

Figure 7: *Time course of monolayer growth of MeT-5A cells (blue square ■), EA.hy926 cells (grey triangle ▲), and their co-culture in both sides of the filter (MeT-5A upper side and EA.hy926 lower side; red rhombus ♦). ***p < 0.001 indicates comparisons of average maximum TER. n = 15-33. Data demonstrated as mean ± SEM.*

13.6 Alterations in the mesothelial barrier function after exposure of MeT-5A cells to PDF supplemented or not with 0.2 mM of 2DG

Snapwell filters with cultured mesothelial MeT-5A cell monolayers were mounted into Ussing chambers for monitoring of the barrier electrical resistance under the effect of PDF supplemented or not with 2DG over an incubation period of 4 hours. Exposure in all PDF significantly increased the R_{TM} outright (CPDF: t_{0h}: 88.50 ± 3.77, BPDF: t_{0h}: 36.00 ± 6.11, LPDF: t_{0h}: 32.50 ± 4.66) compared to control conditions (KRB: 16.73 ± 0.82, $p < 0.001$). In CPDF (t_{1h}: 69.75 ± 3.61, t_{2h}: 60.00 ± 1.78, t_{3h}: 50.75 ± 2.05, t_{4h}: 49.50 ± 2.53, $p < 0.001$) and BPDF (t_{1h}: 29.66 ± 5.36, t_{2h}: 29.33 ± 5.20, $p < 0.001$; t_{3h}: 26.33 ± 6.36, t_{4h}: 25.33 ± 6.64, $p < 0.01$) cases, the increased R_{TM} was preserved throughout the experimental time in contrast to LPDF that the increase was present for 3 hours (t_{1h}: 41.75 ± 4.78, t_{2h}: 33.25 ± 5.39, $p < 0.001$; t_{3h}: 26.25 ± 6.34, $p<0.01$) while at the end, the R_{TM} (t_{4h}: 22.00 ± 6.26) approximated the initial one prior to PDF treatment (**Figure 8A, C, E**).

When 2DG addition was tested, the supplementation of CPDF group significantly mitigated the increased R_{TM} (t_{0h}: 29.33 ± 1.85, $p < 0.01$; t_{1h}: 35.66 ± 6.76, t_{2h}: 31.66 ±

4.25, $p < 0.001$; t_{3h}: 27.00 ± 2.64, $p < 0.05$) compared to control conditions, whereas reversed this effect at the end of the experimental time (t_{4h}: 23.66 ± 2.18) also facilitating the paracellular transport of a 10 kDa dextran (2.78 ± 0.17, $p < 0.001$) but without affecting the paracellular transport of a 70 kDa dextran (0.97 ± 0.04; **Figure 8A, B**). In BPDF (t_{0h}: 24.00 ± 3.39, $p < 0.05$) and LPDF (t_{0h}: 32.50 ± 4.66, t_{1h}: 41.75 ± 4.78, $p < 0.05$) groups, the augmentation in R_{TM} after the 2DG administration was instantly apparent or preserved for an hour, respectively (**Figure 8C, E**) while in both PDF, the paracellular transport was increased only in case of the 10 kDa dextran and not of 70 kDa one (BPDF: 1.44 ± 0.11, $p < 0.05$; LPDF: 1.58 ± 0.07, $p < 0.01$; **Figure 8D, F**).

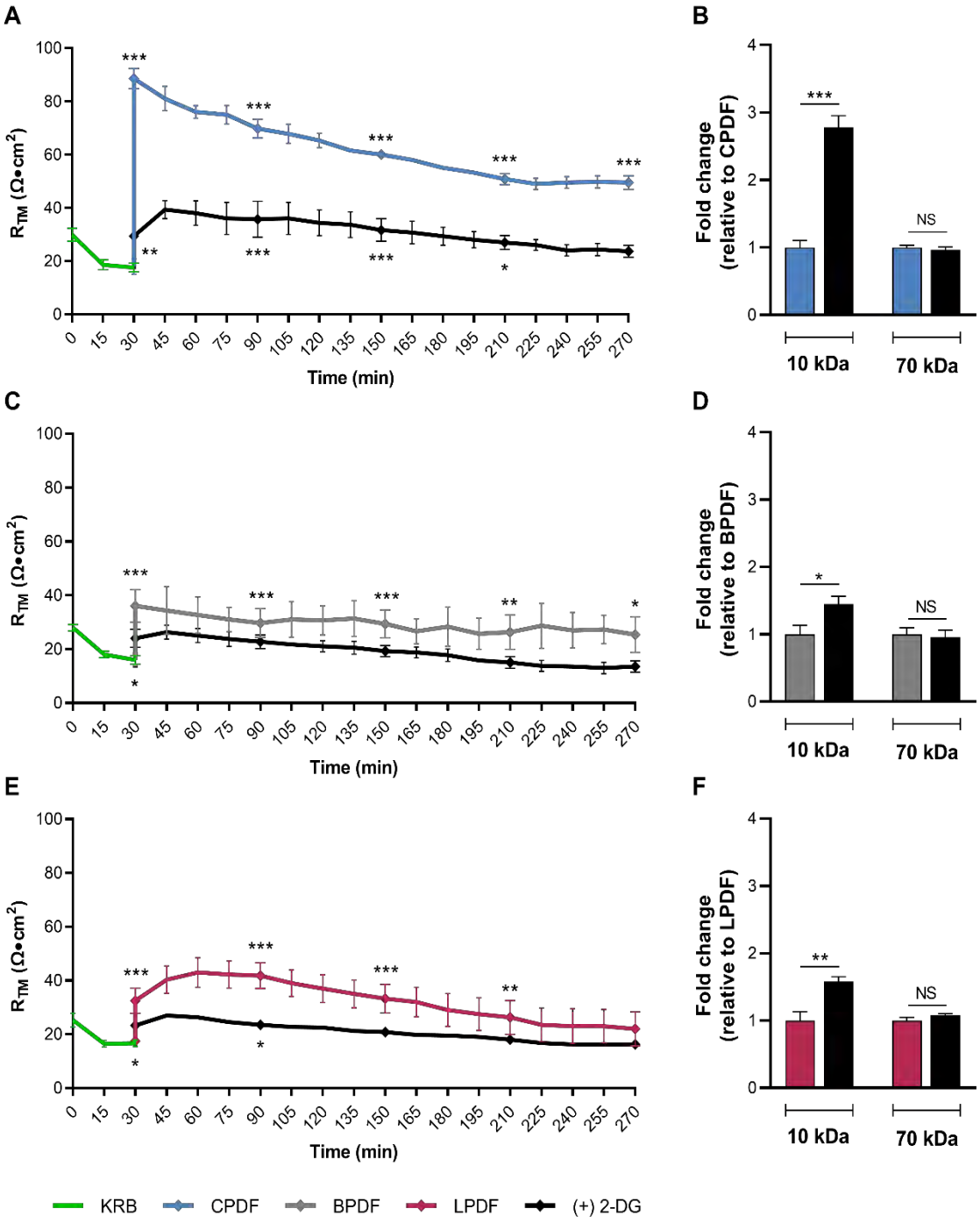

Figure 8: *Effect of CPDF with/without the addition of 2DG* ***(A)*** *on the barrier resistance (R_{TM}) of MeT-5A cells during a 4-hour incubation period, and* ***(B)*** *on the paracellular transport of 10 kDa, 70 kDa dextran expressed as fold change relative to PDF. The same description applies for* ***(C, D**, respectively)** BPDF and* ***(E, F**, respectively)** LPDF. **p < 0.05, **p < 0.01, ***p < 0.001, NS: no significant; n = 3-6. Data demonstrated as mean ± SEM.*

13.7 Alterations in the endothelial barrier function after exposure of EA.hy926 cells to PDF supplemented or not with 0.2 mM of 2DG

As shown in **Figure 9 (A, C, E)**, in all cases of PDF with/without 2DG addition (CPDF: 13.20 ± 1.24, CPDF/2DG: 18.33 ± 0.88, BPDF: 20.33 ± 1.45, BPDF/2DG: 21.75 ± 3.56, LPDF: 13.50 ± 3.09, LPDF/2DG: 17.00 ± 1.52), an instant increase (t_{0h}) in resistance of EA.hy926 cell monolayers was detected compared to control conditions (KRB: 3.95 ± 0.43, $p < 0.001$). Prolonged exposure of cell monolayers in the above experimental conditions did not affect permanently the R_{TM}, however, treatment with CPDF supplemented or not with 2DG maintained the increased resistance of endothelial barrier for 1 (CPDF/2DG: t_{1h}: 12.33 ± 2.40, $p < 0.001$) or 2 hours (CPDF: t_{1h}: 8.60 ± 1.93, $p < 0.001$; t_{2h}: 6.40 ± 2.01, $p < 0.05$), respectively. Moreover, the 2DG addition in BPDF diminished the flux of a 10 kDa dextran (0.82 ± 0.01, $p < 0.01$; **Figure 9D**) but no other significant change was found in the context of paracellular transport.

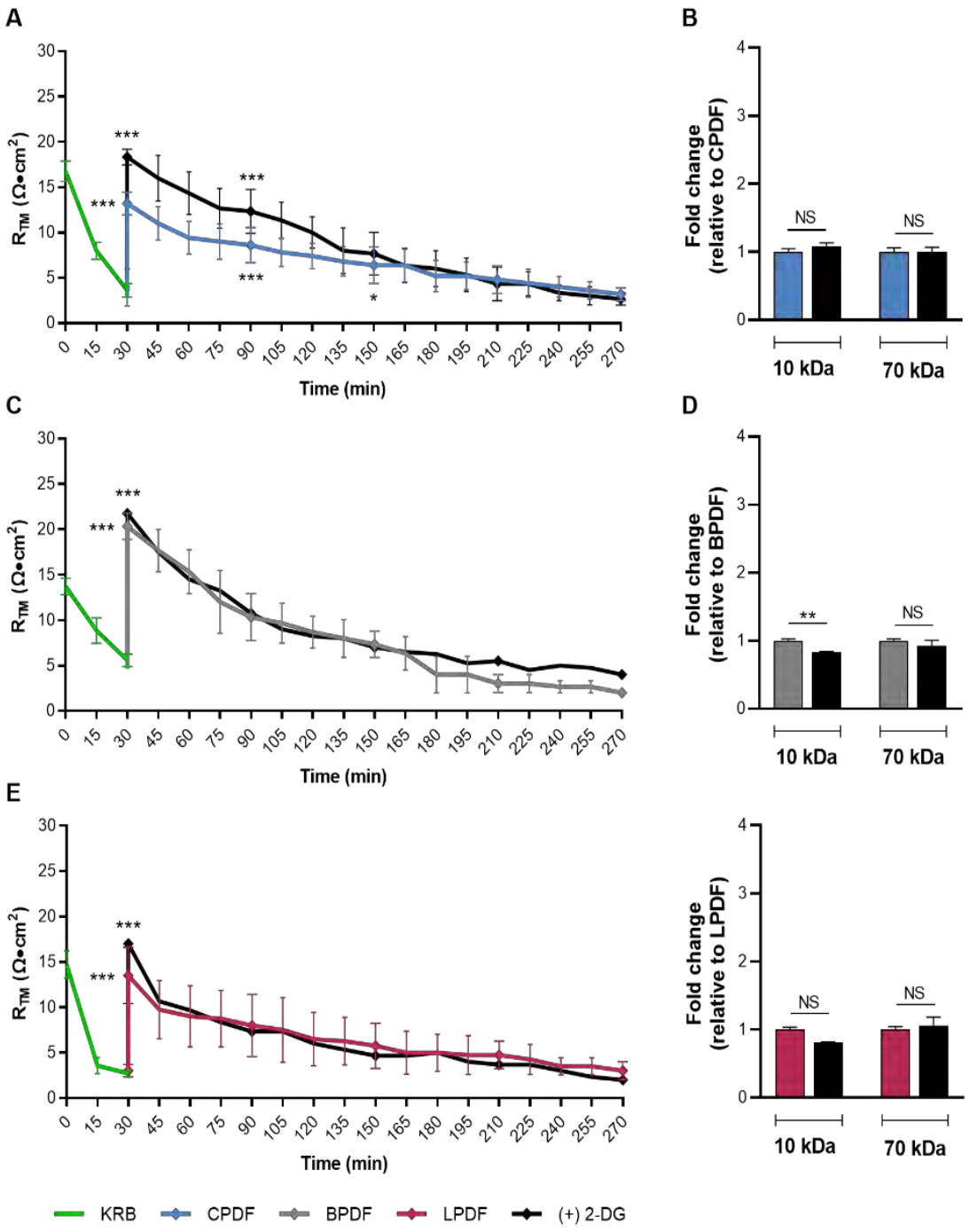

Figure 9: *Effect of CPDF with/without the addition of 2DG* ***(A)*** *on the barrier resistance (R_{TM}) of EA.hy926 cells during a 4-hour incubation period, and* ***(B)*** *on the paracellular transport of 10 kDa, 70 kDa dextran expressed as fold change relative to PDF. The same description applies for* ***(C, D**, respectively)** BPDF and* ***(E, F**, respectively)** LPDF. **p < 0.05, **p < 0.01, ***p < 0.001, NS: no significant; n = 3-6. Data demonstrated as mean ± SEM.*

13.8 Alterations in the combined mesothelial/endothelial barrier function after exposure of an *in vitro* co-culture model to PDF supplemented or not with 0.2 mM of 2DG

Besides the effects of PDF with/without 2DG addition in the mesothelial or endothelial barrier function, an *in vitro* co-culture model of mesothelial cells on the upper side of a Snapwell/Transwell filter and endothelial cells on the bottom side was also developed in order to explore the 2DG efficacy in mesothelial and endothelial combined barrier function and thus, better simulate the *in vivo* conditions. In this model, the CPDF increased the R_{TM} throughout the experimental 4-hour incubation period (t_{0h}: 24.33 ± 7.83, t_{1h}: 29.00 ± 8.00, t_{2h}: 24.33 ± 5.89, $p < 0.001$; t_{3h}: 21.00 ± 5.50, $p < 0.01$; t_{4h}: 19.66 ± 6.76, $p < 0.05$) compared to control (KRB: 9.66 ± 4.54). The addition of 2DG had the same effect but only up to 2 hours of incubation (t_{0h}: 28.00 ± 9.07, $p < 0.001$; t_{1h}: 23.33 ± 4.91, t_{2h}: 23.00 ± 4.72, $p < 0.01$; **Figure 10A**). The differences of the paracellular transport rate of a 10 kDa or 70 kDa dextran between the CPDF and the CPDF supplemented with 2DG were not statistically significant (**Figure 10B**). Moreover, the R_{TM} was sharply increased after exposure in BPDF (t_{0h}: 44.00 ± 8.50, $p < 0.001$) or LPDF (t_{0h}: 22.00 ± 1.52, $p < 0.001$) compared to control, however, this increase was preserved up to 2 hours in the case of BPDF (t_{1h}: 35.33 ± 7.88, $p < 0.01$; t_{2h}: 32.67 ± 6.67, $p < 0.05$) and up to 1 hour in the case of LPDF (t_{1h}: 12.67 ± 1.20, $p < 0.05$). An exact opposite effect was found after the addition of 2DG, which initially induced similar increase in the R_{TM} of both PDF groups (BPDF/2DG: 38.50 ± 5.28, $p < 0.001$; LPDF/2DG: 32.00 ± 2.08, $p < 0.001$) but it was evident only for 1 hour in the BPDF group (t_{1h}: 34.16 ± 5.52, $p < 0.001$) while for 2 hours in the LPDF one (t_{1h}: 22.33 ± 0.88, $p < 0.001$; t_{2h}: 19.00 ± 3.21, $p < 0.01$; **Figure 10C, E**). The effect of 2DG administration was also reflected on the diffusion of the 10 kDa dextran (BPDF/2DG: 1.23 ± 0.01, $p < 0.001$; LPDF/2DG: 0.76 ± 0.01, $p < 0.001$; **Figure 10D, F**).

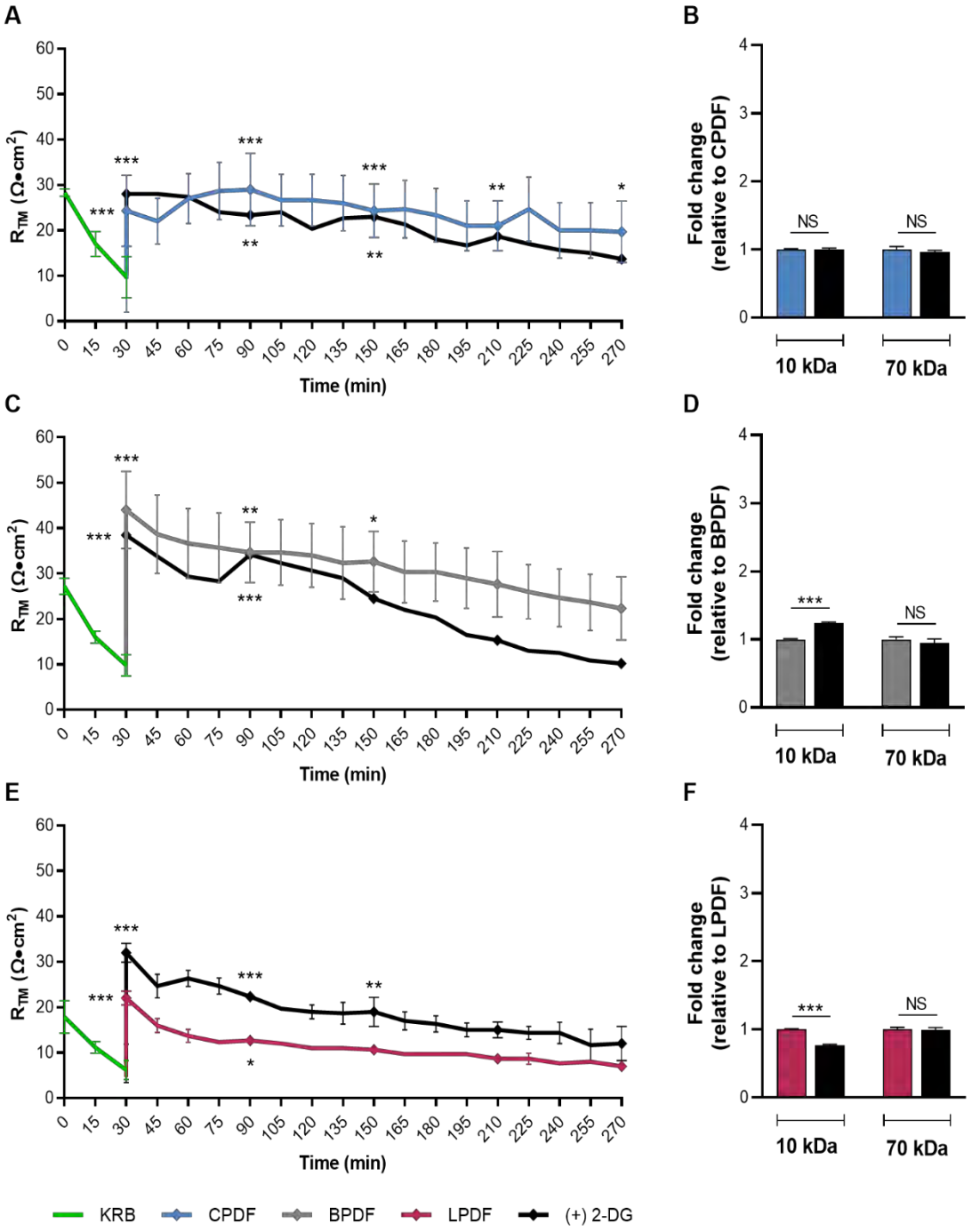

Figure 10: *Effect of CPDF with/without the addition of 2DG* ***(A)*** *on the barrier resistance (R_{TM}) of co-culture in vitro model during a 4-hour incubation period, and* ***(B)*** *on the paracellular transport of 10 kDa, 70 kDa dextran expressed as fold change relative to PDF. The same description applies for* ***(C, D****, respectively****)*** *BPDF and* ***(E, F****, respectively****)*** *LPDF. *p < 0.05, **p < 0.01, ***p < 0.001, NS: no significant; n = 3-6. Data demonstrated as mean ± SEM.*

13.9 Alterations in gene expression levels of molecular determinants of paracellular and transcellular permeability after PDF supplementation with 0.2 mM of 2DG

When the electrophysiological experiments were terminated, the mesothelial and endothelial monolayers were lysed for total RNA extraction to evaluate the effect of 2DG supplementation of PDF in molecular determinants of paracellular and transcellular permeability. As shown in **Figure 11**, the mRNA expression of the TJ components *CLDN-1* to *-5* and *ZO-1* as well as the co-transporter *SGLT2* was significantly altered under the effect of 2DG. In MeT-5A cells, incubation with CPDF/2DG significantly reduced the expression levels of *CLDN3* (-1.44 ± 0.18, $p < 0.01$), *CLDN4* (-0.52 ± 0.02, $p < 0.001$) and *SGLT2* (-0.85 ± 0.03, $p < 0.001$) genes, in contrast to EA.hy926 cells that demonstrated overexpression of *CLDN2* (1.78 ± 0.00, $p < 0.001$), *CLDN4* (1.52 ± 0.15, $p < 0.001$) and *CLDN5* (1.15 ± 0.06, $p < 0.001$). Incubation with BPDF/2DG caused a significant reduction in *CLDN1* (-0.38 ± 0.03, $p < 0.001$), *CLDN3* (-0.91 ± 0.08, $p < 0.001$) and *ZO1* (-1.41 ± 0.24, $p < 0.01$) genes, along with an increase in *CLDN4* (0.91 ± 0.10, $p < 0.01$) and *CLDN5* (1.62 ± 0.37, $p < 0.05$), whereas no significant effect whatsoever was found in endothelial cells. Incubation with LPDF/2DG significantly decreased the expression of *CLDN3* (-1.16 ± 0.18, $p < 0.001$), *CLDN4* (-0.48 ± 0.01, $p < 0.001$) and *SGLT2* (-0.18 ± 0.01, $p < 0.001$) genes in mesothelial cells, while *CLDN2* was overexpressed in both mesothelial (0.31 ± 0.02, $p < 0.001$) and endothelial cells (2.32 ± 0.06, $p < 0.01$).

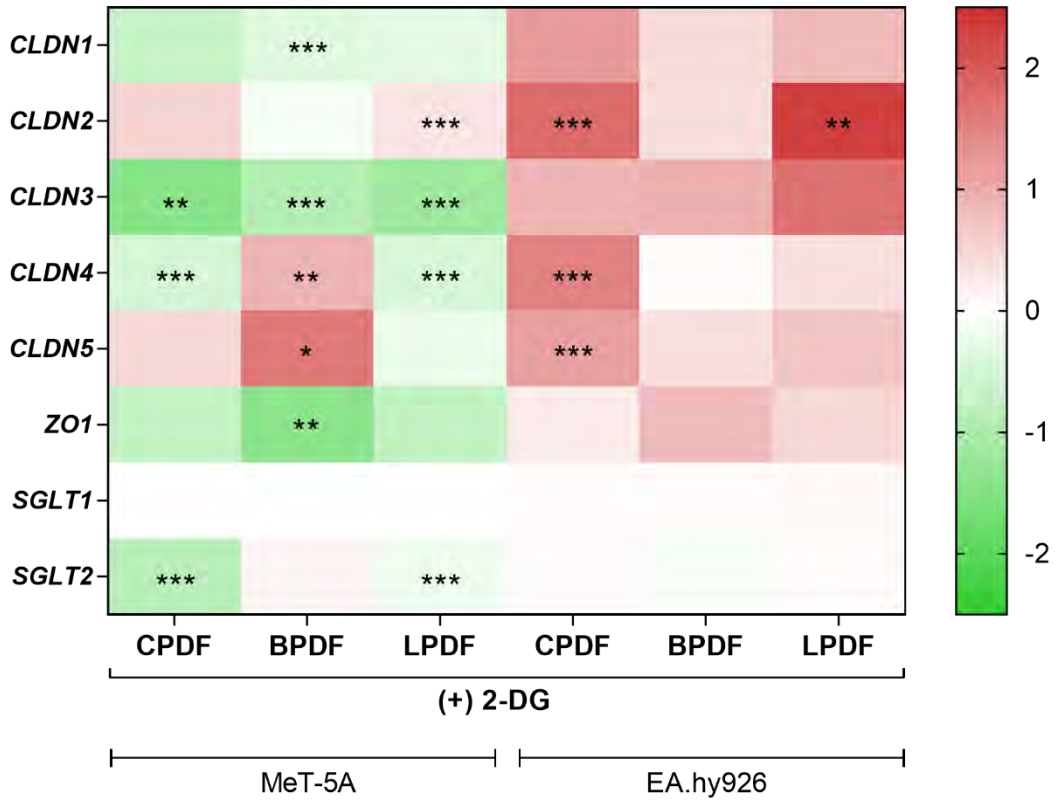

Figure 11: *Heatmap demonstration of the gene expression levels of CLDN1-5, ZO1, SGLT1 and SGLT2 in MeT-5A or EA.hy926 cells incubated with PDF supplemented with 2DG, expressed as fold change relative to PDF per se. Over-expressed genes are in shown in red and under-expressed genes are shown in green. n = 3-4.*

14. Discussion

The efficacy of PD treatment relies on the proper function of the PM as a dialyzing membrane. However, the PM functional integrity deteriorates within a few years post-PD onset, ultimately resulting in pronounced fibrosis and angiogenesis that leads to UF and PD dropout [143,184]. Although peritonitis episodes, along with the PD modality duration and the exposure load to glucose, were considered the main culprits of PM deterioration, recent evidence suggest that the major drivers of this process are the prolonged exposure to PDF and the glucose exposure load that eventually hinder the PD sustainability [119]. High glucose concentration that serves as the osmotic agent and the high GDP content in the PDF contribute to the vasculopathy of PM vessels, mesothelial cell loss and MMT as well as submesothelial thickening and fibrosis [119,183]. Thus, the development of more biocompatible PDF that would prevent or delay the PM deterioration is an area of intense inquiry in order to meet patient needs for a better PD treatment [16].

To this end, novel therapeutic strategies focus on either testing alternative osmotic agents or on the supplementation of currently available PDF with cytoprotective additives that would delay or reverse the PM degeneration without affecting its functional characteristics [197,216]. A very important example of PDF supplementation that has shown potential even in a human clinical trial is the dipeptide AlaGln. The addition of AlaGln has been shown to ameliorate oxidative stress and inflammatory responses, while most importantly in a phase II clinical trial it attenuated protein loss and increased potassium and phosphate removal that are clinically relevant outcomes [13]. More recently, it was demonstrated that both TGF-β stimulation and exposure to PDF induce in mesothelial cells what is called the Warburg effect that refers to aerobic hyper-glycolysis, facilitating not only energy demands but also MMT and subsequent fibrogenesis [17]. This finding suggested that suppression of the Warburg effect could prevent the above deleterious processes.

Indeed, 2DG at a concentration of 0.2 mM was experimentally shown to successfully inhibit the development of peritoneal fibrosis when added in a high-GDP containing PDF [17]. We have also previously reported that *in vitro* administration of 2DG to a concentration range up to 0.5 mM does not induce significant cell death [18]. However, prior to considering 2DG as an efficient PDF additive, its effects on the functional

characteristics of the PM during PD should be precisely described. Therefore, we sought to test *in vitro* the effects of 2DG PDF supplementation on the permeability of the two PM barriers to the transport of water and solutes, the mesothelial and the endothelial cell monolayers.

Here, to make sure that our system would be fit for such a study, we initially performed the collagen gel contraction assay with embedded mesothelial or endothelial cells to assess the impact of 0.2 mM 2DG addition in MMT-/EndoMT-like behaviour. The collagen gel contraction assay serves as a classic tool for the evaluation of the cell phenotype transition based on the decrement in collagenous gel diameter and thus, it is extensively used in the research field of inflammation and wound healing over the past four decades [217–219]. The beneficial antifibrotic effect of 2DG administration was confirmed in mesothelial cells under CPDF incubation as was the case in the study of Si *et al.*, while it was also valid in endothelial cells [17]. More specifically, the CI of MeT-5A and EA.hy926 cells embedded in collagen gels was increased after exposure to CPDF and/or LPDF, accompanied by equivalent alterations at the gene expression level of the mesenchymal markers *αSMA* and *CDH2*, indicating that the long-term PD induces MMT and EndoMT. Although literature is lacking regarding the investigation of PDF-induced MMT by the means of collagen gel contraction assay, it has been shown that high glucose levels significantly impair the wound healing process associated with collagen-rich matrix reorganization, while the expression profile of a multitude of epithelial or mesenchymal markers such as αSMA and N-cadherin has been considered as an unequivocal indicator of MMT/EndoMT process, and studied in relation to PD therapy [31,220,221]. In our study, the addition of 2DG counteracted the increased contractile behaviour of both cell lines exposed to PDF of different composition and thus, our *in vitro* system of 2DG characterization was efficient for further evaluation of the PM barrier function integrity.

Measurement of TER and diffusion rate of fluorescently labelled dextrans of varying sizes comprise common techniques to assess monolayer permeability [222]. In normal conditions with the cell monolayers incubated in regular cell culture medium, the maximum TER of the co-culture model was significantly higher than the TER of the mesothelial monolayer which was also higher than the TER of the endothelial monolayer. These findings are rational given that although the transcapillary permeability was traditionally considered when discussing the PM permeability based

on the three-pore model, increasing evidence strongly support that the mesothelium as well as the capillary endothelium provide a barrier for PD [223–225]. Starting from electrophysiological measurements in human parietal peritoneum to the provision of morphometric evidence of a clearly robust mesothelial monolayer and three distinct capillary layers in the PM of children biopsies and finally, recently published molecular and functional evidence, the barrier contribution of both mesothelium and endothelium in PM has been verified [176,226–229].

Snapwell filters with fully formed cell monolayers were mounted on Ussing chambers to test mesothelial and endothelial barrier behaviour upon exposure of the clinically relevant side of the monolayers to PDF per se or PDF supplemented with 2DG. The Ussing system is widely utilized as a powerful tool for studying permeability characteristics of either membrane tissues or cell monolayers grown on filters in the context of PD [176,227,230–235]. Given that upon introduction of PDF to the peritoneal cavity of a patient, it firstly encounters the apical side of the PM mesothelium and once it penetrates in the PM, it encounters the basolateral side of the capillary walls, as clinically relevant sides were considered the apical one for the cases of mesothelial monolayer and co-culture model, while the basolateral one for the endothelial monolayer. In all three studied PDF, treatment of the mesothelial monolayer caused a sharp increase in the R_{TM} which persisted throughout the experimental time, unlike endothelial monolayer that the increased R_{TM} was preserved for minutes in the case of the two low-GDP PDF (BPDF, LDPF) to 2 hours in the case of high-GDP CPDF without affecting permanently the endothelial barrier function. Taking also into consideration that the PDF-induced increase in the R_{TM} of the co-culture model was significant either throughout the 4-hour incubation period (CPDF) or for 1 to 2 hours (LPDF, BPDF respectively), the most sensitive cell monolayer to the exposure to PDF content is suggested to be the mesothelium which anyhow is the first one coming in direct contact with the PDF clinically.

Interestingly, other *in vitro* studies have also demonstrated significant modifications in the barrier function of either HPMC exposed to glucose or mesothelial cells isolated from PD effluents, along with rearrangements in distribution and expression pattern of TJ components such as Claudin-1, Occludin, ZO-1 [166,167]. The findings regarding the dysregulation of paracellular permeability due to high glucose levels have been reproduced in *in vivo* animal studies in a rat model of diabetes or after treatment with

PDF [169,236]. With regards to paracellular and transcellular permeability of endothelium, a similar effect in response to hyperglycemia has been shown in different endothelial cell types while very recently, the effects of PDF of different composition on the cell-cell junctions associated proteins were highlighted [170,174,237,238].

The efficacy of 2DG as a modulator of the mesothelial and endothelial barrier function in the context of PDF-induced disruption was investigated in electrophysiological, biophysical and molecular level. Supplementation of PDF with 0.2 mM of 2DG significantly ameliorated the mesothelial permeability reinstating the augmented R_{TM} while increasing the paracellular flux of the 10 kDa FITC dextran. This is considered a key finding since the 2DG addition is suggested to accelerate the removal of middle-MW molecules such as the 12 kDa β_2-microglobulin, through the mesothelium irrespective of the PDF type. In fact, the main advantage of hemodiafiltration modality versus conventional HD is the enhanced removal of middle-MW uremic toxins accompanied by superior outcomes and survival, while ineffective clearance has been associated with the detrimental effects of uremia [239–241]. In combination with the absence of significant alterations in the paracellular flux of the 70 kDa FITC dextran which better resembles the size of human albumin (66.5 kDa), 2DG may be a potential candidate to overcome the outstanding clinical problem of hypoalbuminemia that afflicts many ESKD patients [242].

Most importantly, the above findings were accompanied by diminished gene expression levels of sealing and scaffolding TJ components, along with increased *CLDN2* which mediates the diffusive transport of sodium and water [95]. Since it has been shown that de-regulation of claudins is a hallmark of processes relying on cell phenotype transition like carcinogenesis and tumour metastasis, the modified claudin gene expression profile after 2DG administration could potentially be linked to the PD-related antifibrotic role of 2DG [243–245]. Furthermore, the early stages of MMT leading to the loosening of the mesothelial barrier were highlighted in a recent review as an interventional target for preserving the PM functional deterioration during PD [246]. Given the results on collagen gel contraction assay that were reported above, it would be plausible to suggest that the 2DG PDF supplementation presents a dual protective effect by alleviating MMT profibrotic potential while reversing the mesothelial and endothelial barrier function perturbation occurring due to PDF bio-incompatibility. Besides determinants of paracellular transport, we also studied the expression of *SGLT1* and *SGLT2* genes

because of their key role in glucose absorption as shown initially in a rat model and later in HPMC with both SGLT-1 and -2 protein expression to have significantly increased after exposure to PDF [115,165,236,247]. Although the exposure of mesothelial cells to PDF supplemented with 2DG did not significantly modify the *SGLT1* expression, *SGLT2* was decreased under 2DG addition to CPDF or LPDF. This finding demonstrates another cytoprotective effect of 2DG administration, several studies have corroborated that blockade of SGLT2 channel by specific inhibitors mitigates peritoneal fibrosis while improves UF [115,165,248–250].

With regards to endothelium, it was already mentioned that in all cases the sharp increase in monolayer resistance was reinstated stepwise, however the expression of *CLDN-2*, *-4* and *-5* was significantly increased after 2DG addition to CPDF, while a similar effect only in *CLDN2* was detected under LPDF+(2DG) condition. Therefore, the lack of persistent alterations in the permeability of endothelial cells because of 2DG PDF supplementation could be explained by the opposing functional characteristics of these three claudins (Claudin-2 is a pore-forming protein, Claudin-5 is a sealing protein, and Claudin-4 depends on its stoichiometry with other claudins). Our findings are consistent with previously published data about endothelial barrier function and claudin expression in the context of PD [14,201]. More specifically, HUVEC monolayers exposed to CPDF and LDPF for 5 hours with the addition of the cytoprotective agent AlaGln showed restoration at protein expression level of ZO-1 and Claudin-5 [14]. Furthermore, HUVEC monolayers that were exposed to CPDF for 5 hours and were used initially for TER measurements along with assessment of diffusion rate of 10 kDa dextran, and subsequently for immunofluorescence staining of ZO-1 and CLDN5, exhibited increased CLDN5 abundance as in our case with 2DG after 4 hours of exposure [201]. It is important to note that our gene expression level measurements were performed in EA.hy926 monolayers after the end of the PDF exposure in Ussing System experiments, therefore the two models are considered very similar and comparable.

Findings of the mesothelial/endothelial co-culture model resembled these of the mesothelial monolayer except for the LPDF with/without 2DG where an opposite effect was found. Indeed, in the only one comparable to our co-culture model study, the barrier function was attributed mainly to the mesothelial cell monolayer, whereas the paracellular transport was defined by the crosstalk of the mesothelial and endothelial monolayers, which could explain the data variability among PDF type regarding the 10

kDa FITC dextran diffusion rate found in our case [251]. More particularly, in the above study, a decellularized porcine small intestinal submucosa was used as scaffold on top of which human dermal fibroblasts, LP9 mesothelial cells and HUVEC were seeded at days 0, 4 and 7, respectively to mimic the human peritoneum, and TER as well as 4 kDa FITC dextran flux were monitored until day 16. The results indicated that the mesothelial cell monolayer was fully developed at day 7 with the TER to be further increased after HUVEC addition up to day 9, while the permeability to FITC dextran was obstructed approximately by 60% by LP9 and only by 35% by HUVEC. Collectively, these findings indicate that the mesothelial barrier coming in direct contact with PDF during a PD exchange is more sensitive to their supraphysiological glucose composition and subsequently, the main culprit for the inadequate UF function of PM in long-term application of PD.

In conclusion, our data from the present study showed that suppression of the Warburg effect by 2DG administration led to regression of MMT and EndoMT; this antifibrotic effect on both mesothelial and endothelial cells exposed to conventional and bio-compatible PDF of different composition was further accompanied by functional improvement of the PM barriers permeability; which was mirrored at the gene expression level by the changes shown in the gene expression of TJ components. The changes were mostly apparent in the mesothelial than in the endothelial barrier as shown by means of electrophysiology, biophysical and molecular assays. Thus, the supplementation of commercially available PDF with 0.2 mM 2DG could ameliorate the PM barrier function along with the mitigation of the fibrotic process, targeting to the two cornerstones of PD failure, namely the UFF and peritoneal fibrosis. However, these encouraging results of the use of 2DG as a modulating agent in different PDF types should be further explored in order to have a full view of the changes of the molecular counterparts of TJs during PD in order to modulate and improve its performance and lifetime.

REFERENCES

1. Robinson, B. V. Observations upon the Absorption of Fluids by the Peritoneum. *Ann. Surg.* **1897**, *25*, 332–350.
2. Moncrief, J.W. The Birth and Development of Continuous Ambulatory Peritoneal Dialysis. *Contrib. Nephrol.* **2017**, *189*, 85–90.
3. Kramer, A.; Pippias, M.; Noordzij, M.; Stel, V.S.; Afentakis, N.; Ambühl, P.M.; Andrusev, A.M.; Fuster, E.A.; Arribas Monzón, F.E.; Asberg, A.; et al. The European Renal Association - European Dialysis and Transplant Association (ERA-EDTA) Registry Annual Report 2015: a summary. *Clin. Kidney J.* **2018**, *11*, 108–122.
4. Mehrotra, R.; Devuyst, O.; Davies, S.J.; Johnson, D.W. The current state of peritoneal dialysis. *J. Am. Soc. Nephrol.* **2016**, *27*, 3238–3252.
5. Nataatmadja, M.S.; Johnson, D.W.; Pascoe, E.M.; Darssan, D.; Hawley, C.M.; Cho, Y. Associations between peritoneal glucose exposure, glucose degradation product exposure, and peritoneal membrane transport characteristics in Peritoneal Dialysis patients: Secondary analysis of the balANZ Trial. *Perit. Dial. Int.* **2018**, *38*, 349–355.
6. Catalan, M.P.; Santamaría, B.; Reyero, A.; Ortiz, A.; Egido, J.; Ortiz, A. 3,4-di-deoxyglucosone-3-ene promotes leukocyte apoptosis. *Kidney Int.* **2005**, *68*, 1303–1311.
7. Betjes, M.G.H.; Habib, S.M.; Boeschoten, E.W.; Hemke, A.C.; Struijk, D.G.; Westerhuis, R.; Abrahams, A.C.; Korte, M.R. Significant Decreasing Incidence of Encapsulating Peritoneal Sclerosis in the Dutch Population of Peritoneal Dialysis Patients. *Perit. Dial. Int.* **2017**, *37*, 230–234.
8. Johnson, D.W.; Brown, F.G.; Clarke, M.; Boudville, N.; Elias, T.J.; Foo, M.W.Y.; Jones, B.; Kulkarni, H.; Langham, R.; Ranganathan, D.; et al. Effects of biocompatible versus standard fluid on peritoneal dialysis outcomes. *J. Am. Soc. Nephrol.* **2012**, *23*, 1097–1107.
9. van Diepen, A.T.N.; Coester, A.M.; Janmaat, C.J.; Dekker, F.W.; Struijk, D.G.; Krediet, R.T. Comparison of Longitudinal Membrane Function in Peritoneal Dialysis Patients According to Dialysis Fluid Biocompatibility. *Kidney Int.*

Reports **2020**, *5*, 2183–2194.

10. Dousdampanis, P.; Musso, C.G.; Trigka, K. Icodextrin and peritoneal dialysis: advantages and new applications. *Int. Urol. Nephrol.* **2018**, *50*, 495–500.
11. Tjiong, H.L.; Swart, R.; van den Berg, J.W.; Fieren, M.W. Amino Acid-based Peritoneal Dialysis solutions for malnutrition: New Perspectives. *Perit. Dial. Int.* **2009**, *29*, 384–393.
12. Masola, V.; Bonomini, M.; Onisto, M.; Ferraro, P.M.; Arduini, A.; Gambaro, G. Biological effects of XyloCore, a glucose sparing PD solution, on mesothelial cells: Focus on mesothelial-mesenchymal transition, inflammation and angiogenesis. *Nutrients* **2021**, *13*, 2282.
13. Vychytil, A.; Herzog, R.; Probst, P.; Ribitsch, W.; Lhotta, K.; Machold-Fabrizii, V.; Wiesholzer, M.; Kaufmann, M.; Salmhofer, H.; Windpessl, M.; et al. A randomized controlled trial of alanyl-glutamine supplementation in peritoneal dialysis fluid to assess impact on biomarkers of peritoneal health. *Kidney Int.* **2018**, *94*, 1227–1237.
14. Bartosova, M.; Herzog, R.; Ridinger, D.; Levai, E.; Jenei, H.; Zhang, C.; González Mateo, G.T.; Marinovic, I.; Hackert, T.; Bestvater, F.; et al. Alanyl-glutamine restores tight junction organization after disruption by a conventional peritoneal dialysis fluid. *Biomolecules* **2020**, *10*, 1178.
15. Herzog, R.; Sacnun, J.M.; González-Mateo, G.; Bartosova, M.; Bialas, K.; Wagner, A.; Unterwurzacher, M.; Sobieszek, I.J.; Daniel-Fischer, L.; Rusai, K.; et al. Lithium preserves peritoneal membrane integrity by suppressing mesothelial cell αB-crystallin. *Sci. Transl. Med.* **2021**, *13*, eaaz9705.
16. Schmitt, C.P.; Aufricht, C. Is there such a thing as biocompatible peritoneal dialysis fluid? *Pediatr. Nephrol.* **2017**, *32*, 1835–1843.
17. Si, M.; Wang, Q.; Li, Y.; Lin, H.; Luo, D.; Zhao, W.; Dou, X.; Liu, J.; Zhang, H.; Huang, Y.; et al. Inhibition of hyperglycolysis in mesothelial cells prevents peritoneal fibrosis. *Sci. Transl. Med.* **2019**, *11*, eaav5341.
18. Gerogianni, I.; Pitaraki, E.; Jagirdar, R.M.; Kouliou, O.; Giannakou, L.; Giannopoulos, S.; Papazoglou, E.; Hatzoglou, C.; Gourgoulianis, K.I.; Zarogiannis, S.G. 2-Deoxy-glucose enhances the effect of Cisplatin and

Pemetrexed in reducing malignant pleural mesothelioma cell proliferation but not spheroid growth. *Anticancer Res.* **2019**, *39*, 3809–3814.

19. Blackburn, S.C.; Stanton, M.P. Anatomy and physiology of the peritoneum. *Semin. Pediatr. Surg.* **2014**, *23*, 326–330.

20. Tanaka, K.; Hayakawa, T.; Maeda, S.; Kuwahara-Otani, S.; Seki, M. Distribution and ultrastructure of afferent fibers in the parietal peritoneum of the rat. *Anat. Rec. (Hoboken).* **2011**, *294*, 1736–1742.

21. van Baal, J.O.A.M.; Van de Vijver, K.K.; Nieuwland, R.; van Noorden, C.J.F.; van Driel, W.J.; Sturk, A.; Kenter, G.G.; Rikkert, L.G.; Lok, C.A.R. The histophysiology and pathophysiology of the peritoneum. *Tissue Cell* **2017**, *49*, 95–105.

22. Gazvani, R.; Templeton, A. Peritoneal environment, cytokines and angiogenesis in the pathophysiology of endometriosis. *Reproduction* **2002**, *123*, 217–226.

23. Capobianco, A.; Cottone, L.; Monno, A.; Manfredi, A.A.; Rovere-Querini, P. The peritoneum: healing, immunity, and diseases. *J. Pathol.* **2017**, *243*, 137–147.

24. Isaza-Restrepo, A.; Martin-Saavedra, J.S.; Velez-Leal, J.L.; Vargas-Barato, F.; Riveros-Dueñas, R. The peritoneum: Beyond the tissue - A review. *Front. Physiol.* **2018**, *9*, 738.

25. Kastelein, A.W.; Vos, L.M.C.; de Jong, K.H.; van Baal, J.O.A.M.; Nieuwland, R.; van Noorden, C.J.F.; Roovers, J.P.W.R.; Lok, C.A.R. Embryology, anatomy, physiology and pathophysiology of the peritoneum and the peritoneal vasculature. *Semin. Cell Dev. Biol.* **2019**, *92*, 27–36.

26. Healy, J.C.; Reznek, R.H. The peritoneum, mesenteries and omenta: normal anatomy and pathological processes. *Eur. Radiol.* **1998**, *8*, 886–900.

27. Wainwright, S. Langman's Medical Embryology. 11th Edition. *J. Phys. Ther. Educ.* **2010**, *24*, 81.

28. Byrnes, K.G.; Walsh, D.; Dockery, P.; McDermott, K.; Coffey, J.C. Anatomy of the mesentery: Current understanding and mechanisms of attachment. *Semin. Cell Dev. Biol.* **2019**, *92*, 12–17.

29. Michailova, K.N. The serous membranes in the cat. Electron microscopic

observations. *Ann. Anat.* **1996**, *178*, 413–424.

30. Mutsaers, S.E. The mesothelial cell. *Int. J. Biochem. Cell Biol.* **2004**, *36*, 9–16.

31. Mutsaers, S.E.; Birnie, K.; Lansley, S.; Herrick, S.E.; Lim, C.B.; Prêle, C.M. Mesothelial cells in tissue repair and fibrosis. *Front. Pharmacol.* **2015**, *6*, 113.

32. Fang, W.; Qian, J.Q.; Yu, Z.Y.; Chen, S.S. Morphological changes of the peritoneum in peritoneal dialysis patients. *Chin. Med. J. (Engl).* **2004**, *117*, 862–866.

33. Dobbie, J.W.; Anderson, J.D. Ultrastructure, distribution, and density of lamellar bodies in human peritoneum. *Perit. Dial. Int. J. Int. Soc. Perit. Dial.* **1996**, *16*, 482–487.

34. Evanko, S.P.; Tammi, M.I.; Tammi, R.H.; Wight, T.N. Hyaluronan-Dependent Pericellular Matrix. *Adv. Drug Deliv. Rev.* **2007**, *59*, 1351.

35. Kawanishi, K. Diverse properties of the mesothelial cells in health and disease. *Pleura and Peritoneum* **2016**, *1*, 79–89.

36. Beyene, R.T.; Kavalukas, S.L.; Barbul, A. Intra-abdominal adhesions: Anatomy, physiology, pathophysiology, and treatment. *Curr. Probl. Surg.* **2015**, *52*, 271–319.

37. Batra, H.; Antony, V.B. The pleural mesothelium in development and disease. *Front. Physiol.* **2014**, *5*, 284.

38. Kalluri, R.; Weinberg, R.A. The basics of epithelial-mesenchymal transition. *J. Clin. Invest.* **2009**, *119*, 1420–1428.

39. Mutsaers, S.E. *Mesothelial cells: Their structure, function and role in serosal repair*;

40. Citi, S. The mechanobiology of tight junctions. *Biophys. Rev.* **2019**, *11*, 783–793.

41. Otani, T.; Furuse, M. Tight junction structure and function revisited. *Trends Cell Biol.* **2020**, *30*, 805–817.

42. Zihni, C.; Terry, S.J. RhoGTPase signalling at epithelial tight junctions: Bridging the GAP between polarity and cancer. *Int. J. Biochem. Cell Biol.* **2015**, *64*, 120–125.

43. Hartsock, A.; Nelson, W.J. Adherens and tight junctions: Structure, function and

connections to the actin cytoskeleton. *Biochim. Biophys. Acta - Biomembr.* **2008**, *1778*, 660–669.

44. Oshima, A. Structural insights into gap junction channels boosted by cryo-EM. *Curr. Opin. Struct. Biol.* **2020**, *63*, 42–48.

45. Beyer, E.C.; Berthoud, V.M. Gap junction gene and protein families: Connexins, innexins, and pannexins. *Biochim. Biophys. acta. Biomembr.* **2018**, *1860*, 5–8.

46. Nielsen, M.S.; Axelsen, L.N.; Sorgen, P.L.; Verma, V.; Delmar, M.; Holstein-Rathlou, N.-H. Gap Junctions. *Compr Physiol* **2012**, *2*.

47. Kowalczyk, A.P.; Green, K.J. Structure, function, and regulation of desmosomes. *Prog. Mol. Biol. Transl. Sci.* **2013**, *116*, 95–118.

48. Schmidt, A.; Koch, P.J. Desmosomes: Just Cell Adhesion or Is There More? *Cell Adh. Migr.* **2007**, *1*, 28–32.

49. Green, K.J.; Roth-Carter, Q.; Niessen, C.M.; Nichols, S.A. Tracing the Evolutionary Origin of Desmosomes. *Curr. Biol.* **2020**, *30*, R535–R543.

50. Ihrie, R.A.; Marques, M.R.; Nguyen, B.T.; Horner, J.S.; Papazoglu, C.; Bronson, R.T.; Mills, A.A.; Attardi, L.D. Perp is a p63-regulated gene essential for epithelial integrity. *Cell* **2005**, *120*, 843–856.

51. Nievers, M.G.; Schaapveld, R.Q.J.; Sonnenberg, A. Biology and function of hemidesmosomes. *Matrix Biol.* **1999**, *18*, 5–17.

52. Hirako, Y.; Owaribe, K. Hemidesmosomes and Their Unique Transmembrane Protein BP180. *Microsc. Res. Tech* **1998**, *43*, 207–217.

53. Tsuruta, D.; Hashimoto, T.; Hamill, K.J.; Jones, J.C.R. Hemidesmosomes and focal contact proteins: Functions and cross-talk in keratinocytes, bullous diseases and wound healing. *J. Dermatol. Sci.* **2011**, *62*, 7.

54. Hann, L.E.; Hall, D.A.; Black, E.B.; Ferrucci, J.T. Mittelschmerz: Sonographic Demonstration. *JAMA* **1979**, *241*, 2731–2732.

55. Yoshikawa, T.; Hayashi, N.; Maeda, E.; Matsuda, I.; Sasaki, H.; Ohtsu, H.; Ohtomo, K. Peritoneal Fluid Accumulation in Healthy Men and Postmenopausal Women: Evaluation on Pelvic MRI. *Am. J. Roentgenol.* **2013**, *200*, 1181–1185.

56. Tarn, A.C.; Lapworth, R. Biochemical analysis of ascitic (peritoneal) fluid: what

should we measure? *Ann. Clin. Biochem.* **2010**, *47*, 397–407.

57. Abdollahi, A.; Nozarian, Z. Diagnostic value of measurement specific gravity by refractometric and dipstick method in differentiation between transudate and exudate in pleural and peritoneal fluid. *Iran. J. Pathol.* **2016**, *11*, 363–369.

58. Rippe, B. Free water transport, small pore transport and the osmotic pressure gradient three-pore model of peritoneal transport. *Nephrol. Dial. Transplant.* **2008**, *23*, 2147–2153.

59. Seames, E.L.; Moncrief, J.W.; Popovich, R.P. A distributed model of fluid and mass transfer in peritoneal dialysis. *Am. J. Physiol.* **1990**, *258*, R958–R972.

60. Rippe, B. A three-pore model of peritoneal transport. *Perit. Dial. Int.* **1993**, *13*, S35-8.

61. Waniewski, J.; Poleszczuk, J.; Antosiewicz, S.; Baczyński, D.; Gałach, M.; Pietribiasi, M.; Wańkowicz, Z. Can the three pore model correctly describe peritoneal transport of protein? *ASAIO J.* **2014**, *60*, 576–581.

62. Devuyst, O.; Ni, J. Aquaporin-1 in the peritoneal membrane: Implications for water transport across capillaries and peritoneal dialysis. *Biochim. Biophys. Acta - Biomembr.* **2006**, *1758*, 1078–1084.

63. Devuyst, O.; Goffin, E. Water and solute transport in peritoneal dialysis: models and clinical applications. *Nephrol. Dial. Transplant.* **2008**, *23*, 2120–2123.

64. Devuyst, O.; Rippe, B. Water transport across the peritoneal membrane. *Kidney Int.* **2014**, *85*, 750–758.

65. Flessner, M.F. Endothelial Glycocalyx and the Peritoneal Barrier. *Perit. Dial. Int.* **2008**, *28*, 6–12.

66. Kaissling, B.; Le Hir, M. The renal cortical interstitium: Morphological and functional aspects. *Histochem. Cell Biol.* **2008**, *130*, 247–262.

67. Stachowska-Pietka, J.; Waniewski, J.; Flessner, M.F.; Lindholm, B. Concomitant bidirectional transport during peritoneal dialysis can be explained by a structured interstitium. *Am. J. Physiol. - Hear. Circ. Physiol.* **2016**, *310*, H1501–H1511.

68. Rippe, B.; Venturoli, D. Simulations of osmotic ultrafiltration failure in CAPD using a serial three-pore membrane/fiber matrix model. *Am. J. Physiol. - Ren.*

Physiol. **2007**, *292*, F1035–F1043.

69. Fusshoeller, A. Histomorphological and functional changes of the peritoneal membrane during long-term peritoneal dialysis. *Pediatr. Nephrol.* **2008**, *23*, 19–25.

70. Salzer, W.L. Peritoneal dialysis-related peritonitis: challenges and solutions. *Int. J. Nephrol. Renovasc. Dis.* **2018**, *11*, 173–186.

71. Faull, R.J. Peritoneal Defenses Against Infection: Winning the Battle but Losing the War? *Semin. Dial.* **2000**, *13*, 47–53.

72. Yung, S.; Chan, T.M. Pathophysiological Changes to the Peritoneal Membrane during PD-Related Peritonitis: The Role of Mesothelial Cells. *Mediators Inflamm.* **2012**, *2012*, 484167.

73. Visser, C.E.; Brouwer-Steenbergen, J.J.E.; Schadee-Eestermans, I.L.; Meijer, S.; Krediet, R.T.; Beelen, R.H.J. Ingestion of Staphylococcus aureus, Staphylococcus epidermidis, and Escherichia coli by human peritoneal mesothelial cells. *Infect. Immun.* **1996**, *64*, 3425–3428.

74. Kothari, H.; Kaur, G.; Sahoo, S.; Idell, S.; Rao, L.V.M.; Pendurthi, U. Plasmin enhances cell surface tissue factor activity in mesothelial and endothelial cells. *J. Thromb. Haemost.* **2009**, *7*, 121–131.

75. Cheong, Y.C.; Laird, S.M.; Li, T.C.; Shelton, J.B.; Ledger, W.L.; Cooke, I.D. Peritoneal healing and adhesion formation/reformation. *Hum. Reprod. Update* **2001**, *7*, 556–566.

76. Yáñez-Mó, M.; Lara-Pezzi, E.; Selgas, R.; Ramírez-Huesca, M.; Domínguez-Jiménez, C.; Jiménez-Heffernan, J.A.; Aguilera, A.; Sánchez-Tomero, J.A.; Bajo, A.M.; Álvarez, V.; et al. Peritoneal dialysis and epithelial-to-mesenchymal transition of mesothelial cells. *N. Engl. J. Med.* **2003**, *348*, 403–413.

77. Thiery, J.P. Epithelial-mesenchymal transitions in development and pathologies. *Curr. Opin. Cell Biol.* **2003**, *15*, 740–746.

78. Hinz, B.; Phan, S.H.; Thannickal, V.J.; Galli, A.; Bochaton-Piallat, M.L.; Gabbiani, G. The myofibroblast: One function, multiple origins. *Am. J. Pathol.* **2007**, *170*, 1807–1816.

79. Valle, M.T.; Degl'Innocenti, M.L.; Bertelli, R.; Facchetti, P.; Perfumo, F.; Fenoglio, D.; Kunkl, A.; Gusmano, R.; Manca, F. Antigen-presenting function of human peritoneum mesothelial cells. *Clin Exp Immuno!* **1995**, *101*, 172–176.

80. Hausmann, M.J.; Rogachev, B.; Weiler, M.; Chaimovitz, C.; Douvdevani, A. Accessory role of human peritoneal mesothelial cells in antigen presentation and T-cell growth. *Kidney Int.* **2000**, *57*, 476–486.

81. Dasgupta, M.K.; Larabie, M.; Halloran, P.F. Interferon-gamma levels in peritoneal dialysis effluents: Relation to peritonitis. *Kidney Int.* **1994**, *46*, 475–481.

82. Orimo, A.; Weinberg, R.A. Stromal Fibroblasts in Cancer: A Novel Tumor-Promoting Cell Type. *Cell Cycle* **2006**, *5*, 1597–1601.

83. Sandoval, P.; Jiménez-Heffernan, J.A.; Rynne-Vidal, Á.; Pérez-Lozano, M.L.; Gilsanz, Á.; Ruiz-Carpio, V.; Reyes, R.; García-Bordas, J.; Stamatakis, K.; Dotor, J.; et al. Carcinoma-associated fibroblasts derive from mesothelial cells via mesothelial-to-mesenchymal transition in peritoneal metastasis. *J. Pathol.* **2013**, *231*, 517–531.

84. Komarova, Y.; Malik, A.B. Regulation of endothelial permeability via paracellular and transcellular transport pathways. *Annu. Rev. Physiol.* **2010**, *72*, 463–493.

85. Fung, K.Y.Y.; Fairn, G.D.; Lee, W.L. Transcellular vesicular transport in epithelial and endothelial cells: Challenges and opportunities. *Traffic* **2018**, *19*, 5–18.

86. Zihni, C.; Mills, C.; Matter, K.; Balda, M.S. Tight junctions: From simple barriers to multifunctional molecular gates. *Nat. Rev. Mol. Cell Biol.* **2016**, *17*, 564–580.

87. Fischbarg, J. Fluid transport across leaky epithelia: Central role of the tight junction and supporting role of aquaporins. *Physiol. Rev.* **2010**, *90*, 1271–1290.

88. Mineta, K.; Yamamoto, Y.; Yamazaki, Y.; Tanaka, H.; Tada, Y.; Saito, K.; Tamura, A.; Igarashi, M.; Endo, T.; Takeuchi, K.; et al. Predicted expansion of the claudin multigene family. *FEBS Lett.* **2011**, *585*, 606–612.

89. Furuse, M.; Fujita, K.; Hiiragi, T.; Fujimoto, K.; Tsukita, S. Claudin-1 and -2: Novel Integral Membrane Proteins Localizing at Tight Junctions with No

Sequence Similarity to Occludin. *J. Cell Biol.* **1998**, *141*, 1539–1550.

90. Bazzoni, G.; Dejana, E. Endothelial cell-to-cell junctions: molecular organization and role in vascular homeostasis. *Physiol. Rev.* **2004**, *84*, 869–901.

91. Günzel, D. Claudins: vital partners in transcellular and paracellular transport coupling. *Pflugers Arch. Eur. J. Physiol.* **2017**, *469*, 35–44.

92. Ikenouchi, J.; Matsuda, M.; Furuse, M.; Tsukita, S. Regulation of tight junctions during the epithelium-mesenchyme transition: direct repression of the gene expression of claudins/occludin by Snail. *J. Cell Sci.* **2003**, *116*, 1959–1967.

93. Capaldo, C.T.; Nusrat, A. Cytokine regulation of tight junctions. *Biochim Biophys Acta* **2010**, *1788*, 864–871.

94. Günzel, D.; Yu, A.S.L. Claudins and the modulation of tight junction permeability. *Physiol. Rev.* **2013**, *93*, 525–569.

95. Yu, A.S.L. Claudins and the Kidney. *J. Am. Soc. Nephrol.* **2015**, *26*, 11–19.

96. Schulzke, J.D.; Günzel, D.; John, L.J.; Fromm, M. Perspectives on tight junction research. *Ann. N. Y. Acad. Sci.* **2012**, *1257*, 1–19.

97. Van Itallie, C.M.; Fanning, A.S.; Anderson, J.M. Reversal of charge selectivity in cation or anion-selective epithelial lines by expression of different claudins. *Am. J. Physiol. - Ren. Physiol.* **2003**, *285*, 1078–1084.

98. Kovesdy, C.P. Epidemiology of chronic kidney disease: an update 2022. *Kidney Int. Suppl.* **2022**, *12*, 7–11.

99. Thurlow, J.S.; Joshi, M.; Yan, G.; Norris, K.C.; Agodoa, L.Y.; Yuan, C.M.; Nee, R. Global Epidemiology of End-Stage Kidney Disease and Disparities in Kidney Replacement Therapy. *Am. J. Nephrol.* **2021**, *52*, 98–107.

100. McCullough, K.P.; Morgenstern, H.; Saran, R.; Herman, W.H.; Robinson, B.M. Projecting ESRD incidence and prevalence in the United States through 2030. *J. Am. Soc. Nephrol.* **2019**, *30*, 127–135.

101. Kalantar-Zadeh, K.; Jafar, T.H.; Nitsch, D.; Neuen, B.L.; Perkovic, V. Chronic kidney disease. *Lancet* **2021**, *398*, 786–802.

102. Noble, J.; Jouve, T.; Malvezzi, P.; Süsal, C.; Rostaing, L. Transplantation of marginal organs: Immunological aspects and therapeutic perspectives in kidney

transplantation. *Front. Immunol.* **2020**, *10*, 3142.

103. Zazzeroni, L.; Pasquinelli, G.; Nanni, E.; Cremonini, V.; Rubbi, I. Comparison of Quality of Life in Patients Undergoing Hemodialysis and Peritoneal Dialysis: A Systematic Review and Meta-Analysis. *Kidney Blood Press. Res.* **2017**, *42*, 717–727.

104. Bello, A.K.; Okpechi, I.G.; Osman, M.A.; Cho, Y.; Cullis, B.; Htay, H.; Jha, V.; Makusidi, M.A.; McCulloch, M.; Shah, N.; et al. Epidemiology of peritoneal dialysis outcomes. *Nat. Rev. Nephrol.* **2022**, *18*, 779–793.

105. Cho, Y.; Bello, A.K.; Levin, A.; Lunney, M.; Osman, M.A.; Ye, F.; Ashuntantang, G.E.; Bellorin-Font, E.; Gharbi, M.B.; Davison, S.N.; et al. Peritoneal dialysis use and practice patterns: An international survey study. *Am. J. Kidney Dis.* **2021**, *77*, 315–325.

106. Al Sahlawi, M.; Zhao, J.; McCullough, K.; Fuller, D.S.; Boudville, N.; Ito, Y.; Kanjanabuch, T.; Nessim, S.J.; Piraino, B.M.; Pisoni, R.L.; et al. Variation in peritoneal dialysis-related peritonitis outcomes in the peritoneal dialysis outcomes and practice patterns study (PDOPPS). *Am. J. Kidney Dis.* **2022**, *79*, 45-55.e1.

107. Teitelbaum, I. Peritoneal Dialysis. *N. Engl. J. Med.* **2021**, *385*, 1786–1795.

108. Crabtree, J.H.; Chow, K.M. Peritoneal dialysis catheter insertion. *Semin. Nephrol.* **2017**, *37*, 17–29.

109. Jha, V.; Abrahams, A.C.; Al-Hwiesh, A.; Brown, E.A.; Cullis, B.; Dor, F.J.M.F.; Mendu, M.; Ponce, D.; Divino-Filho, J.C. Peritoneal catheter insertion: combating barriers through policy change. *Clin. Kidney J.* **2022**, *15*, 2177–2185.

110. Vardhan, A.; Hutchison, A.J. Peritoneal Dialysis. In *National Kidney Foundation's Primer on Kidney Diseases*; Gilbert, S.F., Weiner, D.E., Eds.; W.B. Saunders, 2014; pp. 520–533 ISBN 9781455746170.

111. Negoi, D.; Nolph, K.D. Automated Peritoneal Dialysis – Indications and Management. *Contrib. Nephrol.* **2006**, *150*, 278–284.

112. Ellam, T.; Wilkie, M. Peritoneal dialysis. *Medicine (Baltimore).* **2015**, *43*, 484–488.

113. Bieber, S.D.; Burkart, J.; Golper, T.A.; Teitelbaum, I.; Mehrotra, R. Comparative outcomes between continuous ambulatory and automated peritoneal dialysis: A narrative review. *Am. J. Kidney Dis.* **2014**, *63*, 1027–1037.

114. Szeto, C.C.; Chow, K.M.; Kwan, B.C.H.; Chung, K.Y.; Leung, C.B.; Li, P.K.T. New-onset hyperglycemia in nondiabetic chinese patients started on peritoneal dialysis. *Am. J. Kidney Dis.* **2007**, *49*, 524–532.

115. Balzer, M.S.; Rong, S.; Nordlohne, J.; Zemtsovski, J.D.; Schmidt, S.; Stapel, B.; Bartosova, M.; von Vietinghoff, S.; Haller, H.; Schmitt, C.P.; et al. SGLT2 inhibition by intraperitoneal dapagliflozin mitigates peritoneal fibrosis and ultrafiltration failure in a mouse model of chronic peritoneal exposure to high-glucose dialysate. *Biomolecules* **2020**, *10*, 1573.

116. Herlihy, S.E.; Starke, H.E.; Lopez-Anton, M.; Cox, N.; Keyhanian, K.; Fraser, D.J.; Gomer, R.H. Peritoneal Dialysis fluid and some of its components potentiate fibrocyte differentiation. *Perit. Dial. Int.* **2016**, *36*, 367–373.

117. Susic, D.; Frohlich, E.D. Salt consumption and cardiovascular, renal, and hypertensive diseases: Clinical and mechanistic aspects. *Curr. Opin. Lipidol.* **2012**, *23*, 11–16.

118. Cappelli, G.; Amore, A.; Bandiani, G.; Cancarini, G.; Coppo, R.; Feriani, M.; Dell'Aquila, R.; Saffioti, S.; Spisni, C.; Stingone, A.; et al. A Peritoneal Dialysis solution prepared from a three-compartment bag: Biological and clinical effects. *Contrib. Nephrol.* **2001**, *131*, 97–106.

119. Bartosova, M.; Schaefer, B.; Vondrak, K.; Sallay, P.; Taylan, C.; Cerkauskiene, R.; Dzierzega, M.; Milosevski-Lomic, G.; Büscher, R.; Zaloszyc, A.; et al. Peritoneal dialysis vintage and glucose exposure but not peritonitis episodes drive peritoneal membrane transformation during the first years of PD. *Front. Physiol.* **2019**, *10*, 356.

120. Goossen, K.; Becker, M.; Marshall, M.R.; Bühn, S.; Breuing, J.; Firanek, C.A.; Hess, S.; Nariai, H.; Sloand, J.A.; Yao, Q.; et al. Icodextrin versus glucose solutions for the once-daily long dwell in Peritoneal Dialysis: An enriched systematic review and meta-analysis of randomized controlled trials. *Am. J. Kidney Dis.* **2020**, *75*, 830–846.

121. Martis, L.; Patel, M.; Giertych, J.; Mongoven, J.; Taminne, M.; Perrier, M.A.; Mendoza, O.; Goud, N.; Costigan, A.; Denjoy, N.; et al. Aseptic peritonitis due to peptidoglycan contamination of pharmacopoeia standard dialysis solution. *Lancet* **2005**, *365*, 588–594.

122. Adam, F.; Singan, M.; Ozelsancak, R.; Torun, D.; Ozdemir, F.; Haberal, M. Icodextrin-associated sterile peritonitis: a recent outbreak in Turkey. *Perit Dial Int* **2007**, *27*, 598–599.

123. Sezer, M.T.; Demir, M.; Ertürk, J.; Yildiz, M. Effects of amino acid peritoneal dialysate in malnutrished peritoneal dialysis patients. *Eur. J. Gen. Med.* **2006**, *3*, 58–63.

124. Twardowski, Z.J. Pathophysiology of peritoneal transport. *Contrib. Nephrol.* **2006**, *150*, 13–19.

125. Khanna, R. Solute and water transport in peritoneal dialysis: A case-based primer. *Am. J. kidney Dis. Off. J. Natl. Kidney Found.* **2017**, *69*, 461–472.

126. Leypoldt, J.K. Solute transport across the peritoneal membrane. *J. Am. Soc. Nephrol. JASN* **2002**, *13 Suppl 1*, S84–S91.

127. Krediet, R.T.; Furgeson, S.; Teitelbaum, I. *The physiology and pathophysiology of peritoneal transport*; Khanna, R., Krediet, R.., Eds.; Nolph and.; Springer, Cham, 2023;

128. Morelle, J.; Devuyst, O. Water and solute transport across the peritoneal membrane. *Curr. Opin. Nephrol. Hypertens.* 2015, *24*, 434–443.

129. Flessner, M.F. Peritoneal ultrafiltration: mechanisms and measures. *Contrib. Nephrol.* **2006**, *150*, 28–36.

130. Waniewski, J. Peritoneal fluid transport: Mechanisms, pathways, methods of assessment. *Arch. Med. Res.* **2013**, *44*, 576–583.

131. Chen, T.W.; Khanna, R.; Moore, H.; Twardowski, Z.J.; Nolph, K.D. Sieving and reflection coefficients for sodium salts and glucose during peritoneal dialysis in rats. *J Am Soc Nephrol* **1991**, *2*, 1092–1100.

132. Malhotra, K.; Khanna, R. Electrolyte Management in Peritoneal Dialysis. In *Nolph and Gokal's Textbook of Peritoneal Dialysis*; Khanna, R., Krediet, R.T.,

Eds.; Springer, Cham, 2021; pp. 1–12.

133. Liakopoulos, V.; Zarogiannis, S.; Hatzoglou, C.; Kourti, P.; Poultsidi, A.; Eleftheriadis, T.; Gourgoulianis, K.; Molyvdas, P.-A.; Stefanidis, I. Inhibition by mercuric chloride of aquaporin-1 in the parietal sheep peritoneum: an electrophysiologic study. *Adv. Perit. Dial.* **2006**, *22*, 7–10.

134. Ni, J.; Verbavatz, J.M.; Rippe, A.; Boisdé, I.; Moulin, P.; Rippe, B.; Verkman, A.S.; Devuyst, O. Aquaporin-1 plays an essential role in water permeability and ultrafiltration during peritoneal dialysis. *Kidney Int.* **2006**, *69*, 1518–1525.

135. Asghar, R.B.; Diskin, A.M.; Spanel, P.; Smith, D.; Davies, S.J. Influence of convection on the diffusive transport and sieving of water and small solutes across the peritoneal membrane. *J. Am. Soc. Nephrol.* **2005**, *16*, 437–443.

136. Aanen, M.C.; Venturoli, D.; Davies, S.J. A detailed analysis of sodium removal by peritoneal dialysis: Comparison with predictions from the three-pore model of membrane function. *Nephrol. Dial. Transplant.* **2005**, *20*, 1192–1200.

137. Jeloka, T.K.; Ersoy, F.F.; Yavuz, M.; Sahu, K.M.; Çamsari, T.; Utaş, C.; Bozfakioglu, S.; Özener, Ç.; Ateş, K.; Ataman, R.; et al. What is the optimal dwell time for maximizing ultrafiltration with icodextrin exchange in automated peritoneal dialysis patients? In *Peritoneal Dialysis International*; Multimed Inc., 2006; Vol. 26, pp. 336–340.

138. Akonur, A.; Guest, S.; Sloand, J.A.; Leypoldt, J.K. Automated peritoneal dialysis prescriptions for enhancing sodium and fluid removal: A predictive analysis of optimized, patient-specific dwell times for the day period. *Perit. Dial. Int.* **2013**, *33*, 646–654.

139. Pérez-Díaz, V.; Pérez-Escudero, A.; Sanz-Ballesteros, S.; Rodríguez-Portela, G.; Valenciano-Martínez, S.; Palomo-Aparicio, S.; Hernández-García, E.; Sánchez-García, L.; Gordillo-Martín, R.; Marcos-Sánchez, H. A new method to increase ultrafiltration in peritoneal dialysis: Steady concentration peritoneal dialysis. *Perit. Dial. Int.* **2016**, *36*, 555–561.

140. Honda, K.; Hamada, C.; Nakayama, M.; Miyazaki, M.; Sherif, A.M.; Harada, T.; Hirano, H. Impact of uremia, diabetes, and peritoneal dialysis itself on the pathogenesis of peritoneal sclerosis: A quantitative study of peritoneal membrane

morphology. *Clin. J. Am. Soc. Nephrol.* **2008**, *3*, 720–728.

141. Mizumasa, T.; Hirakata, H.; Kuroki, Y.; Katafuchi, R.; Yotsueda, H.; Mitsuiki, K.; Nakashima, Y.; Tsuruya, K. Diabetes influences peritoneal morphology in uremic patients at the initiation of peritoneal dialysis. *Perit. Dial. Int. J. Int. Soc. Perit. Dial.* **2013**, *33*, 175–181.

142. Williams, J.D.; Craig, K.J.; Topley, N.; Von Ruhland, C.; Fallon, M.; Newman, G.R.; Mackenzie, R.K.; Williams, G.T. Morphologic changes in the peritoneal membrane of patients with renal disease. *J. Am. Soc. Nephrol.* **2002**, *13*, 470–479.

143. Bajo, M.A.; del Peso, G.; Teitelbaum, I. Peritoneal membrane preservation. *Semin. Nephrol.* **2017**, *37*, 77–92.

144. Szeto, C.C.; Li, P.K.T. Peritoneal dialysis–associated peritonitis. *Clin. J. Am. Soc. Nephrol.* **2019**, *14*, 1100–1105.

145. Cho, Y.; Johnson, D.W. Peritoneal dialysis-related peritonitis: towards improving evidence, practices, and outcomes. *Am. J. kidney Dis. Off. J. Natl. Kidney Found.* **2014**, *64*, 278–289.

146. Kato, S.; Yuzawa, Y.; Tsuboi, N.; Maruyama, S.; Morita, Y.; Matsuguchi, T.; Matsuo, S. Endotoxin-induced chemokine expression in murine peritoneal mesothelial cells: The role of Toll-like receptor 4. *J. Am. Soc. Nephrol.* **2004**, *15*, 1289–1299.

147. Mazzon, E.; Cuzzocrea, S. Role of TNF-α in lung tight junction alteration in mouse model of acute lung inflammation. *Respir. Res.* **2007**, *8*, 1–19.

148. Margetts, P.J.; Kolb, M.; Yu, L.; Hoff, C.M.; Holmes, C.J.; Anthony, D.C.; Gauldie, J. Inflammatory cytokines, angiogenesis, and fibrosis in the rat peritoneum. *Am. J. Pathol.* **2002**, *160*, 2285–2294.

149. Welten, A.G.A.; Zareie, M.; van den Born, J.; ter Wee, P.M.; Schalkwijk, C.G.; Driesprong, B.A.J.; Mul, F.P.J.; Hordijk, P.L.; Beelen, R.H.J.; Hekking, L.H.P. In vitro and in vivo models for peritonitis demonstrate unchanged neutrophil migration after exposure to dialysis fluids. *Nephrol. Dial. Transplant.* **2004**, *19*, 831–839.

150. Bartosova, M.; Schmitt, C.P. Biocompatible peritoneal dialysis: The target is still way off. *Front. Physiol.* 2019, *9*, 1853.

151. Davies, S.J. Longitudinal relationship between solute transport and ultrafiltration capacity in peritoneal dialysis patients. *Kidney Int.* **2004**, *66*, 2437–2445.

152. Davies, S.J.; Phillips, L.; Naish, P.F.; Russell, G.I. Peritoneal glucose exposure and changes in membrane solute transport with time on peritoneal dialysis. *J. Am. Soc. Nephrol.* **2001**, *12*, 1046–1051.

153. Boulanger, E.; Wautier, M.P.; Gane, P.; Mariette, C.; Devuyst, O.; Wautier, J.L. The triggering of human peritoneal mesothelial cell apoptosis and oncosis by glucose and glycoxydation products. *Nephrol. Dial. Transplant.* **2004**, *19*, 2208–2216.

154. Liu, Y.; Dong, Z.; Liu, H.; Zhu, J.; Liu, F.; Chen, G. Transition of mesothelial cell to fibroblast in peritoneal dialysis: EMT, stem cell or bystander? *Perit. Dial. Int.* **2015**, *35*, 14–25.

155. Loureiro, J.; Aguilera, A.; Selgas, R.; Sandoval, P.; Albar-Vizcaíno, P.; Pérez-Lozano, M.L.; Ruiz-Carpio, V.; Majano, P.L.; Lamas, S.; Rodríguez-Pascual, F.; et al. Blocking TGF-β1 protects the peritoneal membrane from dialysate-induced damage. *J. Am. Soc. Nephrol.* **2011**, *22*, 1682–1695.

156. Simon, F.; Tapia, P.; Armisen, R.; Echeverria, C.; Gatica, S.; Vallejos, A.; Pacheco, A.; Sanhueza, M.E.; Alvo, M.; Segovia, E.; et al. Human peritoneal mesothelial cell death induced by high-glucose hypertonic solution involves Ca2+and Na+ions and oxidative stress with the participation of PKC/NOX2 and PI3K/Akt pathways. *Front. Physiol.* **2017**, *8*, 1–17.

157. Honda, K.; Nitta, K.; Horita, S.; Yumura, W.; Nihei, H. Morphological changes in the peritoneal vasculature of patients on CAPD with ultrafiltration failure. *Nephron* **1996**, *72*, 171–176.

158. Shi, Y.; Hu, Y.; Cui, B.; Zhuang, S.; Liu, N. Vascular endothelial growth factor-mediated peritoneal neoangiogenesis in peritoneal dialysis. *Perit. Dial. Int.* **2022**, *42*, 25–38.

159. Combet, S.; Miyata, T.; Moulin, P.; Pouthier, D.; Coffin, E.; Devuyst, O. Vascular proliferation and enhanced expression of endothelial nitric oxide synthase in human peritoneum exposed to long-term peritoneal dialysis. *J. Am. Soc. Nephrol. JASN* **2000**, *11*, 717–728.

160. Aroeira, L.S.; Aguilera, A.; Selgas, R.; Ramírez-Huesca, M.; Pérez-Lozano, M.L.; Cirugeda, A.; Bajo, M.A.; Del Peso, G.; Sánchez-Tomero, J.A.; Jiménez-Heffernan, J.A.; et al. Mesenchymal conversion of mesothelial cells as a mechanism responsible for high solute transport rate in peritoneal dialysis: Role of vascular endothelial growth factor. *Am. J. Kidney Dis.* **2005**, *46*, 938–948.

161. Pecoits-Filho, R.; Araújo, M.R.T.; Lindholm, B.; Stenvinkel, P.; Abensur, H.; Romão, J.E.; Marcondes, M.; De Oliveira, A.H.F.; Noronha, I.L. Plasma and dialysate IL-6 and VEGF concentrations are associated with high peritoneal solute transport rate. *Nephrol Dial Transplant.* **2002**, *17*, 1480–1486.

162. De Vriese, A.S.; Tilton, R.G.; Stephan, C.C.; Lameire, N.H. Vascular endothelial growth factor is essential for hyperglycemia-induced structural and functional alterations of the peritoneal membrane. *J. Am. Soc. Nephrol.* **2001**, *12*, 1734–1741.

163. Boulanger, E.; Grossin, N.; Wautier, M.P.; Taamma, R.; Wautier, J.L. Mesothelial RAGE activation by AGEs enhances VEGF release and potentiates capillary tube formation. *Kidney Int.* **2007**, *71*, 126–133.

164. Jiang, N.; Zhang, Q.; Chau, M.K.; Yip, M.S.; Lui, S.L.; Liu, S.; Chu, K.M.; Ngan, H.Y.; Chan, T.M.; Yung, S. Anti-fibrotic effect of decorin in peritoneal dialysis and PD-associated peritonitis. *EBioMedicine* **2020**, *52*, 102661.

165. Shentu, Y.; Li, Y.; Xie, S.; Jiang, H.; Sun, S.; Lin, R.; Chen, C.; Bai, Y.; Zhang, Y.; Zheng, C.; et al. Empagliflozin, a sodium glucose cotransporter-2 inhibitor, ameliorates peritoneal fibrosis via suppressing TGF-β/Smad signaling. *Int. Immunopharmacol.* **2021**, *93*, 107374.

166. Ito, T.; Yorioka, N.; Kyuden, Y.; Asakimori, Y.; Kiribayashi, K.; Ogawa, T.; Kohno, N. Effect of glucose polymer on the intercellular junctions of cultured human peritoneal mesothelial cells. *Nephron. Clin. Pract.* **2003**, *93*.

167. Kaneda, K.I.; Miyamoto, K.; Nomura, S.; Horiuchi, T. Intercellular localization of occludins and ZO-1 as a solute transport barrier of the mesothelial monolayer. *J. Artif. Organs* **2006**, *9*, 241–250.

168. Retana, C.; Sanchez, E.I.; Gonzalez, S.; Perez-Lopez, A.; Cruz, A.; Lagunas-Munoz, J.; Alfaro-Cruz, C.; Vital-Flores, S.; Reyes, J.L. Retinoic acid improves

morphology of cultured peritoneal mesothelial cells from patients undergoing dialysis. *PLoS One* **2013**, *8*, 1–13.

169. Retana, C.; Sanchez, E.; Perez-Lopez, A.; Cruz, A.; Lagunas, J.; Cruz, C.; Vital, S.; Reyes, J.L. Alterations of intercellular junctions in peritoneal mesothelial cells from patients undergoing dialysis: Effect of retinoic acid. *Perit Dial Int* **2014**, *35*, 275–287.

170. Saker, S.; Stewart, E.A.; Browning, A.C.; Allen, C.L.; Amoaku, W.M. The effect of hyperglycaemia on permeability and the expression of junctional complex molecules in human retinal and choroidal endothelial cells. *Exp. Eye Res.* **2014**, *121*, 161–167.

171. Tien, T.; Barrette, K.F.; Chronopoulos, A.; Roy, S. Effects of high glucose-induced Cx43 downregulation on occludin and ZO-1 expression and tight junction barrier function in retinal endothelial cells. *Investig. Ophthalmol. Vis. Sci.* **2013**, *54*, 6518–6525.

172. Madonna, R.; Montebello, E.; Lazzerini, G.; Zurro, M.; De Caterina, R. NA+/H+ exchanger 1- and aquaporin-1-dependent hyperosmolarity changes decrease nitric oxide production and induce VCAM-I expression in endothelial cells exposed to high glucose. *Int. J. Immunopathol. Pharmacol.* **2010**, *23*, 755–765.

173. Hills, C.E.; Bland, R.; Bennett, J.; Ronco, P.M.; Squires, P.E. High glucose up-regulates ENaC and SGK1 expression in HCD-cells. *Cell. Physiol. Biochem.* **2006**, *18*, 337–346.

174. Norton, L.; Shannon, C.E.; Fourcaudot, M.; Hu, C.; Wang, N.; Ren, W.; Song, J.; Abdul-Ghani, M.; DeFronzo, R.A.; Ren, J.; et al. Sodium-glucose co-transporter (SGLT) and glucose transporter (GLUT) expression in the kidney of type 2 diabetic subjects. *Diabetes, Obes. Metab.* **2017**, *19*, 1322–1326.

175. Freitas, H.S.; Anhê, G.F.; Melo, K.F.S.; Okamoto, M.M.; Oliveira-Souza, M.; Bordin, S.; Machado, U.F. Na+-glucose transporter-2 messenger ribonucleic acid expression in kidney of diabetic rats correlates with glycemic levels: Involvement of hepatocyte nuclear factor-1α expression and activity. *Endocrinology* **2008**, *149*, 717–724.

176. Stefanidis, I.; Liakopoulos, V.; Kourti, P.; Zarogiannis, S.; Poultsidi, A.;

Mertems, P.R.; Salmas, M.; Hatzoglou, C.; Gourgoulianis, K.; Molyvdas, P.A. Amiloride-sensitive sodium channels on the parietal human peritoneum: evidence by ussing-type chamber experiments. *ASAIO J.* **2007**, *53*, 335–338.

177. Mortier, S.; De Vriese, A.S.; McLoughlin, R.M.; Topley, N.; Schaub, T.P.; Passlick-Deetjen, J.; Lameire, N.H. Effects of conventional and new peritoneal dialysis fluids on leukocyte recruitment in the rat peritoneal membrane. *J. Am. Soc. Nephrol.* **2003**, *14*, 1296–1306.

178. Grossin, N.; Wautier, M.-P.; Wautier, J.L.; Gane, P.; Taamma, R.; Boulanger, E. Improved in vitro biocompatibility of bicarbonate-buffered peritoneal dialysis fluid. *Perit Dial Int* **2006**, *26*, 664–670.

179. Bajo, M.A.; Príez-Lozano, M.L.; Albar-Vizcaino, P.; Del Peso, G.; Castro, M.J.; Gonzalez-Mateo, G.; Fernández-Perpén, A.; Aguilera, A.; Sánchez-Villanueva, R.; Sánchez-Tomero, J.A.; et al. Low-GDP peritoneal dialysis fluid ('balance') has less impact in vitro and ex vivo on epithelial-to-mesenchymal transition (EMT) of mesothelial cells than a standard fluid. *Nephrol Dial Transplant.* **2011**, *26*, 282–291.

180. Mortier, S.; Faict, D.; Schalkwijk, C.G.; Lameire, N.H.; De Vriese, A.S. Long-term exposure to new peritoneal dialysis solutions: Effects on the peritoneal membrane. *Kidney Int.* **2004**, *66*, 1257–1265.

181. Mortier, S.; Faict, D.; Lameire, N.H.; De Vriese, A.S. Benefits of switching from a conventional to a low-GDP bicarbonate/lactate-buffered dialysis solution in a rat model. *Kidney Int.* **2005**, *67*, 1559–1565.

182. Rippe, B. Peritoneal angiogenesis in response to dialysis fluid. *Contrib. Nephrol.* **2009**, *163*, 60–66.

183. Krediet, R.T. Aging of the peritoneal dialysis membrane. *Front. Physiol.* **2022**, *13*, 885802.

184. Schaefer, B.; Bartosova, M.; Macher-Goeppinger, S.; Sallay, P.; Vörös, P.; Ranchin, B.; Vondrak, K.; Ariceta, G.; Zaloszyc, A.; Bayazit, A.K.; et al. Neutral pH and low–glucose degradation product dialysis fluids induce major early alterations of the peritoneal membrane in children on peritoneal dialysis. *Kidney Int.* **2018**, *94*, 419–429.

185. Nishimura, H.; Ikehara, O.; Naito, T.; Higuchi, C.; Sanaka, T. Evaluation of taurine as an osmotic agent for peritoneal dialysis solution. *Perit. Dial. Int.* **2009**, *29*, 204–216.

186. Chen, C.; Xia, S.F.; He, J.; Lu, G.; Xie, Z.; Han, H. Roles of taurine in cognitive function of physiology, pathologies and toxication. *Life Sci.* **2019**, *231*, 116584.

187. Seidel, U.; Huebbe, P.; Rimbach, G. Taurine: A regulator of cellular redox homeostasis and skeletal muscle function. *Mol. Nutr. Food Res.* **2019**, *63*, 1800569.

188. Bonomini, M.; Di Silvestre, S.; Di Tomo, P.; Di Pietro, N.; Mandatori, D.; Di Liberato, L.; Sirolli, V.; Chiarelli, F.; Indiveri, C.; Pandolfi, A.; et al. Effect of peritoneal dialysis fluid containing osmo-metabolic agents on human endothelial cells. *Drug Des. Devel. Ther.* **2016**, *10*, 3925–3932.

189. Rago, C.; Lombardi, T.; Di Fulvio, G.; Di Liberato, L.; Arduini, A.; Divino-Filho, J.C.; Bonomini, M. A new peritoneal dialysis solution containing L-carnitine and xylitol for patients on Continuous Ambulatory Peritoneal Dialysis: First clinical experience. *Toxins (Basel)* **2021**, *13*, 174.

190. Ozaki, T.; Fu, H.Y.; Onishi, K.; Yokoyama, S.; Fujita, T.; Tobiume, A.; Sofue, T.; Akimitsu, K.; Minamino, T. Partial replacement of d-glucose with d-allose ameliorates peritoneal injury and hyperglycaemia induced by peritoneal dialysis fluid in rats. *Perit. Dial. Int.* **2023**, *8968608231*.

191. Khajeh, S.; Ganjavi, M.; Panahi, G.; Zare, M.; Zare, M.; Tahami, S.M.; Razban, V. D-allose: Molecular pathways and therapeutic capacity in cancer. *Curr. Mol. Pharmacol.* **2023**, *16*, 801–810.

192. Goyal, S.K.; Samsher; Goyal, R.K. Stevia (Stevia rebaudiana) a bio-sweetener: a review. *Int. J. Food Sci. Nutr.* **2010**, *61*, 1–10.

193. Shivanna, N.; Naika, M.; Khanum, F.; Kaul, V.K. Antioxidant, anti-diabetic and renal protective properties of Stevia rebaudiana. *J. Diabetes Complications* **2013**, *27*, 103–113.

194. Momtazi-Borojeni, A.A.; Esmaeili, S.-A.; Abdollahi, E.; Sahebkar, A. A review on the pharmacology and toxicology of steviol glycosides extracted from Stevia rebaudiana. *Curr. Pharm. Des.* **2017**, *23*, 1616–1622.

195. Kopytina, V.; Pascual-Antón, L.; Toggweiler, N.; Arriero-País, E.M.; Strahl, L.; Albar-Vizcaíno, P.; Sucunza, D.; Vaquero, J.J.; Steppan, S.; Piecha, D.; et al. Steviol glycosides as an alternative osmotic agent for peritoneal dialysis fluid. *Front. Pharmacol.* **2022**, *13*, 868374.

196. Kratochwill, K.; Boehm, M.; Herzog, R.; Lichtenauer, A.M.; Salzer, E.; Lechner, M.; Kuster, L.; Bergmeister, K.; Rizzi, A.; Mayer, B.; et al. Alanyl-glutamine dipeptide restores the cytoprotective stress proteome of mesothelial cells exposed to peritoneal dialysis fluids. *Nephrol. Dial. Transplant* **2012**, *27*, 937–46.

197. Kratochwill, K.; Boehm, M.; Herzog, R.; Gruber, K.; Lichtenauer, A.M.; Kuster, L.; Csaicsich, D.; Gleiss, A.; Alper, S.L.; Aufricht, C.; et al. Addition of alanyl-glutamine to dialysis fluid restores peritoneal cellular stress responses - A first-in-man trial. *PLoS One* **2016**, *11*, e0165045.

198. Herzog, R.; Bartosova, M.; Tarantino, S.; Wagner, A.; Unterwurzacher, M.; Sacnun, J.M.; Lichtenauer, A.M.; Kuster, L.; Schaefer, B.; Alper, S.L.; et al. Peritoneal dialysis fluid supplementation with alanyl-glutamine attenuates conventional dialysis fluid-mediated endothelial cell injury by restoring perturbed cytoprotective responses. *Biomolecules* **2020**, *10*, 1678.

199. Wiesenhofer, F.M.; Herzog, R.; Boehm, M.; Wagner, A.; Unterwurzacher, M.; Kasper, D.C.; Alper, S.L.; Vychytil, A.; Aufricht, C.; Kratochwill, K. Targeted metabolomic profiling of peritoneal dialysis effluents shows anti-oxidative capacity of alanyl-glutamine. *Front. Physiol.* **2018**, *9*, 1961.

200. Herzog, R.; Kuster, L.; Becker, J.; Gluexam, T.; Pils, D.; Spittler, A.; Bhasin, M.K.; Alper, S.L.; Vychytil, A.; Aufricht, C.; et al. Functional and transcriptomic characterization of peritoneal immune-modulation by addition of alanyl-glutamine to dialysis fluid. *Sci. Rep.* **2017**, *7*, 6229.

201. Bartosova, M.; Ridinger, D.; Marinovic, I.; Heigwer, J.; Zhang, C.; Levai, E.; Westhoff, J.H.; Schaefer, F.; Terjung, S.; Hildenbrand, G.; et al. An experimental workflow for studying barrier integrity, permeability, and tight junction composition and localization in a single endothelial cell monolayer: Proof of concept. *Int. J. Mol. Sci.* **2021**, *22*, 1–15.

202. Rusai, K.; Herzog, R.; Kuster, L.; Kratochwill, K.; Aufricht, C. GSK-3β inhibition protects mesothelial cells during experimental peritoneal dialysis

through upregulation of the heat shock response. *Cell Stress Chaperones* **2013**, *18*, 569–579.

203. Bender, T.O.; Böhm, M.; Kratochwill, K.; Vargha, R.; Riesenhuber, A.; Witowski, J.; Jrres, A.; Wieslander, A.; Aufricht, C. Peritoneal dialysis fluids can alter HSP expression in human peritoneal mesothelial cells. *Nephrol. Dial. Transplant.* **2011**, *26*, 1046–1052.

204. Wick, A.N.; Drury, D.R.; Morita, T.N. 2-Deoxyglucose; a metabolic block for glucose. *Proc. Soc. Exp. Biol. Med.* **1955**, *89*, 579–582.

205. Fu, J.; Li, N.; He, M.; Huang, D.; Zhang, P. STAT3 signaling mediates peritoneal fibrosis by activating hyperglycolysis. *Am J Transl Res* **2022**, *14*, 7552–7565.

206. Witowski, J.; Kawka, E.; Rudolf, A.; Jörres, A. New developments in peritoneal fibroblast biology: implications for inflammation and fibrosis in peritoneal dialysis. *Biomed Res. Int.* **2015**, *2015*, 134708.

207. Aroeira, L.S.; Aguilera, A.; Sánchez-Tomero, J.A.; Bajo, M.A.; Del Peso, G.; Jiménez-Heffernan, J.A.; Selgas, R.; López-Cabrera, M. Epithelial to mesenchymal transition and peritoneal membrane failure in peritoneal dialysis patients: pathologic significance and potential therapeutic interventions. *J. Am. Soc. Nephrol.* **2007**, *18*, 2004–2013.

208. Del Peso, G.; Jiménez-Heffernan, J.A.; Bajo, M.A.; Aroeira, L.S.; Aguilera, A.; Fernández-Perpén, A.; Cirugeda, A.; Castro, M.J.; De Gracia, R.; Sánchez-Villanueva, R.; et al. Epithelial-to-mesenchymal transition of mesothelial cells is an early event during peritoneal dialysis and is associated with high peritoneal transport. *Kidney Int. Suppl.* **2008**, *73*.

209. Pletinck, A.; Vanholder, R.; Veys, N.; Van Biesen, W. Protecting the peritoneal membrane: factors beyond peritoneal dialysis solutions. *Nat. Rev. Nephrol.* **2012**, *8*, 542–550.

210. Warburg, O. The metabolism of carcinoma cells. *J. Cancer Res.* **1925**, *9*, 148–163.

211. Ding, H.; Jiang, L.; Xu, J.; Bai, F.; Zhou, Y.; Yuan, Q.; Luo, J.; Zen, K.; Yang, J. Inhibiting aerobic glycolysis suppresses renal interstitial fibroblast activation and renal fibrosis. *Am. J. Physiol. Renal Physiol.* **2017**, *313*, F561–F575.

212. Lunt, S.Y.; Vander Heiden, M.G. Aerobic glycolysis: meeting the metabolic requirements of cell proliferation. *Annu. Rev. Cell Dev. Biol.* **2011**, *27*, 441–464.

213. Chen, J.; Williams, S.; Ho, S.; Loraine, H.; Hagan, D.; Whaley, J.M.; Feder, J.N. Quantitative PCR tissue expression profiling of the human SGLT2 gene and related family members. *Diabetes Ther.* **2010**, *1*, 57–92.

214. Zhou, L.; Cryan, E. V.; D'Andrea, M.R.; Belkowski, S.; Conway, B.R.; Demarest, K.T. Human cardiomyocytes express high level of Na+/glucose cotransporter 1 (SGLT1). *J. Cell. Biochem.* **2003**, *90*, 339–346.

215. Livak, K.J.; Schmittgen, T.D. Analysis of Relative Gene Expression Data Using Real-Time Quantitative PCR and the 2−ΔΔCT Method. *Methods* **2001**, *25*, 402–408.

216. Bonomini, M.; Zammit, V.; Divino-Filho, J.C.; Davies, S.J.; Di Liberato, L.; Arduini, A.; Lambie, M. The osmo-metabolic approach: a novel and tantalizing glucose-sparing strategy in peritoneal dialysis. *J. Nephrol.* **2021**, *34*, 503–519.

217. Bell, E.; Ivarsson, B.; Merrill, C. Production of a tissue-like structure by contraction of collagen lattices by human fibroblasts of different proliferative potential in vitro. *Proc. Natl. Acad. Sci. U. S. A.* **1979**, *76*, 1274–1278.

218. Zolak, J.S.; Jagirdar, R.; Surolia, R.; Karki, S.; Oliva, O.; Hock, T.; Guroji, P.; Ding, Q.; Liu, R.M.; Bolisetty, S.; et al. Pleural mesothelial cell differentiation and invasion in fibrogenic lung injury. *Am. J. Pathol.* **2013**, *182*, 1239–1247.

219. Karki, S.; Surolia, R.; Hock, T.D.; Guroji, P.; Zolak, J.S.; Duggal, R.; Ye, T.; Thannickal, V.J.; Antony, V.B. Wilms' tumor 1 (Wt1) regulates pleural mesothelial cell plasticity and transition into myofibroblasts in idiopathic pulmonary fibrosis. *FASEB J.* **2014**, *28*, 1122–1131.

220. Yu, J.; Choi, S.; Um, J.; Park, K.S. Reduced expression of YAP in dermal fibroblasts is associated with impaired wound healing in type 2 diabetic mice. *Tissue Eng. Regen. Med.* **2017**, *14*, 49–55.

221. Sainio, A.; Jokela, T.; Tammi, M.I.; Järveläinen, H. Hyperglycemic conditions modulate connective tissue reorganization by human vascular smooth muscle cells through stimulation of hyaluronan synthesis. *Glycobiology* **2010**, *20*, 1117–1126.

222. Frost, T.S.; Jiang, L.; Lynch, R.M.; Zohar, Y. Permeability of epithelial/endothelial barriers in transwells and microfluidic bilayer devices. *Micromachines* **2019**, *10*, 533.

223. Stachowska-Pietka, J.; Waniewski, J.; Flessner, M.F.; Lindholm, B. Computer simulations of osmotic ultrafiltration and small-solute transport in peritoneal dialysis: a spatially distributed approach. *Am. J. Physiol. Renal Physiol.* **2012**, *302*, F1331-41.

224. Morelle, J.; Sow, A.; Fustin, C.A.; Fillée, C.; Garcia-Lopez, E.; Lindholm, B.; Goffin, E.; Vandemaele, F.; Rippe, B.; Oberg, C.M.; et al. Mechanisms of crystalloid versus colloid osmosis across the peritoneal membrane. *J. Am. Soc. Nephrol.* **2018**, *29*, 1875–1886.

225. Devuyst, O. Assessing transport across the peritoneal membrane: Precision medicine in dialysis. *Perit. Dial. Int.* **2021**, *41*, 349–351.

226. Schaefer, B.; Bartosova, M.; MacHer-Goeppinger, S.; Ujszaszi, A.; Wallwiener, M.; Nyarangi-Dix, J.; Sallay, P.; Burkhardt, D.; Querfeld, U.; Pfeifle, V.; et al. Quantitative histomorphometry of the healthy peritoneum. *Sci. Rep.* **2016**, *6*, 21344.

227. Piccapane, F.; Gerbino, A.; Carmosino, M.; Milano, S.; Arduini, A.; Debellis, L.; Svelto, M.; Caroppo, R.; Procino, G. Aquaporin-1 facilitates transmesothelial water permeability: In vitro and ex vivo evidence and possible implications in peritoneal dialysis. *Int. J. Mol. Sci.* **2021**, *22*, 12535.

228. Marinovic, I.; Bartosova, M.; Levai, E.; Herzog, R.; Hausmann, M.; Zhang, C.; Pap, D.; Zarogiannis, S.; Kratochwill, K.; Schmitt, C.P. Molecular and functional characterization of the peritoneal mesothelial and endothelial cell barrier. *Nephron. Dial. Transpl.* **2023**, *37*.

229. Levai, E.; Marinovic, I.; Bartosova, M.; Zhang, C.; Schaefer, B.; Jenei, H.; Du, Z.; Drozdz, D.; Klaus, G.; Arbeiter, K.; et al. Human peritoneal tight junction, transporter and channel expression in health and kidney failure, and associated solute transport. *Sci. Rep.* **2023**, *13*, 17429.

230. Kourti, P.; Zarogiannis, S.G.; Liakopoulos, V.; Karioti, A.; Eleftheriadis, T.; Hatzoglou, C.; Gourgoulianis, K.; Molyvdas, P.A.; Stefanidis, I. Endothelin-1

acutely reduces the permeability of visceral sheep peritoneum in vitro through both endothelin-A and endothelin-B receptors. *Artif. Organs* **2013**, *37*, 308–312.

231. Ussing, H.H.; Zerahn, K. Active transport of sodium as the source of electric current in the short-circuited isolated frog skin. *Acta Physiol. Scand.* **1951**, *23*, 110–127.

232. Simon, M. Peritoneal mesothelium in vitro: an electrophysiologic study. *Perit Dial Int* **1996**, *16*, 393–397.

233. Zarogiannis, S.; Stefanidis, I.; Hatzoglou, C.; Liakopoulos, V.; Gourgoulianis, K.; Molyvdas, P.-A. Effect of adrenaline on the electrophysiologic profile of isolated visceral sheep peritoneum. *Adv Perit Dial* **2004**, *20*, 23–26.

234. Zarogiannis, S.; Kourti, P.; Hatzoglou, C.; Liakopoulos, V.; Poultsidi, A.; Gourgoulianis, K.; Molyvdas, P.-A.; Stefanidis, I. Influence of the sodium transport inhibition by amiloride on the transmesothelial resistance of isolated visceral sheep peritoneum. *Adv. Perit. Dial.* **2005**, *21*, 5–8.

235. Stefanidis, I.; Zarogiannis, S.; Hatzoglou, C.; Liakopoulos, V.; Kourti, P.; Poultsidi, A.; Mertens, P.R.; Gourgoulianis, K.; Molyvdas, P.-A. Enhancement of the transmesothelial resistance of the parietal sheep peritoneum by epinephrine in vitro: ussing-type chamber experiments. *Artif. Organs* **2005**, *29*, 919–922.

236. Debray-García, Y.; Sánchez, E.I.; Rodríguez-Muñoz, R.; Venegas, M.A.; Velazquez, J.; Reyes, J.L. Diabetes and exposure to peritoneal dialysis solutions alter tight junction proteins and glucose transporters of rat peritoneal mesothelial cells. *Life Sci.* **2016**, *161*, 78–89.

237. Horiuchi, T.; Matsunaga, K.; Banno, M.; Nakano, Y.; Nishimura, K.; Hanzawa, C.; Miyamoto, K.I.; Nomura, S.; Ohta, Y. HPMCs induce greater intercellular delocalization of tight junction-associated proteins due to a higher susceptibility to H2O2 compared with HUVECs. *Perit. Dial. Int.* **2009**, *29*, 217–226.

238. Sacnun, J.M.; Hoogenboom, R.; Eibensteiner, F.; Sobieszek, I.J.; Unterwurzacher, M.; Wagner, A.; Herzog, R.; Kratochwill, K. Proteome-wide differential effects of peritoneal dialysis fluid properties in an in vitro human endothelial cell model. *Int. J. Mol. Sci.* **2022**, *23*, 8010.

239. Lauri, K.; Arund, J.; Holmar, J.; Tanner, R.; Kalle, S.; Luman, M.; Fridolin, I.

Removal of urea, β2-microglobulin, and indoxyl sulfate assessed by absorbance and fluorescence in the spent dialysate during hemodialysis. *ASAIO J.* **2020**, *66*, 698–705.

240. Voigt, M.; Gebert, M.; Haug, U.; Hulko, M.; Storr, M.; Boschetti-de-Fierro, A.; Beck, W.; Krause, B. Retention of beneficial molecules and coagulation factors during haemodialysis and haemodiafiltration. *Sci. Rep.* **2019**, *9*, 6370.

241. Masakane, I.; Sakurai, K. Current approaches to middle molecule removal: room for innovation. *Nephrol. Dial. Transplant.* **2018**, *33*, iii12–iii21.

242. Ward, R.A.; Beck, W.; Bernardo, A.A.; Alves, F.C.; Stenvinkel, P.; Lindholm, B. Hypoalbuminemia: a price worth paying for improved dialytic removal of middle-molecular-weight uremic toxins? *Nephrol. Dial. Transplant.* **2019**, *34*, 901–907.

243. Wang, D.W.; Zhang, W.H.; Danil, G.; Yang, K.; Hu, J.K. The role and mechanism of claudins in cancer. *Front. Oncol.* **2022**, *12*, 1051497.

244. Nehme, Z.; Roehlen, N.; Dhawan, P.; Baumert, T.F. Tight junction protein signaling and cancer biology. *Cells* **2023**, *12*, 243.

245. Venugopal, S.; Anwer, S.; Szászi, K. Claudin-2: Roles beyond permeability functions. *Int. J. Mol. Sci.* **2019**, *20*, 5655.

246. Kang, D.H. Loosening of the mesothelial barrier as an early therapeutic target to preserve peritoneal function in peritoneal dialysis. *Kidney Res. Clin. Pract.* **2020**, *39*, 136–144.

247. Eleftheriadis, T.; Pissas, G.; Antoniadi, G.; Nikolaou, E.; Golfinopoulos, S.; Liakopoulos, V.; Stefanidis, I. Activation of general control nonderepressible-2 kinase ameliorates glucotoxicity in human peritoneal mesothelial cells, preserves their integrity, and prevents mesothelial to mesenchymal transition. *Biomolecules* **2019**, *9*, 832.

248. Zhou, Y.; Fan, J.; Zheng, C.; Yin, P.; Wu, H.; Li, X.; Luo, N.; Yu, X.; Chen, C. SGLT-2 inhibitors reduce glucose absorption from peritoneal dialysis solution by suppressing the activity of SGLT-2. *Biomed. Pharmacother.* **2019**, *109*, 1327–1338.

249. Lai, J.W.; Lin, H.J.; Chou, C.Y. SGLT-2 inhibitors may increase ultrafiltration in incident peritoneal dialysis patients: a case report. *BMC Nephrol.* **2023**, *24*, 106.

250. Vorobiov, M.; Rogachev, B.; Riff, R.; Chaimowitz, C.; Neulander, E.Z.; Basok, A.; Shnaider, A.; Douvdevani, A.; Haviv, Y.S. Blockade of sodium–glucose co-transporters improves peritoneal ultrafiltration in uraemic rodent models. *Perit Dial Int* **2023**, 8968608231165865.

251. Herbert, S.L.; Fick, A.; Heydarian, M.; Metzger, M.; Wöckel, A.; Rudel, T.; Kozjak-Pavlovic, V.; Wulff, C. Establishment of the SIS scaffold-based 3D model of human peritoneum for studying the dissemination of ovarian cancer. *J. Tissue Eng.* **2022**, *13*, 20417314221088510.